NASA CONTRACTOR REPORT

NASA CR-1859

ANALYTICAL AND EXPERIMENTAL INVESTIGATION OF AIRCRAFT METAL STRUCTURES REINFORCED WITH FILAMENTARY COMPOSITES

Phase I: Concept Development and Feasibility

by S. Dicken and R. R. June

Prepared by
THE BOEING COMPANY
Seattle, Wash.
for Langley Research Center

19960605 030

NATIONAL AERONAUTICS AND SPACE ADMINISTRATION · WASHINGTON, D. C. · DECEMBER 1971

1. Report No. NASA CR-1859	2. Government Accession No.	3. Recipient's Catalog No.
4. Title and Subtitle ANALYTICAL AND EXPERIMENTAL INVESTIGATION OF AIRCRAFT METAL STRUCTURES REINFORCED WITH FILAMENTARY COMPOSITES. Phase I - Concept Development and Feasibility		5. Report Date December 1971
		6. Performing Organization Code
7. Author(s) S. Oken and R. R. June		8. Performing Organization Report No.
		10. Work Unit No.
9. Performing Organization Name and Address The Boeing Company Commercial Airplane Group Seattle, Washington		11. Contract or Grant No. NAS 1-8858
		13. Type of Report and Period Covered Contractor Report
12. Sponsoring Agency Name and Address National Aeronautics and Space Administration Washington, DC 20546		14. Sponsoring Agency Code

15. Supplementary Notes

16. Abstract

    This report covers the analytical and experimental investigations in phase I of a three-phase program performed to establish the feasibility of reinforcing metal aircraft structures with advanced filamentary composites. The interactions resulting from combining the two types of materials into single assemblies as well as their ability to function structurally were studied. The combinations studied were boron–epoxy reinforced aluminum, boron–epoxy reinforced titanium, and boron–polyimide reinforced titanium. The concepts used unidirectional composites as reinforcement in the primary loading direction and metal for carrying the transverse loads as well as its portion of the primary load. The program established that several realistic concepts could be fabricated, that these concepts could perform to a level that would result in significant weight savings, and that there are means for predicting their capability within a reasonable degree of accuracy. This program also encountered problems related to the application of polyimide systems that resulted in their relatively poor and variable performance.

17. Key Words (Suggested by Author(s)) Filamentary composites Composite reinforced metals Boron–epoxy Boron–polyimide Aircraft structures	18. Distribution Statement Unclassified — Unlimited

19. Security Classif. (of this report) Unclassified	20. Security Classif. (of this page) Unclassified	21. No. of Pages 129	22. Price* $3.00

FOREWORD

CONTENTS

TABLES

FIGURES

ANALYTICAL AND EXPERIMENTAL INVESTIGATION OF AIRCRAFT METAL STRUCTURES REINFORCED WITH FILAMENTARY COMPOSITES

Phase I – Concept Development and Feasibility

By S. Oken and R. R. June

The Boeing Company

SUMMARY

This report covers the analytical and experimental investigations in phase I of a three-phase program performed to establish the feasibility of reinforcing metal aircraft structures with advanced filamentary composites. The interactions resulting from combining the two types of materials into single assemblies as well as their ability to function structurally were studied.

In this work, existing material systems and processes were used with only minor changes. The material systems that were investigated are described in detail in appendix B and are listed below.

- Aluminum-boron-epoxy

- Titanium-boron-epoxy

- Titanium-boron-polyimide

The concepts studied used unidirectional composites as reinforcement in the primary loading direction and metal for carrying the transverse loads as well as its portion of the primary load. The basic investigations performed to provide data for developing design concepts and establish their feasibility included the following:

- Bonding development—Evaluated capability of existing adhesive systems and changes to their cure cycles to alleviate residual thermal stresses.

- Residual thermal stress—Established stress-free temperature of adhesives to establish a basis for determining the magnitude of residual thermal stresses.

- Composite load transfer—Established effective techniques for introducing load to advanced filamentary composites.

- Compression stress-strain—Established stress-strain relationships for various metal-composite material systems.

- Plate bending—Evaluated use of transformed section techniques for determining bending stiffness of composite-reinforced plates.

- Plate buckling—Developed experimental data and investigated buckling characteristics of flat metal plates reinforced with composite.

- Column crippling and buckling—Performed experimental investigations to establish the feasibility of reinforcing structural shapes with composites.

- Sandwich crippling and buckling—Performed experimental investigations to establish the capabilities of honeycomb sandwich construction incorporating composite-reinforced metal skins.

- Concept verification panels—Performed experimental and theoretical investigations to establish the capabilities and efficiencies of several stiffened-panel concepts incorporating unidirectional boron composite as reinforcement in the primary load direction.

The results obtained from the above investigations proved the feasibility of reinforcing metal aircraft structures with advanced filamentary composites. This program established that several realistic concepts could be fabricated, that these concepts could perform to a level that would result in significant weight savings, and that there are means for predicting their capability within a reasonable degree of accuracy. This program also encountered problems related to the application of polyimide systems that resulted in their relatively poor and variable performance.

During this program, new analytical procedures were developed. Column analysis using transformed section techniques was used. A buckling analysis for anisotropic, layered plates and plate sections is being developed under a contract modification, and the results are expected to be published when complete.

In the following phases of this program, creep and fatigue characteristics will be observed and damage containment capabilities will be developed. Finally, full-size components will be designed, fabricated, and tested.

INTRODUCTION

Several approaches have been studied to determine feasible means for using filamentary composites in aircraft structures. Some of the applications are pointed toward secondary structure and others toward primary structure. Some designs use composite to carry all the load and others use the composite to reinforce metal structures in the primary load direction. The latter application has many advantages and has a good possibility of providing the initial approach for using composites for primary aircraft structure.

Efficient use of composites holds a high priority because of high initial cost. The metal structure reinforcement concept uses composites in smaller amounts and in a unidirectional form. The composites are loaded in a mode that takes maximum advantage of the fiber properties.

Manufacturing assemblies incorporating composite-reinforced metal offer many advantages. The metal portions will use existing forming and metal-removal technology. Laminate fabrication, by using unidirectional construction, is reduced to its simplest form. The manner in which concepts have been conceived permits the attachment problems to revert to conventional designs by incorporating load transition sections that terminate in all-metal sections. Conventional adhesives and processes have proven adequate for assembling composites to metal structure. The residual stresses and curvatures resulting from elevated-temperature curing of the adhesives were studied in this program.

Preliminary studies performed prior to this work have shown that the reinforced-metal concept results in significant weight savings when compared with conventional metal structure. Further studies were performed in this program to investigate the most promising of these concepts and their relative merits.

The material systems investigated in this program were selected for use at temperatures consistent with the environments of two groups of aircraft (see app. C). The aluminum-boron-epoxy and titanium-boron-epoxy systems were evaluated for use in subsonic aircraft with an operating temperature range of -65° to 160° F (219° to 344° K). The titanium-boron-polyimide system was evaluated for a supersonic transport application with an operating temperature range of -65° to 450° F (219° to 506° K).

The program revolved around an investigation of the basic structural element consisting of a metal substrate, a unidirectional composite reinforcement, and a stepped metal transition region for properly loading the composite. Studies were performed investigating the merits of candidate constituents and the manner in which they performed together. Methods of specimen fabrication are discussed in appendix B. Special attention was given to a stepped metal transition region design that provided equal stiffness load paths to each fiber.

The final investigations were concerned with various arrangements of structural elements to establish efficient concepts for carrying load. These concepts were committed primarily to adhesive-bonded construction, although, in some instances, mechanical fastening was considered to prevent adhesive peel during panel postbuckling.

SYMBOLS

The units used for physical quantities defined in this paper are given in both the U.S. customary units and in the international system of units (SI) (ref. 1). Conversion factors pertinent to the present investigation are presented in appendix A.

A	area, square inches (square centimeters)
b	breadth or width, inches (centimeters)
b_s	stringer spacing, inches (centimeters)
c	distance from neutral axis to extreme fiber or fixity coefficient, inches (centimeters)
cm	centimeter
E	modulus of elasticity, pounds per square inch (newtons per square meter)
in.	inch
I	moment of inertia, quartic inches (quartic centimeters)
kip	1000 pounds
ksi	kips per square inch
L	length, inches (centimeters)
lb	pound
m	meter
N	newton
N_x	load intensity, kips per inch (newtons per meter)
P	load, pounds
psi	pounds per square inch
Q	static moment of section, cubic inches (cubic centimeters)
r	radius of gyration, inches (centimeters)
s	total beam span, inches (centimeters)
t	thickness, inches (centimeters)
t_e	weight effective skin thickness, inches (centimeters)
T	temperature, degrees Fahrenheit (Kelvin)
T_o	stress-free temperature, degrees Fahrenheit (Kelvin)
V	vertical shearing force, pounds (newtons)
w	width
ΔT	change in temperature, degrees Fahrenheit (Kelvin)
δ	deflection, inches (centimeters)
ϵ	strain, inches per inch (centimeters per centimeter)
κ	coefficient of thermal expansion, inches per inch per degree Fahrenheit (meters per meter per degree Kelvin)
μ	Poisson's ratio
ρ	density
Σ	summation
σ	stress, pounds per square inch (newtons per square meter)

Subscripts

Al	aluminum
B	boron
c	composite
e	effective
m	metal
me	metal equivalent
r	matrix or adhesive
Ti	titanium

BONDING DEVELOPMENT

Objective

The objective of the bonding development portion of this program was to select suitable bonding materials and processes to bond boron-epoxy composite to aluminum or titanium and to bond boron-polyimide composite to titanium. The evaluation considered use-temperatures consistent with applicable aircraft environments—-65° F to 160° F (219° K to 344° K) for the epoxy composites and -65° F to 450° F (219° K to 505° K) for the polyimide systems.

Approach

Candidate adhesive systems and processes were selected from metal bonding technology currently available at The Boeing Company. This provided baseline property data as well as state-of-the-art processing information. Four epoxy systems with different curing temperatures were evaluated as well as two polyimide systems. Each system was evaluated on the basis of interlaminar shear or lap shear strengths. Studies also were made of epoxy cure cycle modifications that would lessen the effects of residual thermal stress.

Test Specimens

The basic specimens used in this evaluation consisted of short-beam interlaminar shear and standard metal-to-metal lap shear specimens. Details of these specimens are shown in figures 1, 2, and 3.

Testing and Results

The short-beam specimens were tested in three-point bending, as shown in figure 4. The test span was five times the thickness of the specimen. The elevated-temperature test specimens were heated in an enclosure during testing. For the -65° F tests, liquid nitrogen was metered into an enclosure to cool the specimen. A thermocouple taped to the specimen was used to control the temperature. The failure load of each specimen was recorded and used to develop the interlaminar shear strength. A summary of the test data in terms of interlaminar shear is shown in figures 5 and 6.

Discussion

Four adhesive systems for bonding boron-epoxy composites to aluminum were selected for evaluation: BP-907, AF 126, FM 123, and Epon 927. (See app. C.) These systems were selected because of their high shear strengths and because they provide a range of cure temperatures. (The magnitude of the residual bonding stresses is a function of cure temperature.) Excessive cure temperatures induce potentially high residual thermal stresses that, in turn, may affect the metal-to-composite bond strength. Also, these stresses are magnified when aluminum is used with a composite because of the large differences in thermal expansion. Epon 927 was selected for evaluation because it cures at room temperature and would minimize this effect. AF 126 and FM 123 were selected because of their high strengths.

Figure 7 shows metal-to-metal lap shear strengths of the AF 126, FM 123, and Epon 927 adhesive systems used in design at Boeing. BP-907 was also investigated to determine the practicability of using the composite matrix as an adhesive thus combining composite curing and bonding in the same process cycle.

The short-beam interlaminar shear data for the aluminum-epoxy systems are shown in figure 5. Interlaminar shear strength is shown as a function of test temperature for three adhesive systems when cured following the recommended curing cycle. These results showed that all of the candidate adhesives developed interlaminar shear strengths that are acceptable for bonded metal aircraft structure. The higher strength levels available using BP-907, AF 126, or FM 123 were desirable, but, due to the large differences in coefficients of thermal expansion of the adherends, the low-temperature-curing adhesive (Epon 927) was preferred for assembling aluminum composite system to minimize residual bonding stresses and assembly distortions.

The possibility of combining the laminating and bonding processes using AF 126 adhesive and the laminating cure cycle was also evaluated. Curves 3P and 3K of figure 5 show that the bond strength is significantly reduced by the higher cure temperature. Part distortion, because of the higher cure temperature, would also be intolerable.

A shorter time and higher temperature curing cycle than normally recommended for Epon 927 was investigated. The standard cure for this system is 120 hr at room temperature in a vacuum. This modification not only reduced fabrication time appreciably, but also improved the adhesive shear strength as shown in figure 5.

Cure-cycle modifications were also studied for the AF 126 and FM 123 systems. Lap shear test specimens were fabricated to compare the standard cure cycle with two modified cure cycles where the temperature was reduced and the time increased. Test results, presented in table 1, indicate that the modified cures sacrifice strength. The lower shear strength after exposure to humidity is interpreted as an indication of an incomplete cure. This phase of the study was terminated.

When production of larger assemblies began, normal shop tolerances produced gaps between surfaces to be bonded. The room temperature cured adhesive layers [0.005 in. (0.13 cm) thick] could not fill all these spaces, and bond-line voids resulted. Curves 3H, 3I, and 3J (fig. 5) indicated that increasing the Epon 927 adhesive thickness to fill these voids would reduce interlaminar shear strength. Therefore, a subsequent study, employing lap shear specimens, was conducted. It showed that the use of Epon 933 (Epon 927 filled with fiberglass and asbestos), combined with Epon 927, gave satisfactory bond-line strength. Table 2 shows the results of this series of tests. All of these specimens were cured at room temperature for 48 hr, then postcured at 160° F (344° K) for 2 hr. This modified cure cycle was used in all subsequent bonding of boron-epoxy composite to aluminum.

Two adhesive systems were evaluated for bonding boron-epoxy composite to titanium: BP-907 and AF 126. Results of interlaminar shear tests using the short-beam specimen are shown in curves 3L, 3N, and 3O of figure 6. These results showed that both systems provided shear strengths in excess of 2500 psi at room temperature, the level normally required for aircraft structural usage. AF 126 was selected for bonding boron-epoxy composite to titanium because it is a standard adhesive system used at Boeing. Discussions of titanium conversion coatings using Pasa Jel and phosphate fluoride treatments for preparation of titanium for bonding may be found in the "Composite Load Transfer" section.

Two systems were evaluated for bonding boron-polyimide composite to titanium. One was a laminating resin, 35-520 Pyralin, and the other an adhesive, FM 34 (see app. C). Both of these were preselected as the best candidate systems available for use with this program. An evaluation was conducted using the short-beam interlaminar shear test. Results are shown in figure 6. Both systems produced strengths in excess of 5000 psi (34.5 MN/m^2) at room temperature and retained strengths in excess of 3000 psi (20.7 MN/m^2) at the maximum design temperature of 450° F (505° K). Test results for the 35-520 Pyralin system are shown by curve 3U. Curves 3Q, 3R, 3S, and 3T show data developed using the FM 34 adhesive system. The specimens from lot 3Q, which were to be tested at 450° F (505° K), were inadvertently tested at 160° F (344° K). The 3R replacement specimens failed at significantly lower stress levels than Group 3Q, therefore, the 3S specimens were made and tested. No known process or material parameters were changed between lots. The large scatter indicated by the curves is interpreted as being due to process sensitivity. The polyimide systems contain solvents and give off reaction products during cure that make successful bonding very sensitive to venting, pressure application, temperature, and part geometry. In general, all results were lower than desired, but both systems were considered adequate. Subsequently, 35-520 Pyralin was used as the bond to the titanium step fittings coincident with the laminating subassembly process. The FM 34 was used as an adhesive as required in bonding the laminate-step fitting subassembly to a metal part.

Conclusions

Bonding of boron-epoxy composites to aluminum was accomplished using standard adhesives and processes. Shear strengths attained were equivalent to test data obtained with the adhesives used in present aircraft designs. The combination of Epon 927 and Epon 933 was the adhesive system selected for assembling boron-epoxy laminates to aluminum for use-temperatures consistent with subsonic aircraft (-65° F to 160° F) (219° K to 344° K).

Bonding of boron-epoxy composite to titanium was accomplished using standard adhesives and processes. AF 126 adhesive was selected for assembling composites to titanium in components to be evaluated for potential applications in subsonic aircraft. Pasa Jel and phosphate fluoride conversion coating of titanium were both satisfactory and were both used in subsequent work. Test data ("Composite Load Transfer" section) indicated that the phosphate fluoride coating was slightly superior to Pasa Jel for epoxy bonding.

Both of the polyimide systems evaluated, 35-520 Pyralin laminating resin and FM 34 adhesive, were considered satisfactory for bonding the composite to titanium. Pasa Jel conversion coating of the titanium, and rigid adherence to process control procedures are required to produce bonds that will consistently develop full boron filament strength.

TABLE 1.—AVERAGE LAP SHEAR STRENGTH WITH VARIOUS CURE CYCLES AND EXPOSURE ENVIRONMENTS

		10-hr cure cycle				2-hr standard cure	
		175° F (353° K)		185° F (358° K)		240° F (389° K)	
Adhesive	Exposure	lb/in^2	MN/m^2	lb/in^2	MN/m^2	lb/in^2	MN/m^2
AF 126	Control[a]	4240	29.24	5280	36.40	5500	37.92
	Humidity[b]	4075	28.09	4465	30.78	5500	37.92
	Skydrol[c]	4940	34.06	5090	35.09	4800	33.09
FM 123-2	Control[a]	4465	30.78	4655	32.09	4800	33.09
	Humidity[b]	3550	24.47	4165	28.71	4700	32.40
	Skydrol[c]	4740	32.68	4830	33.30	4800	33.09
FM 123-5	Control[a]	5230	36.05	4630	31.92	5300	36.54
	Humidity[b]	4360	30.06	4600	31.71	4600	31.71
	Skydrol[c]	5220	35.98	5410	37.29	5200	35.85

[a]Test results are single lap shear bond strenghts developed with 7075-T6 aluminum adherend.

[b]Humidity exposure: Test panels and test coupons were subjected to 28 days of continuous exposure to condensing humidity at 120° F (322° K) per FTM STD 141, method 6201. The test specimens were tested within 4 hr after removal from the humidity cabinet.

[c]Skydrol exposure: Test coupons were immersed in Skydrol 500A for 7 days at 160° F (344° K) and tested within 0.5 hr after removal.

TABLE 2.—LAP SHEAR STRENGTHS OF ROOM-TEMPERATURE BONDS[a]

Adhesive	Lap shear strength	
	lb/in.^{2}	MN/m^2
Epon 927 adhesive film, 0.010 in. (0.0254 cm) thick	3040	20.96
	2780	19.17
	2960	20.41
	3200	22.06
	3070	21.17
	3010 av	20.75 av
Epon 933 filled resin	2540	17.51
	2400	16.55
	2440	16.82
	2400	16.55
	2800	19.30
	2520 av	17.35 av
Epon 927 adhesive film, 0.010 in. (0.0254 cm) thick, with Epon 933 filled resin	3510	24.20
	3540	24.41
	3430	23.65
	3370	23.23
	3520	24.27
	3480 av	23.95 av
Epon 927 adhesive film, 0.010 inch (0.0254 cm) thick, with Epon 933 filled resin, bondline shimmed open 0.010 in. (0.0254 cm)	3530	24.34
	3360	23.16
	3520	24.27
	3100	21.37
	3320	22.89
	3360 av	23.21 av

[a]Substrate: 7075-T6 aluminum
Cure cycle: 48 hr at room temperature, then 2 hr at 160° F (344° K)
Test specimen: standard lap shear per figure 2
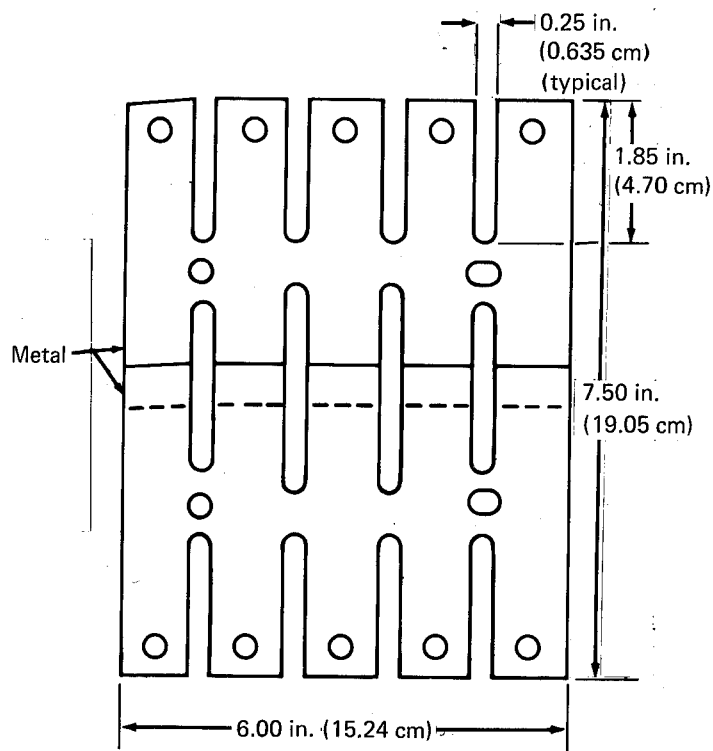
FIGURE 1.—STANDARD LAP SHEAR
SPECIMEN ASSEMBLY

0.25 in.
(0.635 cm)
(typical)

1.85 in.
(4.70 cm)

7.50 in.
(19.05 cm)

Metal

6.00 in. (15.24 cm)

Note: Sheared from assembly
shown in figure 1.

0.050 in.
(0.127 cm)

Metal

0.50 in.
(1.27 cm)

1.00 in.
(2.54 cm)
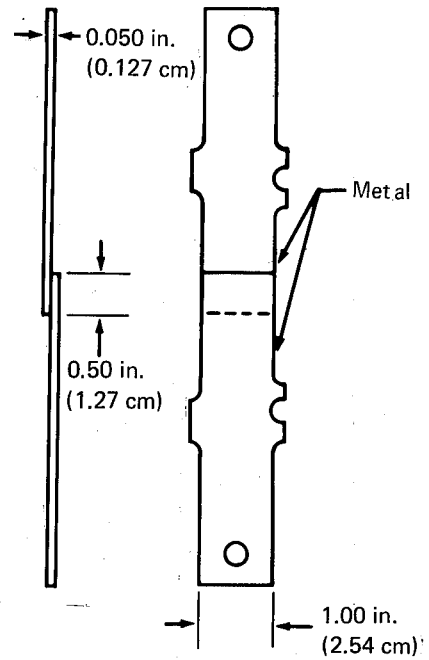
FIGURE 2.—LAP SHEAR
TEST SPECIMEN

0.50 in.
(1.27 cm)

7t
(0.88 in., 2.24 cm)

P

t

Composite (10 ply)
Adhesive
Metal 0.016 in. (0.041 cm)
Adhesive
Composite (10 ply)

5t

P/2   P/2
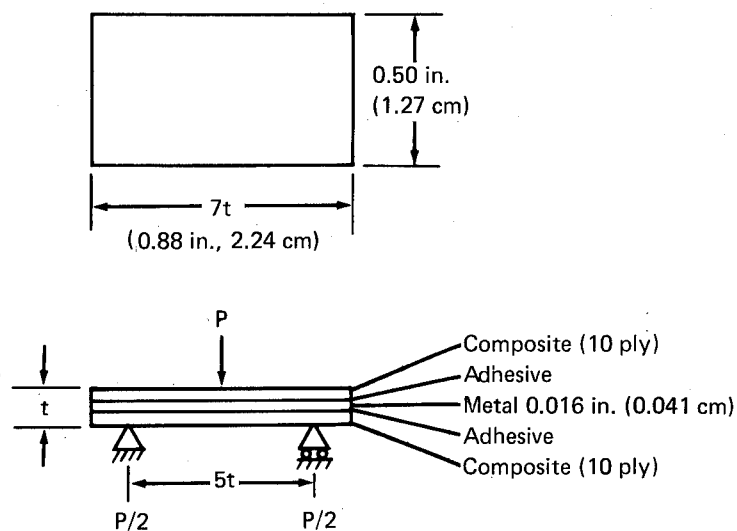
FIGURE 3.—SHORT-BEAM, THREE-POINT-BEND, INTERLAMINAR SHEAR SPECIMEN
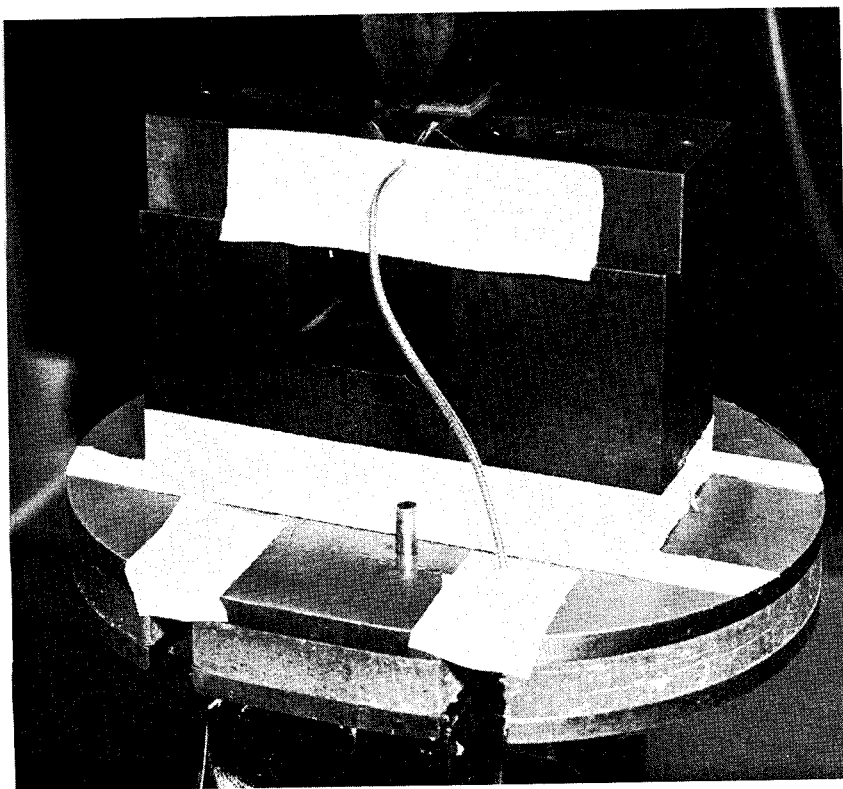
FIGURE 4.—SHORT-BEAM INTERLAMINAR SHEAR TEST SETUP

3M—BP-907
3K—AF 126
3H—EPON 927
3P—AF 126 cured with BP-907 cure cycle
3I—Epon 927 with 0.005 in. (0.012 cm) thick adhesive cured
    2 hr at 160° F (344° K)
3J—Epon 927 with 0.010 in. (0.025 cm) thick adhesive cured
    2 hr at 160° F (344° K)
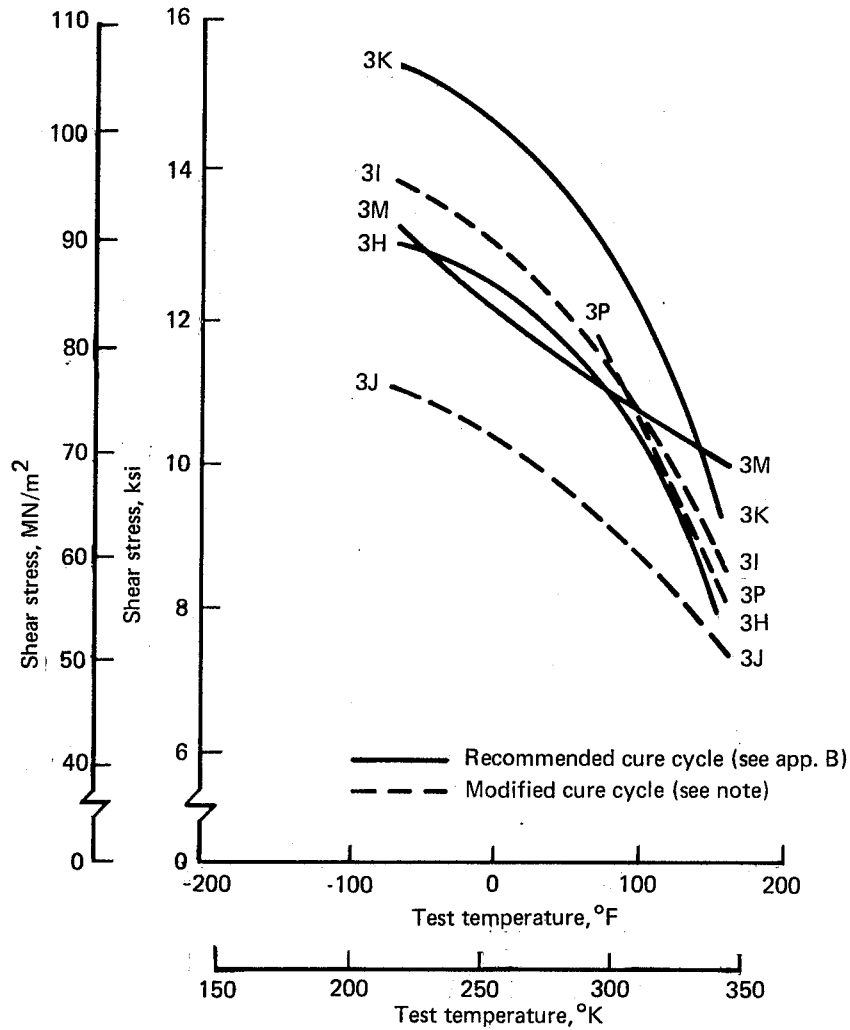
FIGURE 5.—ALUMINUM-BORON-EPOXY SHORT-BEAM INTERLAMINAR
SHEAR STRENGTH

3N—BP-907 adhesive
3L—AF 126 Pasa Jel conversion coating
3O—AF 126 phosphate fluoride conversion
   coating
3U—35-520 Pyralin
3Q—FM 34
3R—FM 34
3S—FM 34
3T—FM 34

Titanium-boron-epoxy

Titanium-boron-polyimide

Test temperature, °F

Test temperature, °K
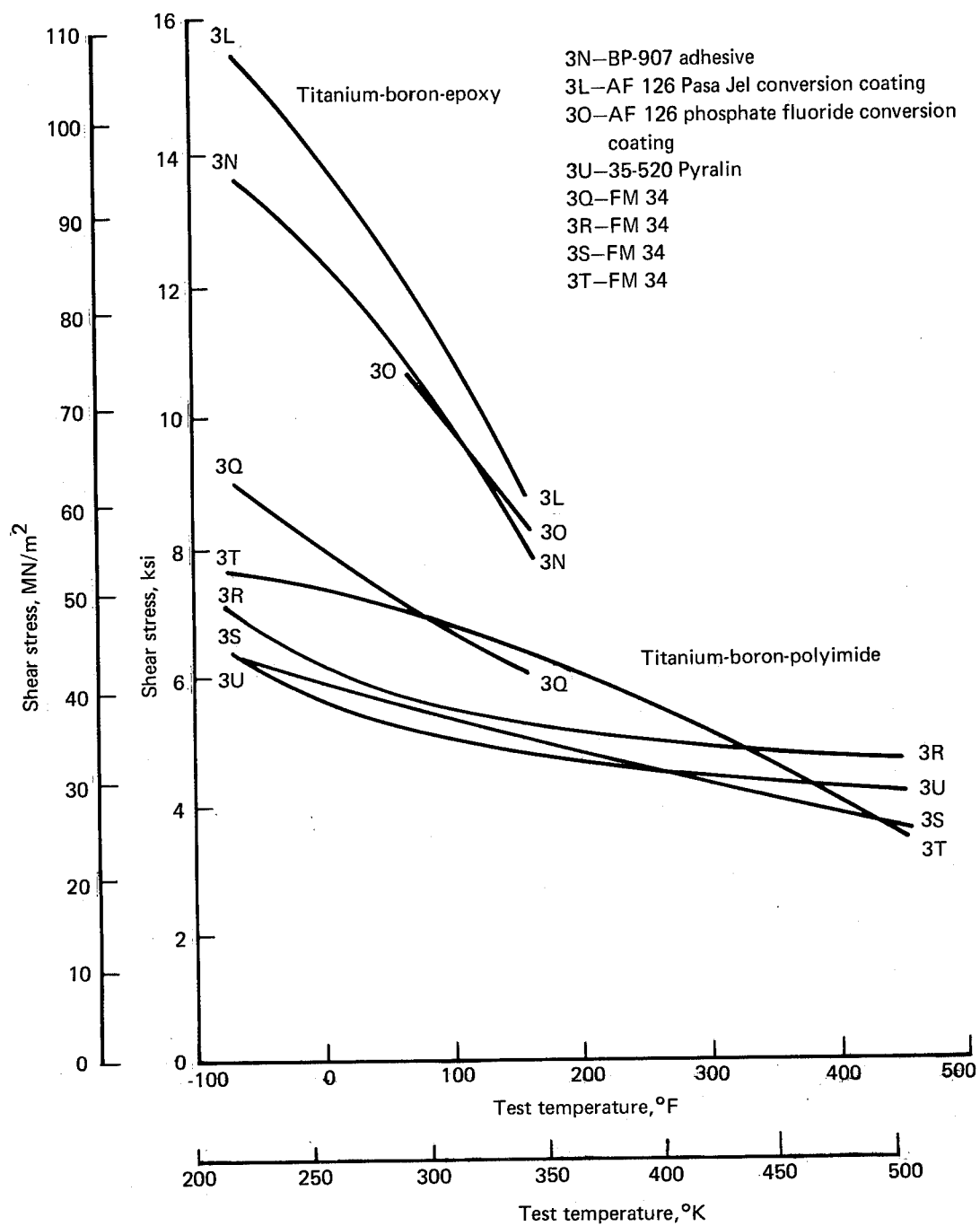
*FIGURE 6.—TITANIUM-BORON COMPOSITE SHORT-BEAM
INTERLAMINAR SHEAR STRENGTH*

15

Lap length = 0.50 in. (1.27 cm)
7075-T6 aluminum adherend

AF 126
FM 123

Epon 927
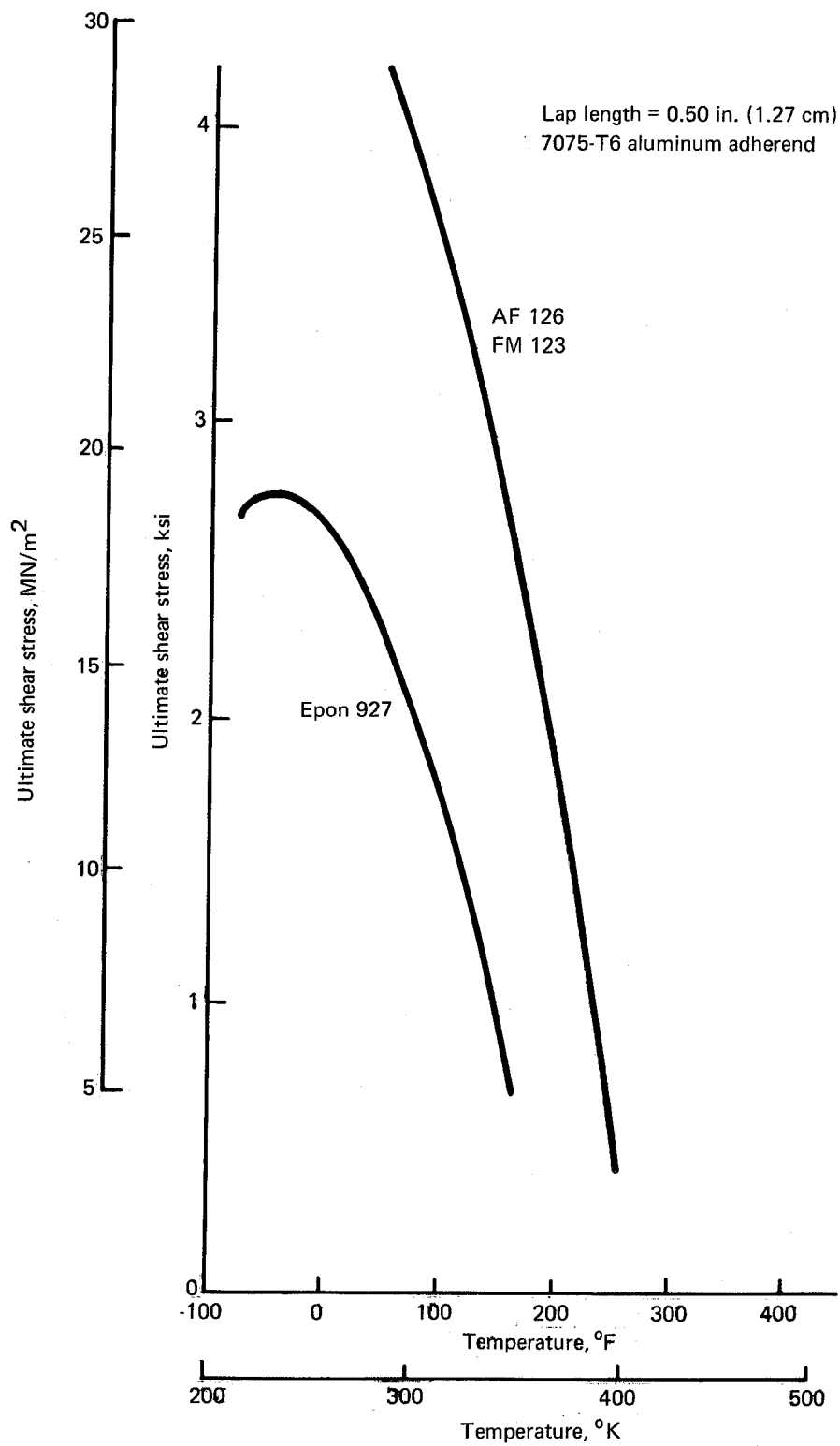
FIGURE 7.—LAP SHEAR PROPERTIES OF EPOXY ADHESIVES

RESIDUAL THERMAL STRESS

Objective

Thermally induced stress occurs when materials of differing thermal expansion are joined at one temperature and then exist at another temperature. Prediction of these thermal stresses is dependent on knowledge of the temperature at which the assembly is stress free. The objective of this phase of the investigation was to determine the stress-free temperature for boron-composite/metal assemblies bonded with various adhesive systems.

Approach

The approach was to fabricate composite/metal specimens that act like bimetallic strips. Based on the curvature assumed by these specimens at room temperature, the stress-free temperature was computed using Timoshenko's "Analysis of Bi-Metal Thermostats" (ref. 1 and app. D). The stress-free temperature was then measured, and these results were compared with the calculations.

Test Specimens

Typical test specimen geometry is shown in figure 8; detailed data are listed on table 3. Five plies of unidirectional boron composite were bonded to aluminum or titanium strips 0.025 in. (0.063 cm) thick. The specimens were cured in a vacuum bag and were flat when the adhesive bond was established. At the completion of the cure cycle, the specimens were allowed to cool to room temperature where they assumed a curved shape as shown in figure 9.

Testing and Results

The curvature of the specimens mentioned in the preceding section is a function of the constituent material properties, the specimen geometry, and the temperature difference between room temperature and the stress-free temperature. The curvatures of the specimens were measured by matching them with arcs drawn to known curvatures and by using measured offsets from fixed chord lengths. Using the relationships shown in appendix D and the measured radius of curvature, the stress-free temperature was computed. Each specimen was then placed in an oven and observed while the specimen temperature was increased. The temperature at which each specimen matched a flat surface plate (the stress-free temperature T_o) was recorded. This procedure was repeated several times with each specimen (minimum of eight) within an approximate accuracy of $\pm 10^\circ$ F (5.5° K). The midspan deflections, radii of curvatures, and stress-free temperatures are listed in table 4.

Discussion

Figure 10 shows the correlation of stress-free temperature determined by test and by computation using the measured curvature of the specimens. The dashed 45° line shown in this figure represents an exact match between these methods. Using the dashed line as a reference, the test data deviation is within 10%, as indicated by the solid lines. The accuracy of the calculated values depends on the differences in thermal expansion coefficients of the constituent materials; small differences cause greater percentages of error in the

17

calculations. This was quite evident when evaluating specimens that incorporated titanium, which has a coefficient of thermal expansion similar to that of boron composites.

No consistent relationship was found between the maximum cure temperature and the stress-free temperature, as may be seen in figure 11. Some of the cure cycles required that temperature be held at an intermediate level early in the curing process and then increased at a specific rate until the maximum temperature was attained. The stress-free temperature can be created at any point when sufficient cross-polymerization has occurred to enable the bond or matrix to resist the subsequent thermal stresses at higher temperature.

Three of the data points shown in figure 11 indicate that the stress-free temperature is higher than the maximum cure temperature. This was interpreted as primarily resulting from experimental error. A small portion of this difference could be caused by the volumetric contraction that typically occurs during the polymerization process. However, it is felt that this contribution was negligible.

The results obtained from this study, combined with additional analyses, may be used to evaluate thermal stress in composite/metal assemblies. Figure 12 shows the results obtained with this type of analysis. Thermal stress is shown as a function of constituent area ratios and the temperature difference between use-temperature and stress-free temperature. The relationship shown in figure 12 is limited to applications in which the assembly is constrained against out-of-plane deformation during temperature change. Symmetric distribution of composites and stiffened structures designed to maintain their shapes, such as honeycomb sandwich and hat-stiffened panels, are examples that satisfy this requirement.

Conclusions

The calculated stress-free temperatures of structural laminates are in good agreement with values determined experimentally. The accuracy of the calculations however, is very sensitive to the values of thermal expansion coefficients used for determining stress-free temperatures.

TABLE 3.—RESIDUAL THERMAL STRESS SPECIMEN DATA

Specimen	Matrix	Metal	Adhesive	Cure temperature		Time at temperature, hr	t_{total}[a]		t_{metal}	
				°F	°K		in.	cm	in.	cm
4A	BP-907	7075-T6	AF 126	245	391	1.5	0.060	0.152	0.025	0.063
4B	BP-907	7075-T6	Epon 927	160	344	2.0	0.058	0.147	0.025	0.063
4C	BP-907	Ti-6Al-4V	BP-907	350	450	1.5	0.056	0.142	0.025	0.063
4D	BP-907	Ti-6Al-4V	BP-907	350	450	1.5	0.050	0.127	0.025	0.063
4E	BP-907	Ti-6Al-4V	BP-907	350	450	1.5	0.050	0.127	0.025	0.063
4F	BP-907	Ti-6Al-4V	AF 126	245	391	1.5	0.056	0.142	0.025	0.063
4G	BP-907	Ti-6Al-4V	AF 126	350	450	1.5	0.056	0.142	0.025	0.063
4H	35-520	Ti-6Al-4V	35-520	350	450	1.5	0.064	0.162	0.025	0.063
4I	35-520	Ti-6Al-4V	FM 34	350	450	2.0	0.064	0.162	0.025	0.063

[a]See figure 8.

TABLE 4.—STRESS-FREE TEMPERATURE DATA

Specimen	Deflection at center		Radius of curvature		$T_{o_{calc}}$		$T_{o_{test}}$	
	in.	cm	in.	cm	°F	°K	°F	°K
4A	0.47	1.19	26.7	68	244	391	210	372
4B	0.27	0.69	48.9	124	154	341	145	336
4C	0.30	0.76	42.1	107	475	519	390	472
4D	0.27	0.69	45.9	116	395	475	365	458
4E	0.255	0.65	48.1	122	380	467	350	450
4F	0.15	0.38	82.5	210	278	410	265	403
4G	0.135	0.34	96.2	245	247	393	215	375
4H	0.14	0.36	89.2	227	304	424	275	408
4I	0.11	0.28	114	290	254	397	290	416

19
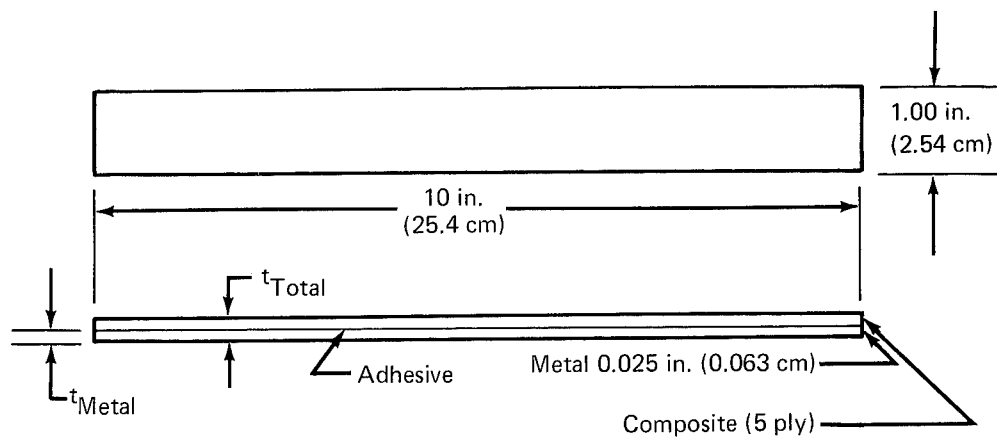
FIGURE 8.—RESIDUAL THERMAL STRESS SPECIMEN CONFIGURATION (TYPICAL)
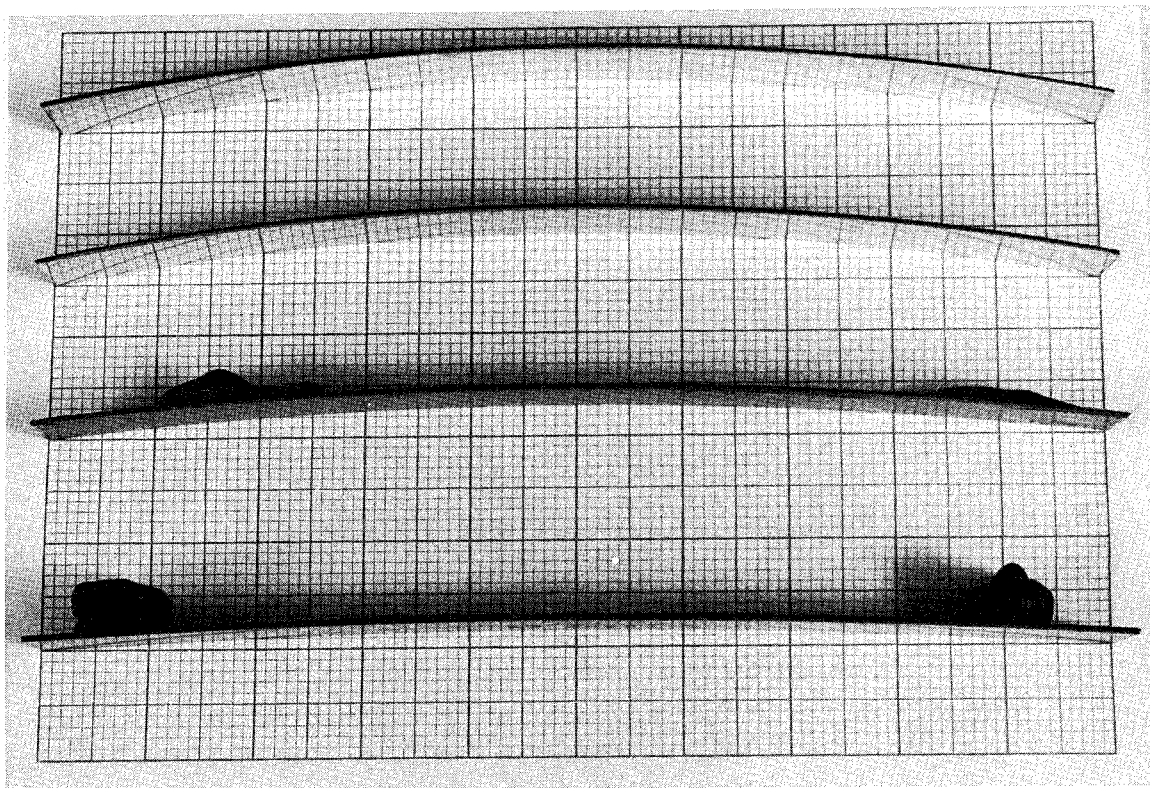
FIGURE 9.—TYPICAL RESIDUAL THERMAL STRESS SPECIMEN CURVATURES
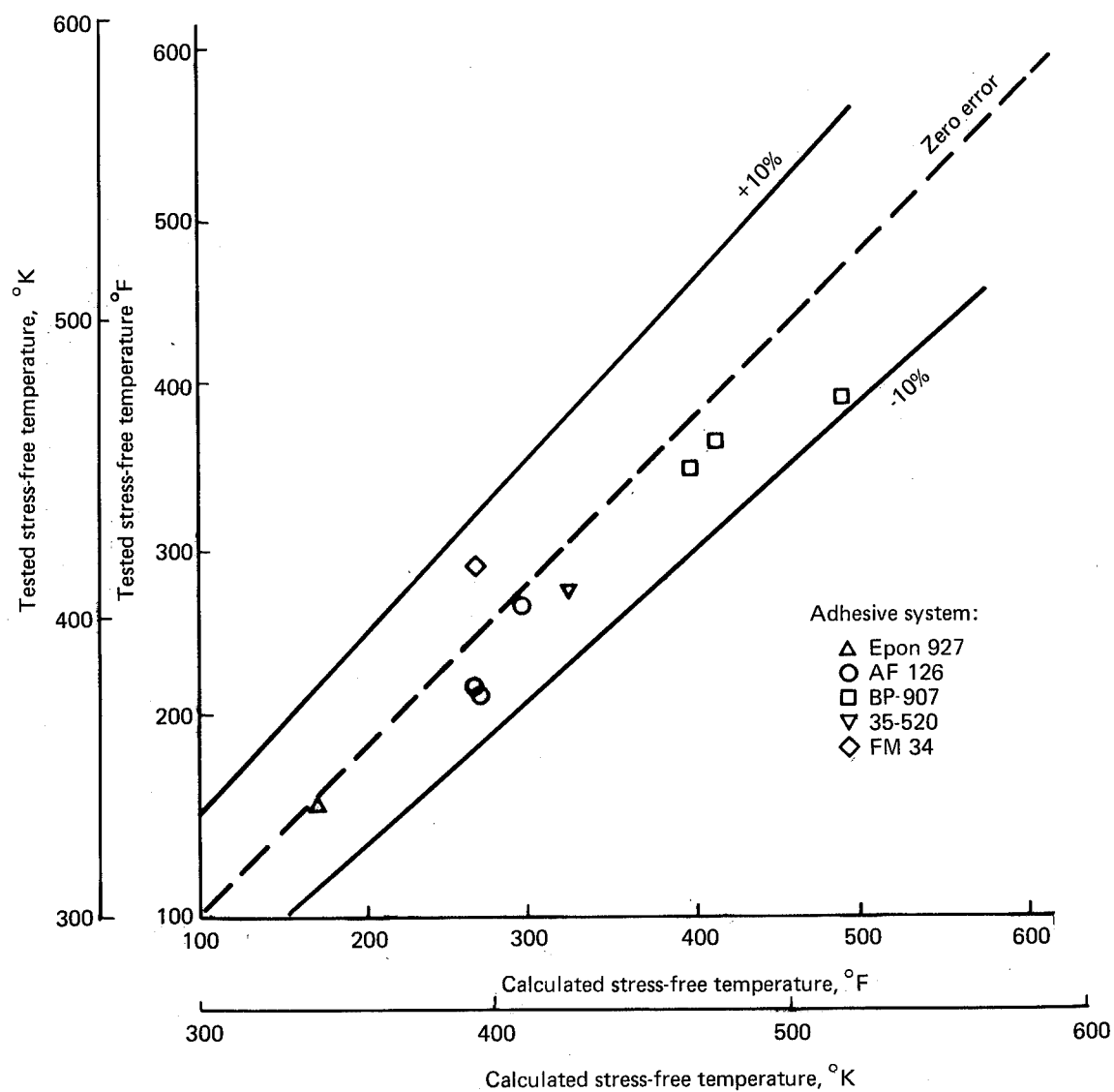
FIGURE 10.—MEASURED AND CALCULATED STRESS-FREE
TEMPERATURE FOR DIFFERENT ADHESIVE SYSTEMS
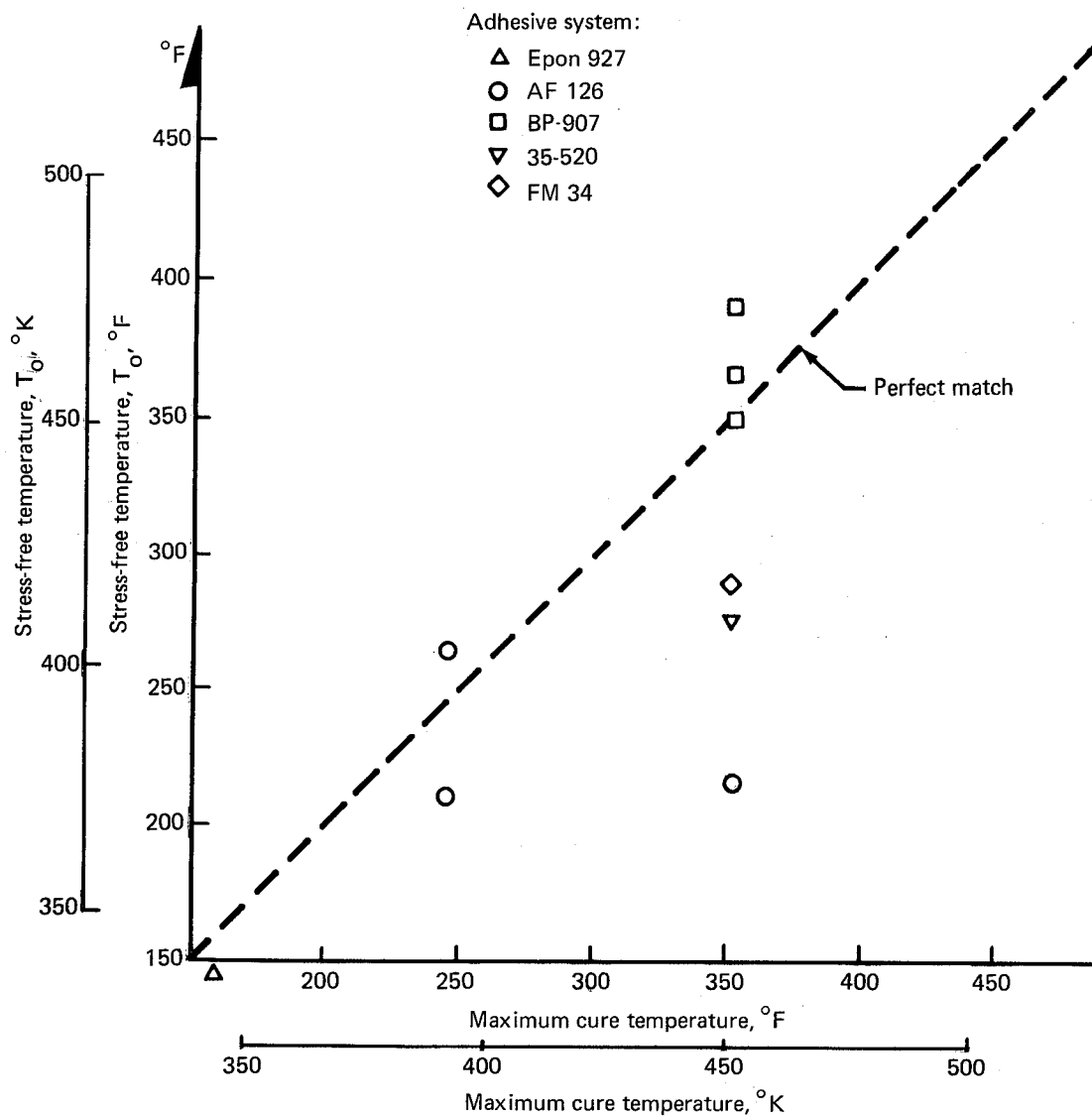
FIGURE 11.—COMPARISON OF MEASURED STRESS-FREE
         TEMPERATURE AND MAXIMUM CURE TEMPERATURE
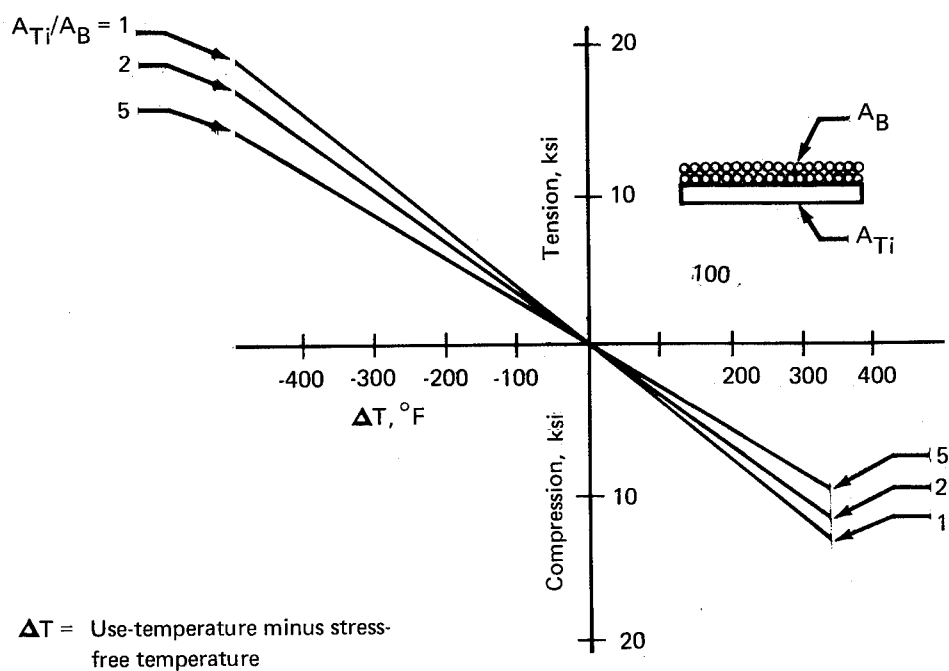
FIGURE 12.—INDUCED THERMAL STRESS IN TITANIUM

COMPOSITE LOAD TRANSFER

Objective

The objective of this portion of the program was to establish an effective load transition region between metal and composite.

Approach

Prior to this program, Boeing had used a room temperature boron fiber stress tension allowable of 360 ksi (2482 MN/m^2). This corresponds to the strain level developed at the proportional limit of titanium and, therefore, probably represents the maximum useful strain for using boron-epoxy as reinforcement for titanium structures. This level was consistently achieved by using a stepped titanium load transfer fitting to introduce loads evenly to each fiber. Using this as a base, an investigation of the stepped transition joint was begun to examine the effect of step length on static strength and to examine theoretically and experimentally the stress distribution in the transition area.

Initial room temperature testing of boron-epoxy specimens in this program produced fiber stress levels ranging from 220 to 270 ksi (1517 to 1861 MN/m^2). These results were unreasonably low when compared with the expected performance noted above. Subsequent evaluations of these specimens indicated that the poor performance was due to inferior composite-to-titanium bonds. The scope of the study was enlarged to evaluate selected material and process variables in an effort to achieve better bonding.

Test Specimens

To investigate process variables, three test methods were used: step shear, lap shear, and drum peel. The step-shear specimens consisted of a five-ply composite with stepped 6Al-4V titanium transition fittings, as shown in figure 13. Standard lap-shear and drum-peel specimens were fabricated as shown in figures 1, 2, and 14. A summary of the titanium surface-preparation, material, and process variables investigated with these specimens is shown in table 5.

After the process study was concluded, testing to satisfy the primary objective was resumed using the transition region test specimens shown in figure 15; detailed data are listed in table 6.

Testing and Results

Eighteen combinations of material and process variables were studied by using the three test methods. The five-ply composite step-shear specimens were tested in tension in a Universal test machine using hydraulic grips to prevent slippage. A summary of test results, in terms of boron stress developed, is shown in table 5. Lap-shear and drum-peel specimens were tested; the results are summarized in table 5. Based on the results obtained from these investigations, improved processes were selected and incorporated into a new set of specimens. These specimens used boron-epoxy or boron-polyimide systems, transition regions having different step lengths, and different metal face skins.

The results of the transition region tests, in terms of boron stresses, are plotted as a function of test temperatures in figure 16. The results, in terms of the maximum stresses developed in the steps, are plotted as a function of test temperatures in figure 17.

Discussion

Process verification tests.—Significant improvements in fiber failure stress level with epoxy adhesive were achieved in two specimen groups: 5A3 and 5A15. Specimen 5A3 incorporated the phosphate fluoride coating change (app. C), while specimen 5A15 combined the phosphate fluoride conversion coating change with a primer change and added adhesive in the step area. The additional adhesive made it necessary to increase the thickness of the titanium end fitting, which required additional filler plies and an undesirable weight increase. For this reason, only the conversion coating change was adopted.

Two groups of test specimens were fabricated using boron-polyimide composite. They were used to evaluate the addition of adhesive in the step area. A comparison of the test results of the two groups showed that the additional adhesive (specimen 5A18) did not improve the load transfer capability when compared to using the available matrix (specimen 5A17) for the bonding to the titanium load transfer fittings.

Transition region tests.—The effect of step length was evaluated by testing specimens at room temperature. Average results, shown in figure 16, indicate that fiber stress at failure increased with decreasing step length. These average results are perhaps misleading. The results of three tests with boron-epoxy specimens incorporating a step length of 0.50 in. (1.27 cm) were 355, 370, and 378 ksi (2477, 2551, and 2606 MN/m^2). This scatter, within one test group, covers the range of the indicated trend. A similar condition exists with the boron-polyimide results. Therefore, it was concluded that step length in the range of 0.30 to 0.50 in. (0.76 to 1.27 cm) is not critical for static strength of the systems examined.

Both elevated- and reduced-temperature tests were conducted using steps 0.40 in. (1.02 cm) long. The results are shown in figure 16. Load transfer to boron-epoxy composite is adequate at room temperature and reduced temperature, and drops to 92% of room temperature strength at 160° F (344° K). The elevated-temperature creep tests of phase II should provide additional insight in this area.

Boron-polyimide specimens were tested to establish load-transfer capabilities over a temperature range of -65° to 450° F (219° to 505° K). Three specimens with steps 0.40 in. (1.02 cm) long were tested at -65° F (219° K), 70° F (293° K), and 450° F (505° K). Also, three specimens with steps 0.30 in. (0.76 cm) long and three with steps 0.50 in. (1.27 cm) long were tested at room temperature. A summary of these results is shown in figure 16. In general, the specimens failed in a cohesive manner in the step-joint area. Boron fiber stresses of 320 ksi (2206 MN/m^2) were developed at room temperature and -65° F (219° K) and 260 ksi (1793 MN/m^2) at 450° F (505° K). The test results showed that static strength is not significantly affected in the load-transfer region by varying the step lengths in the range investigated (0.30 to 0.50 in.—0.76 to 1.27 cm).

An analytical study, performed early in this program, provides additional insight into the behavior of the load transfer region. The analysis used the basic material properties in conjunction with a finite element computer program using a matrix displacement method. The results are shown in figure 18. Predicted surface strain levels are compared to strain gage measurements taken at the center of the steps of a test specimen. The strain distribution was

predicted reasonably well using a simple model made up of approximately 200 rod and plate elements. The titanium fitting and the adhesive were represented by plate elements. The boron fibers were represented by rod elements placed at the horizontal interfaces of the plates, as shown in figure 18. The maximum strain in the joint occurs at the last step. Another strain peak occurs in the vicinity of the first step. Of the 27 failures that occurred during the above evaluation (data in fig. 16), 24 initiated in one of these two steps. Figure 17 shows the maximum net area stress that occurred in the step region during the above testing. The tensile yield strength of titanium (6Al-4V, condition III), based on 0.2% offset, is also shown in figure 17. There appears to be some correlation between the maximum joint stresses and the base-metal properties. Assuming that the failures in the best of the epoxy tests (shown as triangles in fig. 17) are caused by titanium yield, it would follow that the 450° F (505° K) performance of boron-polyimide is definitely titanium limited. The 0.2% offset data were used for this comparison only because they were readily available. Some other property, such as proportional limit, will probably provide a better correlation. Additional study, possibly including high heat treat steel step details, appears worthwhile.

Two additional tests were performed to evaluate the effect of thickness and type of metal skin covering the composite. As shown in figure 15 and table 6, the majority of the load transfer specimens were sheathed with 0.007-in. (0.018-cm) titanium. This thickness was increased to 0.025 in. (0.064 cm) in one group of specimens. Another was covered with 0.025-in. (0.064-cm) 7075-T6 aluminum skin. Failures occurred at average fiber stress levels of 370 ksi (2553 MN/m^2) and 349 ksi (2410 MN/m^2) for the titanium and aluminum specimens, respectively. The peak stress in the metal is included in the data of figure 17. The results obtained from the specimens sheathed with titanium were not significantly different than those previously obtained with the thinner titanium sheathing, but the results for those specimens using aluminum were appreciably lower than expected. In addition, two of the three aluminum-sheathed specimens failed at the center of the specimen rather than in the usually critical joint area. Further investigation in this area might prove useful. In all subsequent specimen tests, this stepped joint was used and the stepped metal was titanium (6Al-4V) regardless of the face sheet material.

Figure 19 is a photo of one of the stiffener terminations in a panel evaluated in this program. In this design, a 70-ply load transition region did not require any greater distance than the standard five-ply laminate. This is significant because it illustrates how stepped chem-milled fittings can be used in a practical manner without requiring unduly long lengths that could cause both weight and cost penalties.

Conclusions

The basic objectives of this phase of the investigation were accomplished. Boron-epoxy composite load transfer regions can be made that will develop 360 ksi (2482 MN/m^2) fiber stress at room temperature. Strength levels obtained with the boron-polyimide systems were less than with the boron-epoxy, but 320 ksi (2206 MN/m^2) was developed at room temperature and 80% of this at 450° F (505° K). Step length, in the range investigated, did not significantly affect the strength of the joint. The strain distribution within the joint was successfully predicted and compared well with measured strains. An additional study demonstrated that the surface treating process for bonding BP-907 epoxy composite to titanium should be altered to employ phosphate fluoride rather than Pasa Jel.

Three potentially useful areas for further investigation were identified: (1) determine the properties or characteristics of titanium that govern load transfer region failures; (2) examine other materials that would improve the joint strength; and (3) extend the evaluation of sheathing material, material gage effects, and adhesive strain sensitivity.

TABLE 5.–PROCESS VERIFICATION SPECIMEN DATA

Specimen	Conversion coating	Primer	Additional step adhesive	Matrix	Filler plies	Pressure application			Step specimen boron stress[b]		Lap shear stress[b]		Drum peel torque[c]	
						Step shear	Lap shear	Drum peel	ksi	MN/m²	ksi	MN/m²	in-lb	cm-N
5A1	PJ	EC 2320	None	BP-907	BP-907	Bag	Bag	Bag	307.1	2115	4136	28.49	5.05	57.41
5A2	PJ	EC 2320	None	BP-907	BP-907	Caul			289.2	1992	–		–	
5A3	PF	EC 2320	None	BP-907	BP-907	Bag	Bag	Bag	350.4	2414	4746	3,269	7.37	83.79
5A4	PF	EC 2320	None	BP-907	BP-907	Caul			327.3	2755	–		–	
5A5	PF	BR 127	None	BP-907	BP-907	Bag	Bag	Bag	321.9	2217	4326	29.80	6.45	73.33
5A6	PF	BR 127	None	BP-907	BP-907	Caul			280.7	1934	–		–	
5A7	PJ	EC 2320	BP-907	BP-907	BP-907	Bag	Bag	Bag	311.8	2148	5202	35.84	19.12	217.39
5A8	PJ	EC 2320	BP-907	BP-907	BP-907	Caul			262.7	1810	–		–	
5A9	PF	BR 127	BP-907	BP-907	BP-907	Bag	Bag	Bag	325.6	2243	3824	26.34	3.67	41.72
5A10	PF	BR 127	BP-907	BP-907	BP-907	Caul			257.6	1774	–		–	
5A11	PJ	EC 2320	AF 126	BP-907	BP-907	Bag	Bag	Bag	288.7	1989	5202	35.84	19.12	217.39
5A12	PJ	EC 2320	AF 126	BP-907	BP-907	Caul			284.5	1960	–		–	
5A13	PF	EC 2320	AF 126	BP-907	BP-907	Bag	Bag	Bag	338.5	2352	6108	42.08	26.68	303.35
5A14	PF	EC 2320	AF 126	BP-907	BP-907	Caul			323.6	2229	–		–	
5A15	PF	BR 127	AF 126	BP-907	BP-907	Bag	Bag	Bag	352.9	2431	5574	38.40	27.39	311.42
5A16	PF	BR 127	AF 126	BP-907	BP-907	Caul			348.3	2399	–		–	
5A17	PJ	BR 34	None	35-520	35-520	Bag	Bag	Bag	227.8	1569	3815	26.28	5.8	65.92
5A18	PJ	BR 34	FM 34	35-520	35-520	Bag	Bag	Bag	221.8	1528	2840	19.56	11.0	125.07

[a]PJ = Pasa Jel
PF = Phosphate fluoride
[b]Average of five tests
[c]Average of three tests

TABLE 6.–TRANSITION REGION TEST SPECIMEN DATA

Specimen	Step length		Metal skin	Adhesive layer	Filler plies	Composite matrix
	in.	cm				
5B1	0.30	0.76	0.007 Ti	AF 126	BP-907	BP-907
5B2	0.40	1.01	0.007 Ti	AF 126	BP-907	BP-907
5B3	0.50	1.27	0.007 Ti	AF 126	BP-907	BP-907
5B4	0.30	0.76	0.007 Ti	FM 34	35-520	BP-907
5B5	0.40	1.01	0.007 Ti	FM 34	35-520	35-520
5B6	0.50	1.27	0.007 Ti	FM 34	35-520	35-520
5B7	0.40	1.01	0.025 Ti	AF 126	BP-907	BP-907
5B8	0.40	1.01	0.025 Al	AF 126	BP-907	BP-907
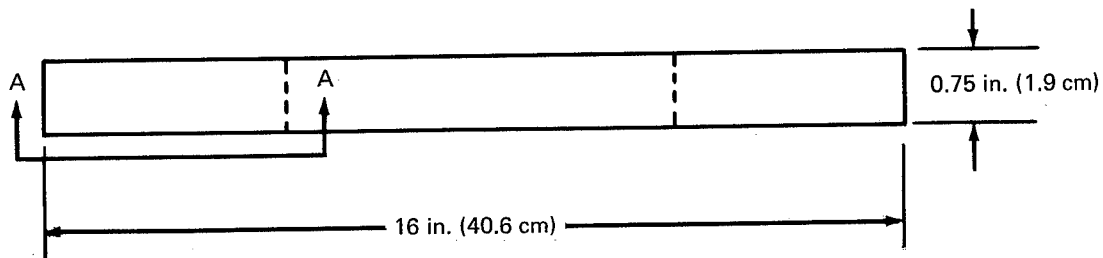
Five-Step Strap Specimen Plan View

0.75 in. (1.9 cm)

16 in. (40.6 cm)

Boron

Typical step = 0.50 in. long by
0.0055 in. thick
(1.27 cm by 0.14 mm)

Titanium
step fitting

5.00 in. (17.7 cm)

0.008 in. (0.020 cm) filler plies
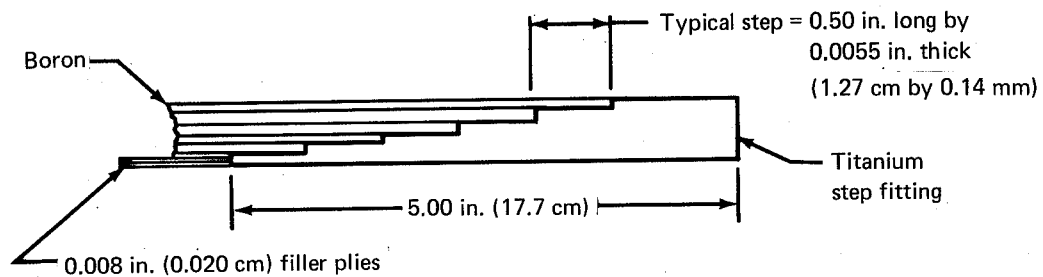
A-A
(Typical Section Through Transition Region)

FIGURE 13.—PROCESS VERIFICATION SPECIMEN CONFIGURATION—MATRIX SHEAR

1.5 in. (3.81 cm)

A   A

14 in. (35.6 cm)

1 in. (2.54 cm)

Specimen Plan View

0.010 in. (0.025 cm) typical

Five-ply boron composite
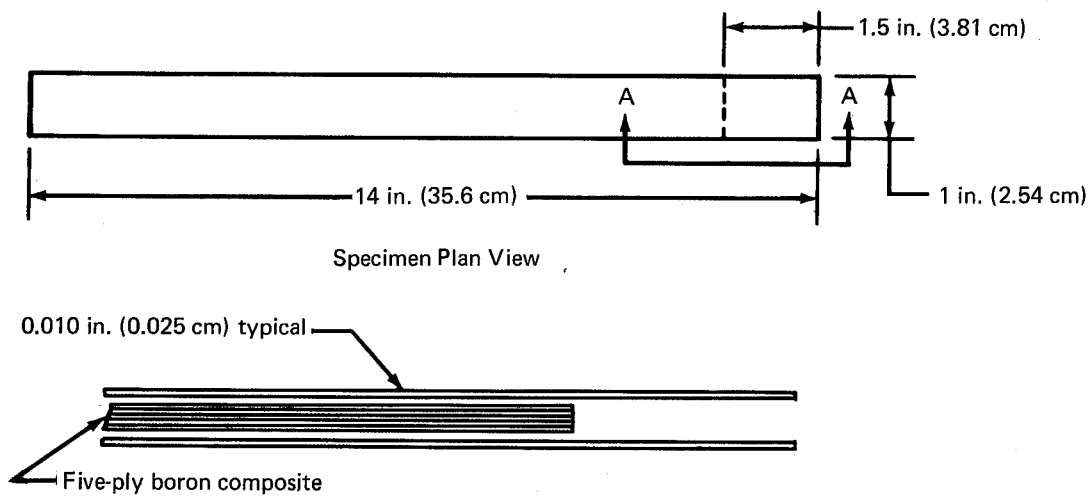
A-A
(Typical Section of End Where Peel Is Initiated)

FIGURE 14.—PROCESS VERIFICATION TEST SPECIMEN
CONFIGURATION—DRUM PEEL

2.00 in. (5.08 cm)

A   A

16.00 in. (40.6 cm)

Specimen Plan View

Metal skin
Adhesive
0.005 in. (0.013 cm)
Filler
0.008 in. (0.020 cm)
Boron composite
Adhesive
0.005 in. (0.013 cm)

5 in. (12.7 cm)

Ti-6A1-4V,
condition III

Typical step 0.0055 in. (0.014 cm) thick
(see table 6 for length)
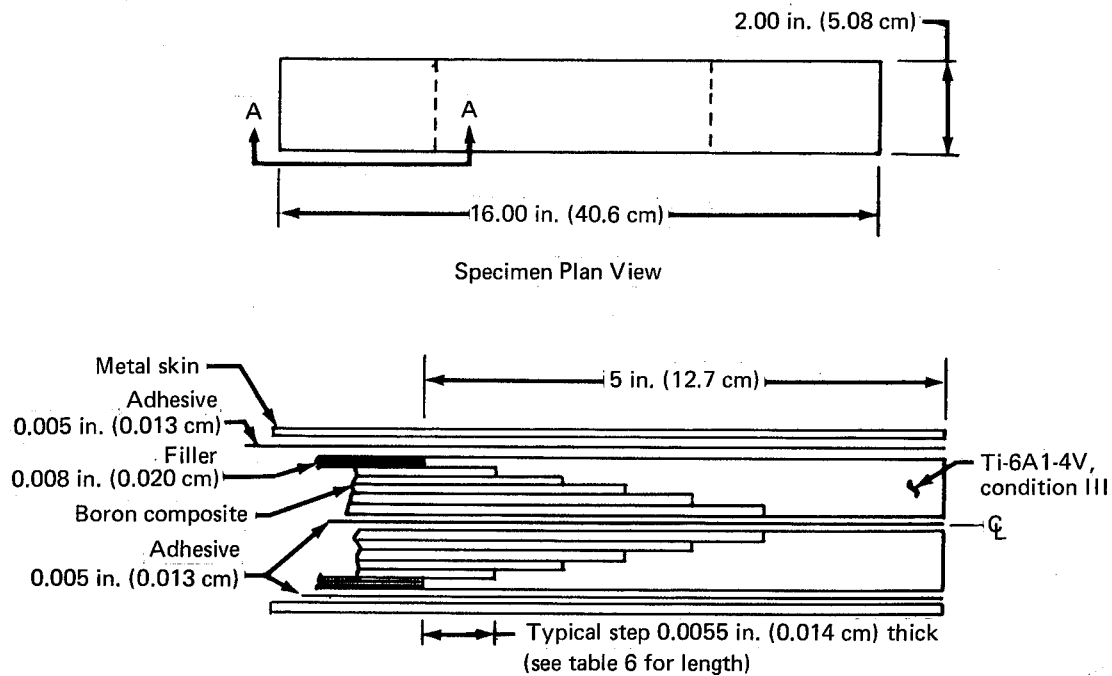
A-A
(Typical Section Through Transition Region)
FIGURE 15.—TRANSITION REGION TEST SPECIMEN CONFIGURATION
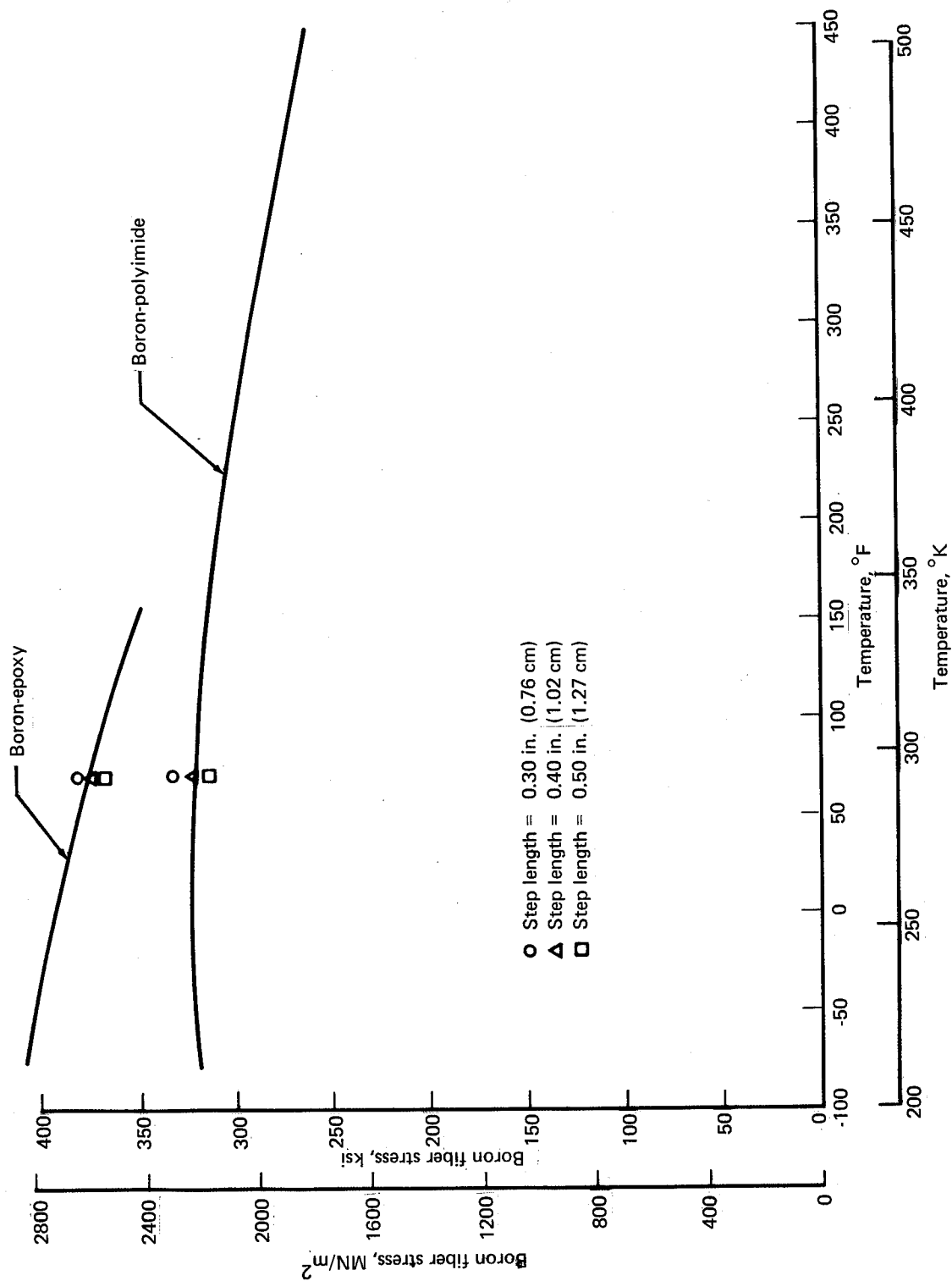
FIGURE 16.—INFLUENCE OF TEST TEMPERATURE ON AVERAGE BORON FILAMENT TENSILE STRESS AT FAILURE IN LOAD TRANSFER SPECIMENS
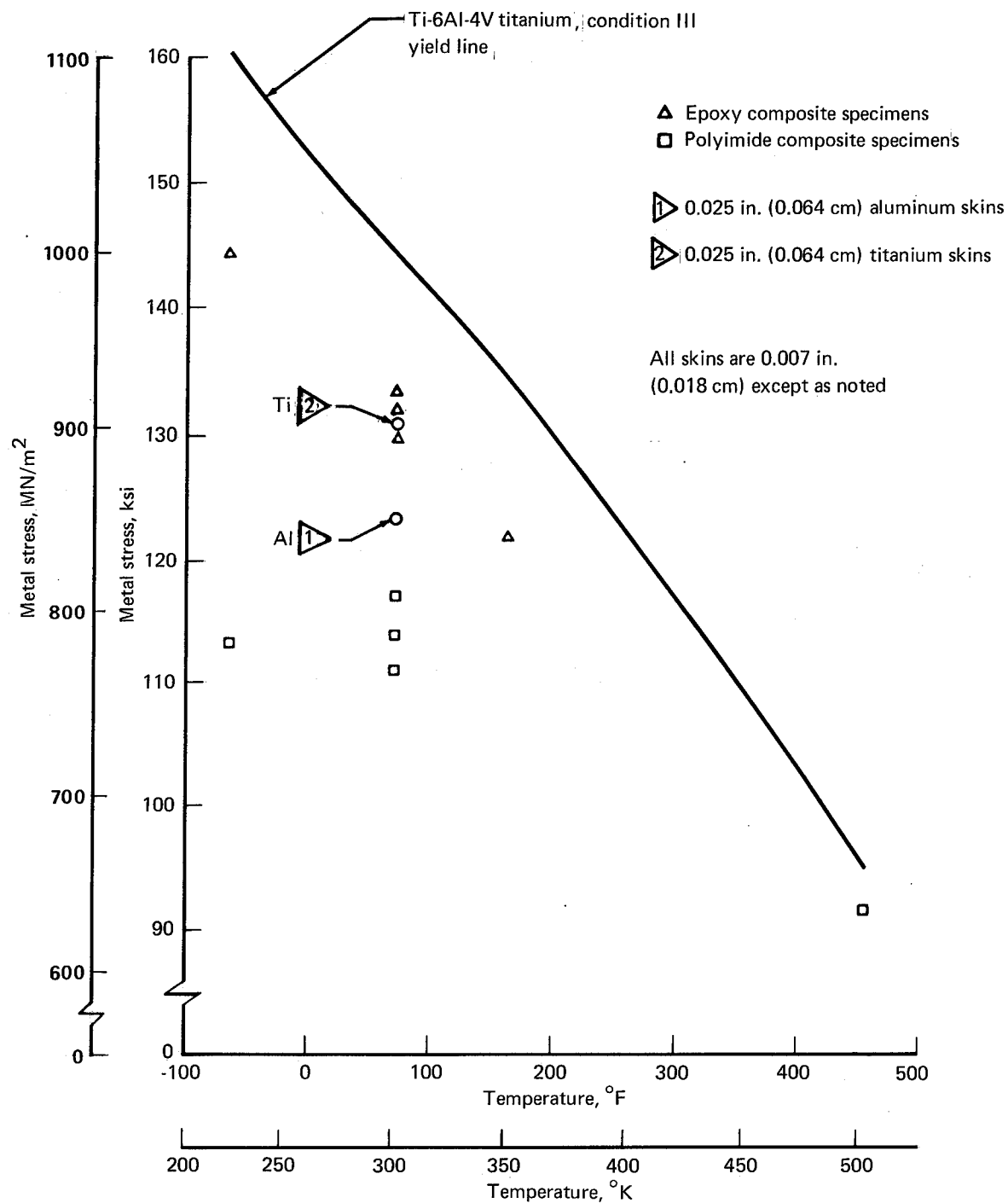
FIGURE 17.—MAXIMUM TITANIUM FITTING TENSILE STRESSES
ATTAINED AT TEMPERATURES TESTED
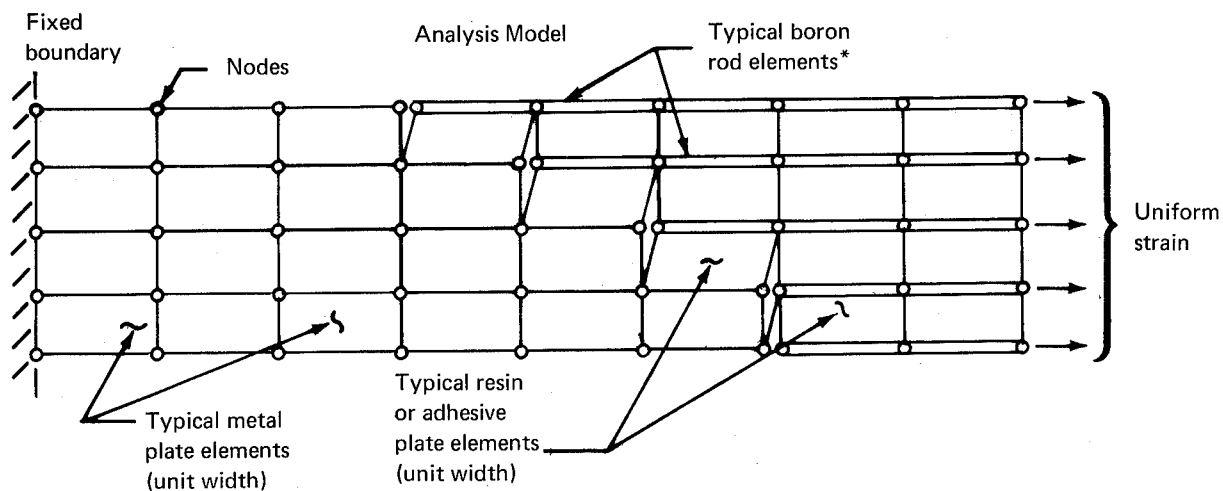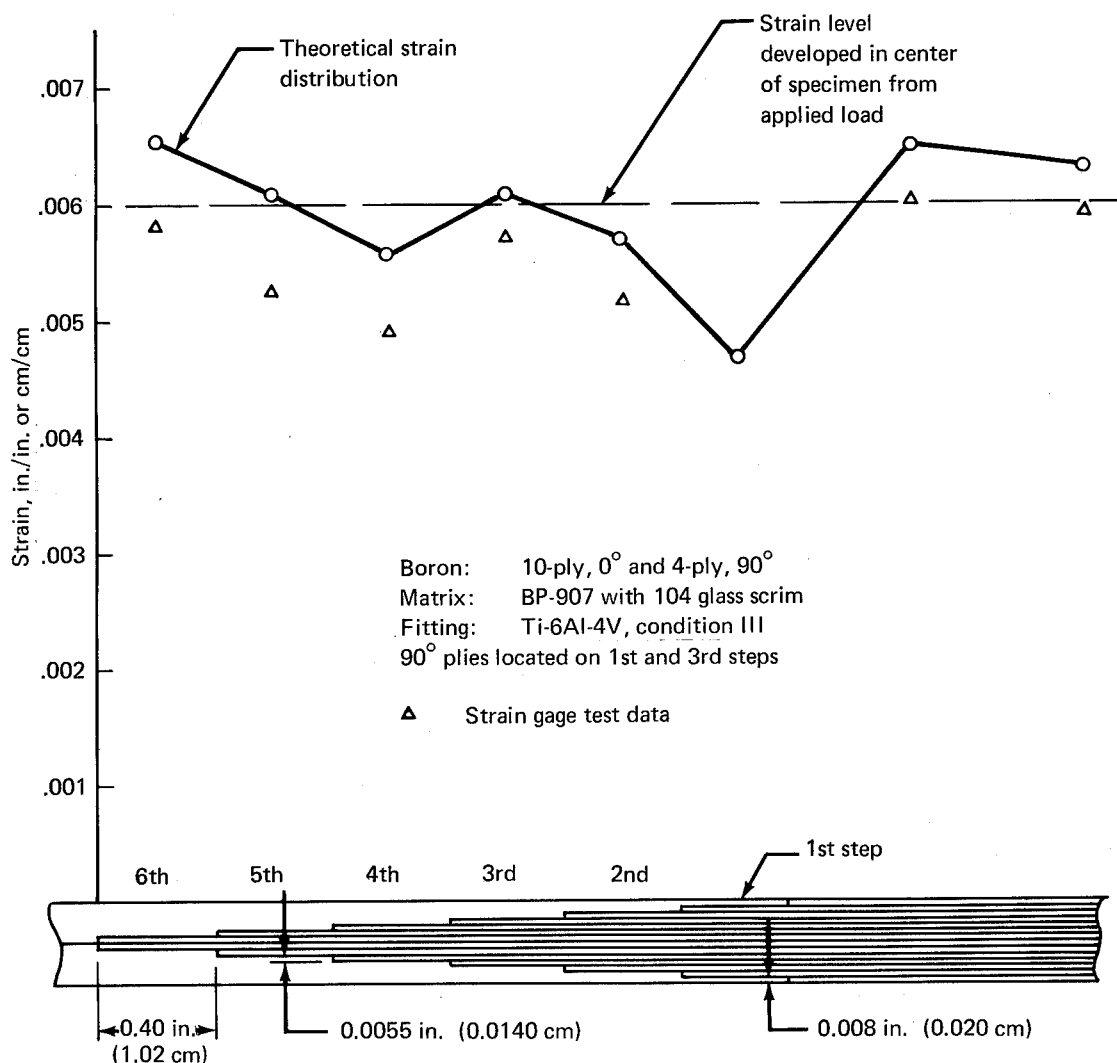
FIGURE 18.—STEP JOINT STRAIN DISTRIBUTION
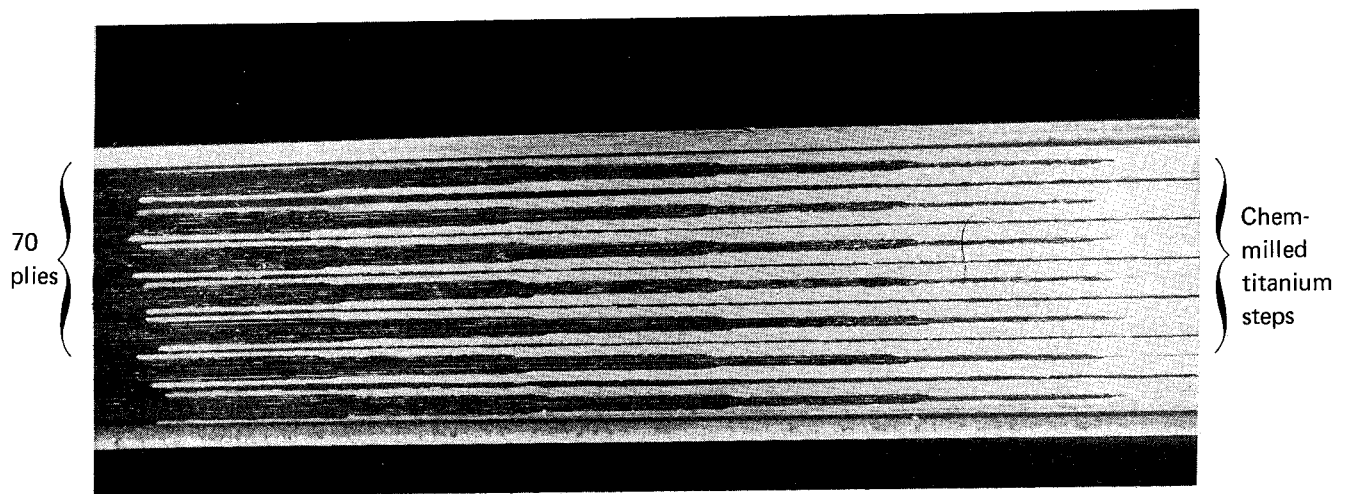
FIGURE 19.—70-PLY LOAD TRANSITION

70 plies

Chem-milled titanium steps

COMPRESSION STRESS-STRAIN

Objective

The objectives of this phase of the program were to determine the compressive stress-strain response and Poisson's ratio of boron composite reinforced metal.

Approach

The approach selected for this investigation was to predict, and then verify by test, the elastic modulus of boron composite combined with metallic face sheets. The material combinations evaluated were aluminum-boron-epoxy, titanium-boron-epoxy, and titanium-boron-polyimide. In addition, the effects of temperature and metal skin thickness were examined.

Test Specimens

The test specimens selected were metal/boron-composite-faced honeycomb core columns, as shown in figure 20. Titanium step transitions were provided at each end of each boron composite face skin to ensure uniform filament loading. A relatively large specimen was selected to provide appreciable composite cross-sectional area and a gaging zone well away from regions with boundary effects.

Testing and Results

The specimens were tested in compression between parallel plates. All specimens had an axial strain gage bonded to each face. In addition, an extensometer with a 4-in. (10.16-cm) gage length was also employed. Two specimens were tested at each test condition. Half of these specimens had transverse strain gages on each face for Poisson's ratio determination (see fig. 21 for a typical test setup). All failures occurred in the load transfer region (fig. 22).

The elastic modulus of each specimen was predicted using the constituent materials properties shown in table C-3 of appendix C and the calculation method shown in appendix D. The specimen elastic modulus obtained from the tests was computed using the linear portion of the load strain results from each face. The indicated face strains were averaged to correct for bending, but bending was significant in only a few tests. These averaged results agreed with the extensometer results with only one exception. In that test, conducted at 450° F (505° K), the strain gage data were 34% higher than the extensometer data, and it was concluded that the extensometer slipped. The predicted modulus values and the test results are summarized in table 7. Typical load/strain curves are shown in figure 23.

Discussion

Predicted and measured modulus values agreed very well, as shown in table 7. The maximum deviation of the test results from the predicted values was 7%.

The effect of temperature on modulus is shown in figure 24. Predicted modulus values are shown as solid lines and compared with test data. Specimen modulus was not significantly affected by temperature over the range of temperatures examined. In all cases, the test values at room temperature were lower than predicted.

Tests were also conducted to evaluate the thickness of the metal sheathing skin on the effective modulus of the reinforced skins. These results are shown in figure 25, where test moduli are compared to predicted moduli. Again, general agreement between predictions and test results was achieved.

The results from each strain gage and extensometer were examined for indications of yielding. In all tests where aluminum face sheets were employed, the ultimate strain exceeded 0.005, and many exceeded 0.006. In no case was there a pronounced specimen yield point, and in four of the 14 tests, strain was linear to the ultimate load.

Previous work performed by Zender and Dexter (ref. 3) also showed that compression yield strains of composite-reinforced aluminum occur beyond the compression yield strain of the metal itself. The aluminum sheathing is in a state of tension due to bonding to the composite at the elevated cure temperature of the adhesive. This effect provides an increased elastic range in compression.

Similarly, the group of specimens having titanium face sheets showed no distinct proportional limit, and four of 10 tests were linear to failure. Secant modulus at failure (ultimate stress divided by ultimate strain) was computed for each specimen and compared to the elastic modulus. The maximum variation between these moduli was 4.5%.

The values of Poisson's ratio, tabulated in table 7, were somewhat higher than anticipated. It was suspected that the honeycomb core cells acted as small truss structures and affected these results. To evaluate this hypothesis, a specimen having 0.025-in. (0.06-cm) aluminum face skins and 8.1 lb/ft^3 (0.131 g/cm^3) honeycomb core (no composite) was tested. The measured value of Poisson's ratio for the specimen was 0.398 compared to 0.33 for sheet aluminum, thereby substantiating that honeycomb does influence transverse strains in compression-loaded sandwich construction.

Conclusions and Recommendations

The elastic compression stress-strain response of boron-composite/metal systems may be predicted within 7% to 10% using a simple transformed area approach and typical material properties. The compression strengths attained in this portion of the program were limited by failures in the stepped load transfer region at boron filament stresses of approximately 350 ksi (2413 MN/m^2) for epoxy systems and approximately 160 ksi (1103 MN/m^2) for the polyimide systems.

Measured Poisson's ratios were somewhat higher than anticipated. The honeycomb core in the test specimens apparently contributed to this behavior. Additional investigation in this area is recommended.

TABLE 7.–COMPRESSION STRESS-STRAIN PREDICTIONS AND TEST DATA

Specimen	Metal skin, in.	Adhesive layers	Filler plies and composite matrix	Honeycomb core	Test temp		Predicted modulus		Test modulus, avg		Poisson's ratio
					°F	°K	ksi × 10³	MN/m² × 10³	ksi × 10³	MN/m² × 10³	
6A	0.006 Al	AF 126	BP 907	Aluminum	70	294	19.6	135	18.3	126.1	0.490
6B	0.012 Al	AF 126	BP 907	Aluminum	70	294	18.4	127	17.5	120.6	0.403
					165	330	18.1	125	17.3	119.2	0.400
					-65	219	18.5	127.5	18.2	125.3	0.375
6C	0.012 Ti	AF 126	BP 907	Aluminum	70	294	20.0	138	19.0	131	0.396
6D	0.025 Al	AF 126	BP 907	Aluminum	70	294	16.6	114.2	15.7	108.2	0.380
					165	330	16.4	113	16.3	112.2	0.381
					-65	219	16.8	116	17.1	118	0.375
6E	0.012 Ti	FM 34	35-520	Polyimide	70	294	20.4	140.8	19.8	136.5	0.347
					-65	219	21.0	145	21.2	146	0.332
					450	506	19.8	136.5	20.6	142	0.344
6F	0.025 Ti	FM 34	35-520	Polyimide	450	506	18.6	128.1	18.7	129	0.306

1.00 in.
(2.54 cm)

4.00 in.
(10.2 cm)

Titanium
step joint

Spacer

A

2.00 in.
(5.08 cm)
spacer
length

5.00 in.
(12.7 cm)
transition
length

20.00 in.
(50.8 cm)

0.50 in.
(1.27 cm)
(typ)

Sym
C L

A

Metal skin
Adhesive
Filler
Composite
Adhesive
Honeycomb

A-A
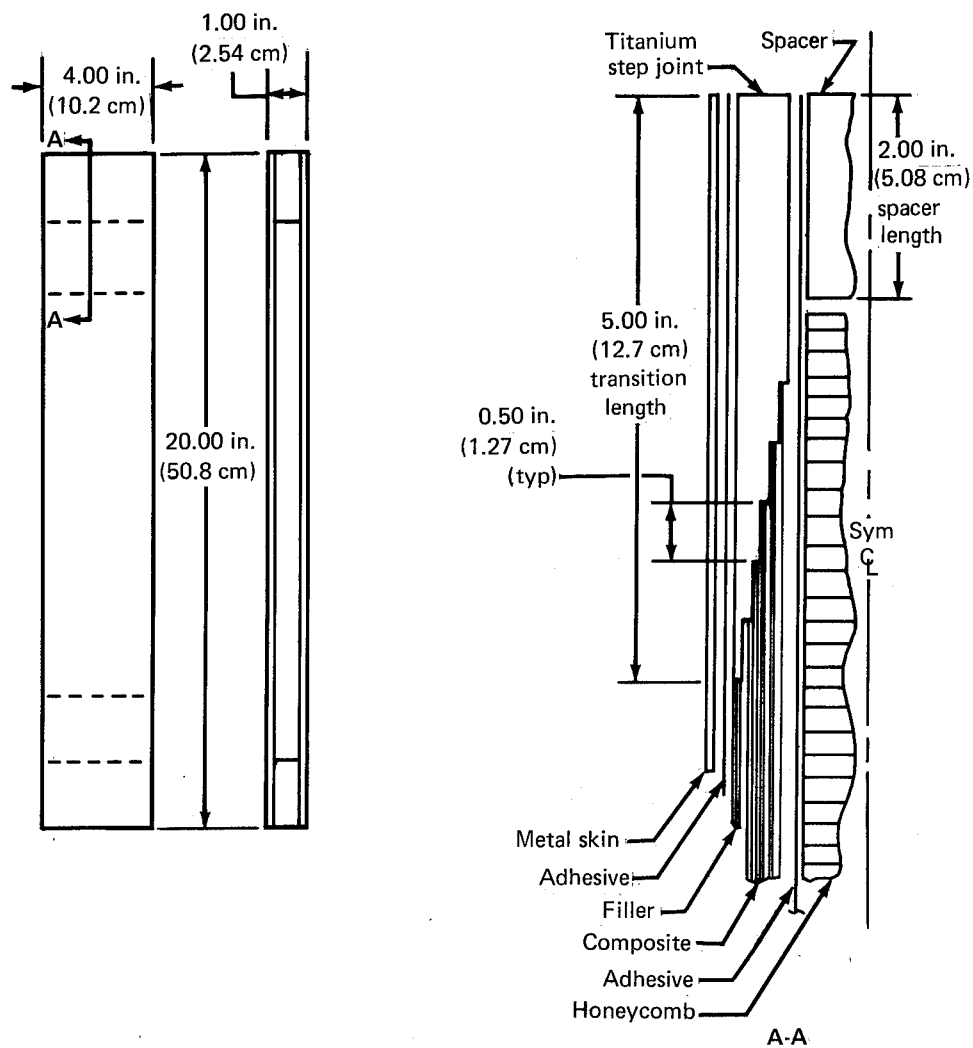
FIGURE 20.—COMPRESSION STRESS-STRAIN SPECIMENS
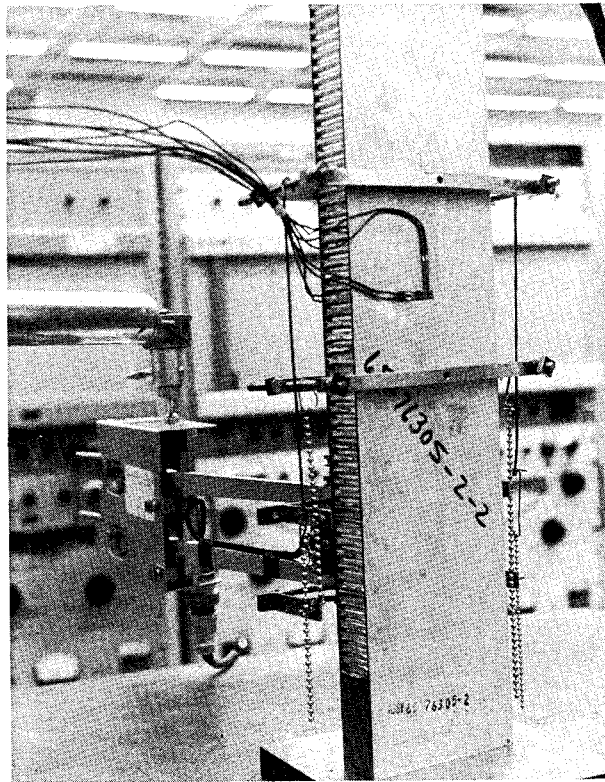
FIGURE 21.—COMPRESSION STRESS-STRAIN TEST SETUP (TYPICAL)
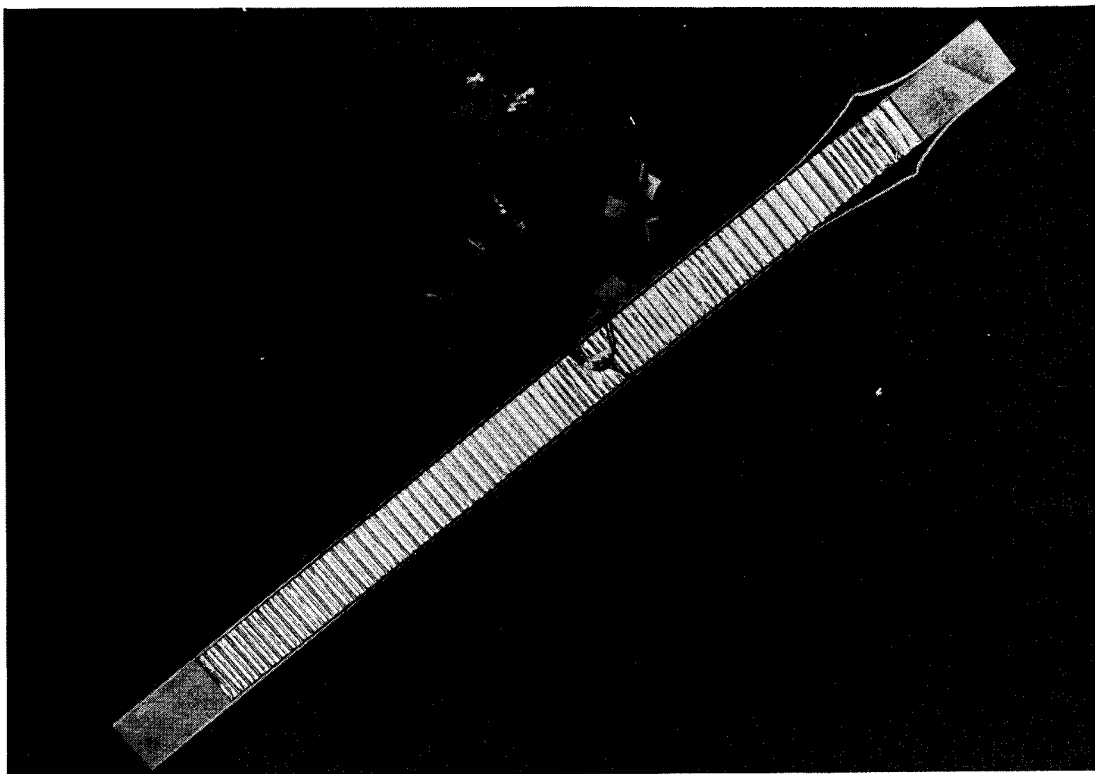
FIGURE 22.—COMPRESSION STRESS-STRAIN FAILURE (TYPICAL)
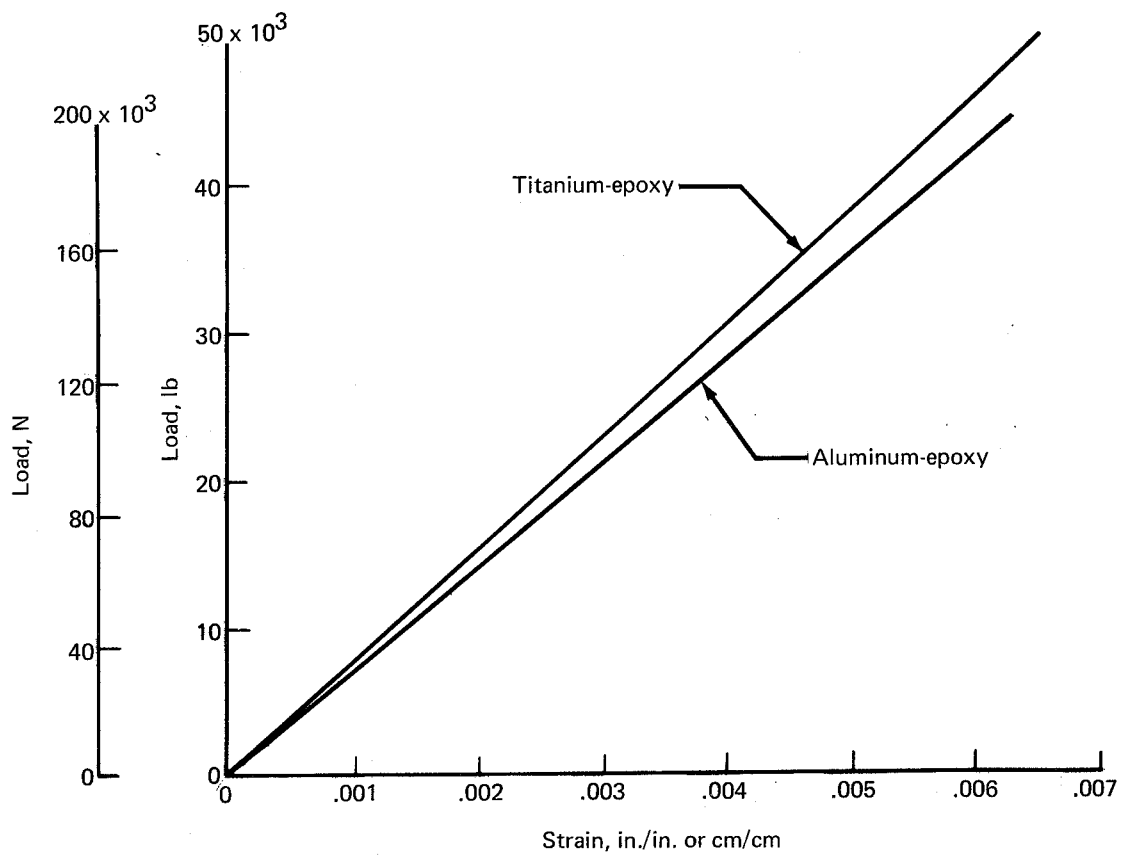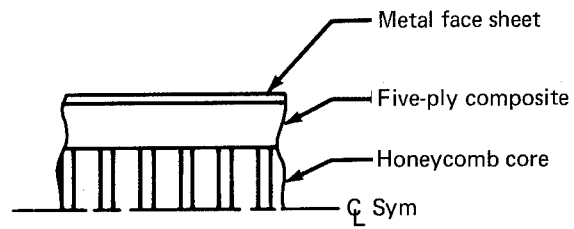
FIGURE 23.—TYPICAL COMPRESSION LOAD-STRAIN RESULTS (ROOM TEMPERATURE)
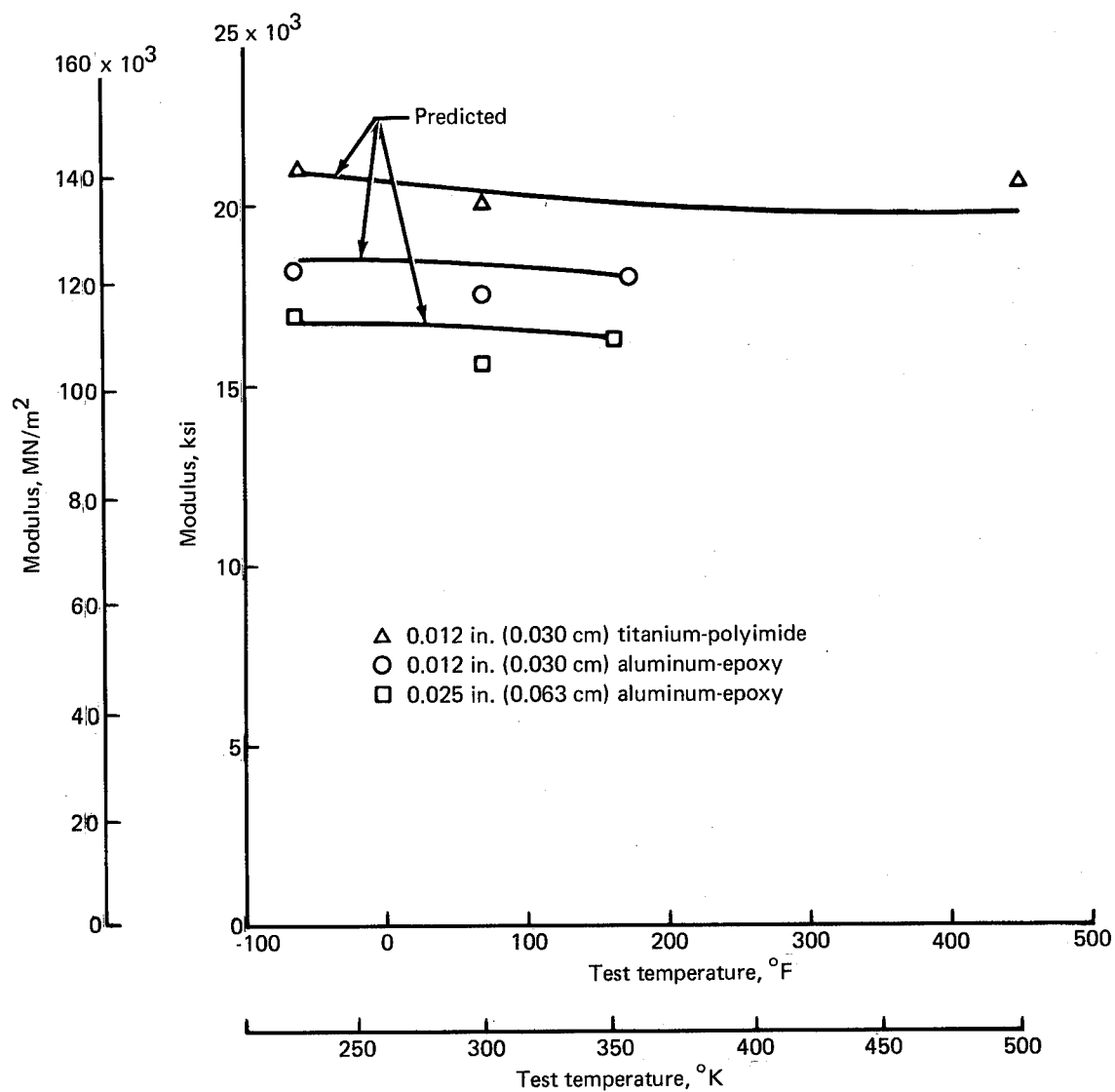
FIGURE 24.—INFLUENCE OF TEMPERATURE ON THE COMPRESSION
MODULUS OF COMPOSITE METAL SYSTEMS
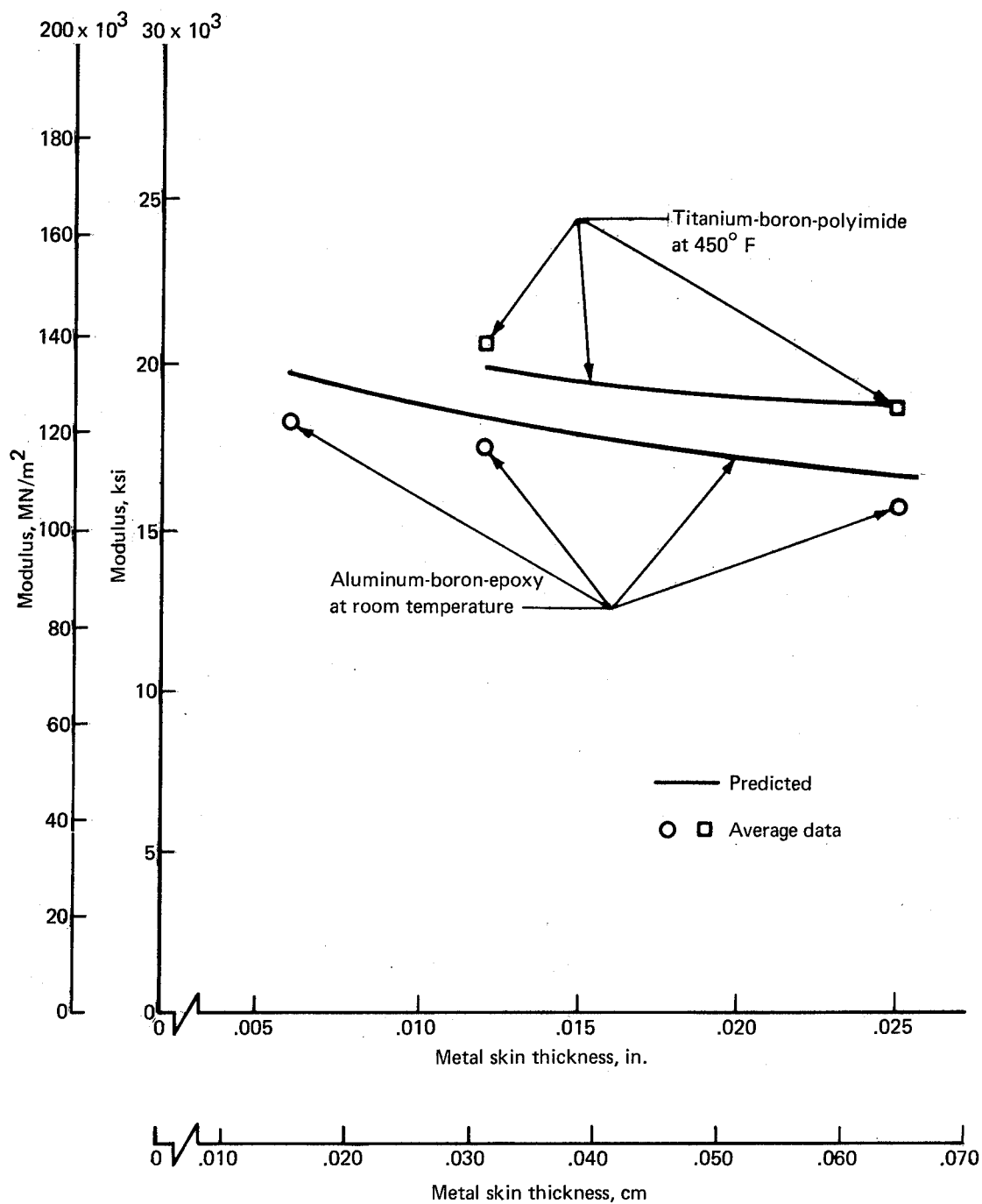
FIGURE 25.—VARIATION OF COMPRESSION MODULUS WITH METAL SKIN THICKNESS

PLATE BENDING

Objective

The objective of this portion of the program was to determine the bending response of metal plates reinforced with composites.

Approach

One of the basic elements that must be understood for the analysis and design of composite-reinforced metal construction is a simple plate in bending. Titanium plates were reinforced with different amounts of boron-epoxy composites. Some of these plates were tested in bending with the titanium in compression, and others were tested with the titanium in tension. Plots of center span deflection, as a function of load, were generated during the tests. Theoretical deflections were calculated and compared with the test results in the elastic regions. These comparisons were used to establish the theoretical capability of predicting the bending stiffness of the reinforced plates.

Test Specimens

Specimens fabricated for test in this category consisted of titanium plates reinforced with unidirectional boron-epoxy composites. Three plies of BP-907 were placed on the bond side of the composite to simulate filler plies that would normally be used in conjunction with stepped transition regions. Epon 927 was used to assemble the composite to the titanium. A detailed description of the three groups of specimens fabricated is shown in figure 26 and table 8.

Testing and Results

Six specimens of each type were tested in bending. Three were tested with the titanium in compression and three were tested with the titanium in tension. All specimens were loaded in a manner that produced principal curvature in the filament direction.

The specimens were tested in four-point bending in the fixture shown in figure 27. The reaction points were 3.5 in. (8.89 cm) apart. The load was applied equally at two points that divided the span into three equal 1.166-in. (2.96-cm) parts. All specimens were tested until load-center span deflection plots indicated a failure had occurred. Table 9 shows the 500-lb (2224 N) load-deflection data. Table 10 shows failure load, component stresses, and failure modes.

Discussion

Theoretical deflections were calculated at a load of 500-lb (2224 N) and compared to the test deflection at this loading. At this loading, all the materials were well within their elastic range, thereby permitting the use of standard beam equations for the analysis.

An average of five measurements was used to establish the thickness of each specimen. Thickness variations between specimens were assumed to be caused by bond-line variations. The composite beam was then transformed into an equivalent all-titanium beam by varying the constituent material areas by the ratio of their moduli of elasticity to that of titanium. The section properties of the transformed beam sections were then used in conjunction with the modulus of elasticity of titanium to find the theoretical deflections by use of the following equation (assumed plate bending effects would be insignificant):

$$\text{Center Span Deflection} = 0.03549 \frac{Ps^3}{E_{Ti} I_{\text{Transformed Beam}}}$$

A comparison of the theoretical and test center span deflections is shown in table 9. The average deviation equaled +3.1% and ranged from +9.9% to -8.8%. These results are of the same order that can be expected with homogeneous materials and are well within the limits imposed by the accuracy to which the specimens and data could be measured. Specimen 7A2 can be used to illustrate the sensitivity of the data to the specimen geometry. This specimen showed the greatest deviation between experimental and theoretical predictions. The thickness varied by +0.001 in. (0.00254 cm). If the thickness of this specimen was lowered one thousandth to 0.095 in. (0.241 cm), which was within the measured spread, the resulting error would be lowered from 9.9% to a more than acceptable 1.4%.

The specimens were tested to failure and the resulting maximum stresses are summarized in table 10. All stresses were calculated using elastic beam analysis and, in some cases, may be unrealistically high. The plate deflection curves plotted during testing, as well as the apparent stresses calculated at maximum loads, showed that the titanium had yielded. In general, the boron fiber stresses obtained were acceptable. In the few instances where low failure stresses were encountered, a bond failure was indicated. The shear stresses developed in the bond interface were as high as could be expected. In general, failure occurred after metal yielding was experienced, which is consistent with all-metal bonded construction.

Conclusions

The bending stiffness of composite-reinforced metal plates can be accurately established with relatively simple procedures, such as transformation to an equivalent one-material plate, by using constituent areas and moduli. After being transformed, simple beam relationships can be used to accurately predict bending deflections.

TABLE 8.—PLATE ELEMENT BEND SPECIMEN DATA

Specimen	Titanium thickness		Adhesive	Filler	Composite
	in.	cm			
7A	0.020	0.0508	1-ply Epon 927	3-ply BP-907	12-ply boron BP-907
7B	0.032	0.0812	1-ply Epon 927	3-ply BP-907	10-ply boron BP-907
7C	0.040	0.0816	1-ply Epon 927	3-ply BP-907	8-ply boron BP-907

TABLE 9.—PLATE ELEMENT BEND SPECIMEN DEFLECTION DATA AT 500-LB (2220-N) LOAD

Specimen	Average thickness		Test deflection		Calculated deflection		Percent deviation[a]
	in.	cm	in.	cm	in.	cm	
7A1	0.096	0.244	0.137	0.348	0.1244	0.3160	9.2
7A2	0.096	0.244	0.138	0.351	0.1244	0.3160	9.9
7A3	0.096	0.244	0.154	0.391	0.1443	0.3665	6.3
7A4	0.092	0.234	0.157	0.399	0.1434	0.3642	8.7
7A5	0.095	0.241	0.137	0.348	0.1359	0.3452	0.8
7A6	0.095	0.241	0.133	0.338	0.1359	0.3452	-0.2
7B1	0.095	0.241	0.135	0.343	0.1281	0.3254	5.1
7B2	0.095	0.241	0.142	0.361	0.1281	0.3254	9.8
7B3	0.095	0.241	0.134	0.340	0.1281	0.3254	4.4
7B4	0.095	0.241	0.130	0.330	0.1227	0.3117	5.6
7B5	0.097	0.246	0.125	0.318	0.1227	0.3117	1.8
7B6	0.091	0.231	0.149	0.378	0.1451	0.3686	2.6
7C1	0.092	0.234	0.127	0.323	0.1392	0.3536	-8.8
7C2	0.094	0.239	—	—	—	—	—
7C3	0.095	0.241	0.128	0.325	0.1269	0.3223	0.9
7C4	0.096	0.244	0.122	0.310	0.1250	0.3175	-2.4
7C5	0.096	0.244	0.115	0.292	0.1250	0.3175	-8.0
7C6	0.096	0.244	0.135	0.343	0.1250	0.3175	7.4

[a]Average = + 3.1

TABLE 10.–STRESS AT FAILURE LOAD[a]

Specimen	Failure load		Boron stress[b]		Titanium stress[b]		Bond shear		Failure mode
	lb	N	ksi	MN/m^2	ksi	MN/m^2	ksi	N/m^2 x 10^4	
7A1	678	3017	320-T	2210-T	118-C	810-C	1654	1141	Composite tension failure
7A2	877	3903	414-T	2860-T	152-C	1050-C	2137	1474	Composite tension failure
7A3	828	3685	439-T	3030-T	150-C	1030-C	2065	1424	Composite tension failure
7A4	783	3484	434-C	2990-T	138-T	950-T	1886	1301	Excess metal yield plus composite compression failure
7A5	1200	5340	609-C	4200-C	218-T	1500-T	3048	2102	Excess metal yield plus composite compression failure
7A6	1210	5385	614-C	4230-C	220-T	1520-T	3073	2119	Excess metal yield plus composite compression failure
7B1	880	3916	417-T	2880-T	155-C	1070-C	3009	2075	Bond failure
7B2	745	3315	354-T	2440-T	131-C	900-C	2585	1783	Composite tension failure
7B3	590	2626	280-T	1930-T	104-C	720-C	2017	1391	Bond failure
7B4	1105	4917	512-C	3530-C	180-T	1240-T	3463	2388	Composite compression failure
7B5	875	3894	401-C	2770-C	149-T	1030-T	2924	2017	Bond failure
7B6	640	2848	333-C	2300-C	118-T	810-T	2246	1549	Bond failure
7C1	808	3596	403-T	2780-T	150-C	1030-C	3204	2210	Composite tension failure
7C2	440	1958	210-T	1450-T	79-C	540-C	1704	1175	Bond failure
7C3	764	3400	357-T	2460-T	134-C	920-C	2924	2017	Bond failure
7C4	921	4098	424-C	2920-C	158-T	1090-T	3478	2399	Bond failure
7C5	867	3858	399-C	2750-C	149-T	1030-T	3274	2258	Bond failure
7C6	702	3124	323-C	2230-C	120-T	830-T	2654	1830	Bond failure

Note: All stresses are calculated using elastic beam theory.

T = tension, C = compression.

46

Fiber
←—direction—→

2.00 in. (5.08 cm)

4.00 in.
(10.16 cm)

— Titanium
— Adhesive
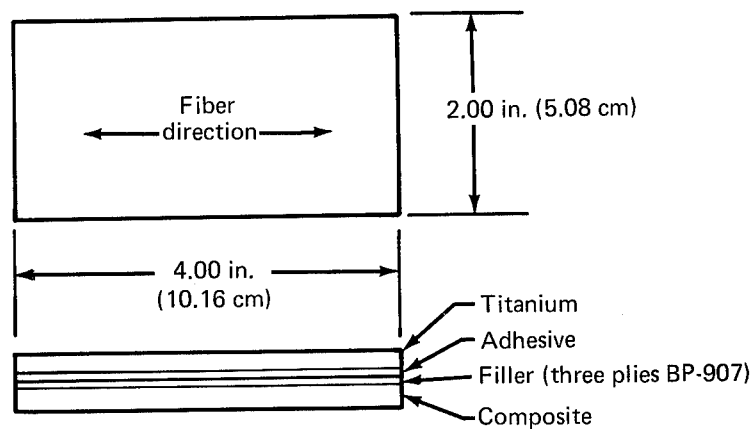— Filler (three plies BP-907)
—Composite

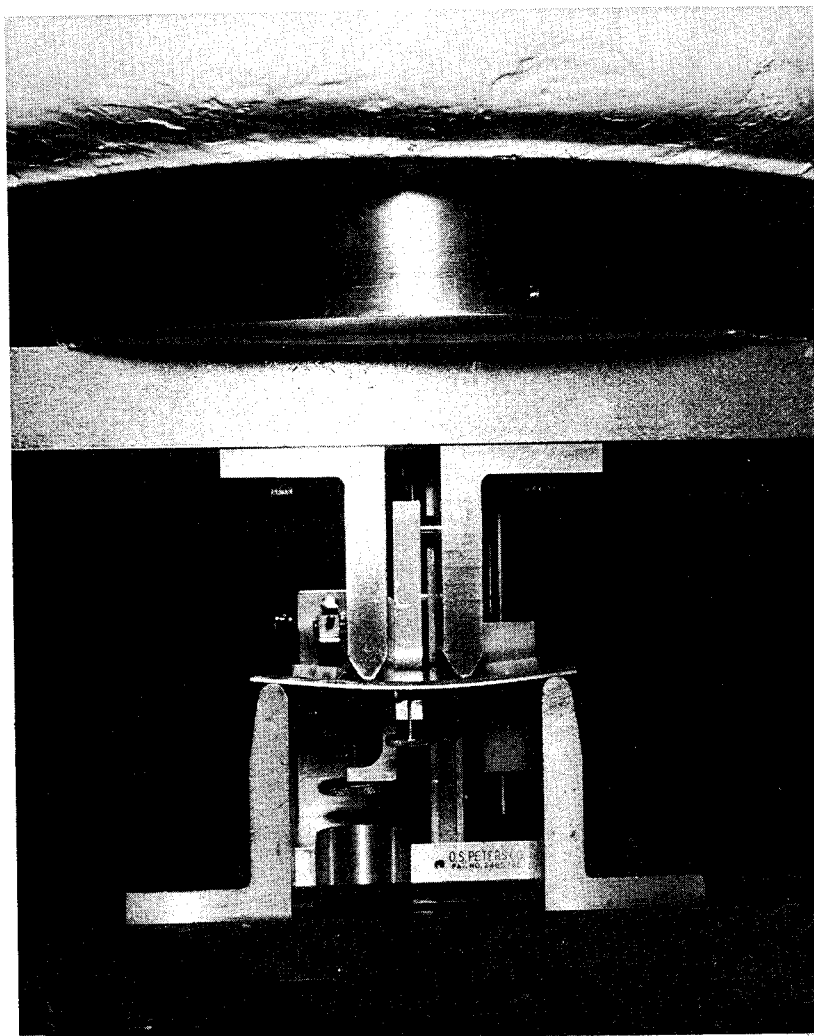FIGURE 26.—TYPICAL PLATE ELEMENT BEND SPECIMEN

FIGURE 27.—PLATE BEND SPECIMEN TEST

PLATE BUCKLING

The following is a preliminary summary of the plate buckling work. Under a contract modification, a buckling analysis for anisotropic layered plates and plate sections is being developed, and the final results are expected to be published in a separate document when complete (ref. 5).

Objective

The objective of this work was to investigate the buckling characteristics of flat metal plates reinforced with composites. This work included both experiments and theoretical analysis development. The test data were used as a base for evaluating the capability of the plate buckling prediction techniques.

Approach

Flat titanium plates reinforced with unidirectional boron-epoxy laminates were prepared. The variables that were incorporated included metal thickness, degree of reinforcement, and symmetrical versus unsymmetrical material distribution. These plates were placed in a test jig that provided clamped conditions at the loaded ends and simple or free boundary conditions at the sides, as required. Compression testing was performed in a 120 kip (5.34×10^5 N) Universal testing machine. Theoretical predictions were then compared with the test data.

Test Specimens

Eight specimen designs were made. Half were symmetrically laminated (composite on both sides of titanium plate) and half were unsymmetrically laminated (composite on one side of titanium plate). They were sized to provide a test section of 3.00 in. (7.62 cm) by 9.00 in. (22.86 cm). Additional length was added to facilitate the incorporation of stepped transition regions at the ends.

The metal plates were all 6Al-4V titanium. The laminates were made from boron/BP-907 composites and also incorporated chem-milled stepped titanium transition regions at the ends. The metal and composites were assembled with a room temperature curing adhesive to eliminate distortion. A summary of the plate designs is shown in figure 28 and table 11.

Testing and Results

Forty-eight plate specimens were tested. These were tested with the loaded edges clamped and with the sides either free or simply supported. Where simply supported sides were employed, knife-edge supports were installed and a feeler gage was used to ensure that proper contact was made with the test panels. The test sections measured 9.0 in. (22.86 cm) in length between clamps and 2.98 in. (7.57 cm) in width between knife edges. A typical test setup is shown in figures 29 and 30.

In-plane shortening versus load curves were developed during tests. The critical buckling loads of the plates tested with knife-edge side supports were determined from these curves. Slope lines representing the effective moduli of the plates were superimposed on the test curves. The point at which the test curves deviated from the theoretical slope lines was used to determine the critical load for each plate. The plates tested with their sides free were loaded until their load curves reached a maximum. These loads were used as the critical buckling loads.

The test data were reduced and the critical loads established. Figures 31 and 32 show a summary of these buckling test data and a comparison with theoretical calculations. In addition, the test data are tabulated in table 12.

Discussion

Initially, it was intended to use the RA5 program to develop our theoretical plate buckling predictions. Because of usage problems encountered with this program (repeatability, reliability), it was decided to develop a new analytical program. An important feature of this new analysis is that it represents an "exact" solution for a multilayered plate with unsymmetric lamination. It treats extensional but not shear coupling between bending and extension. A general description of this program follows.

The total potential energy of the flat plate is formulated in terms of the in-plane displacements u and v, the lateral displacement w, and the external loading. The equilibrium equations and corresponding consistent boundary conditions are obtained from the minimization of the total potential energy. The displacement functions assume two opposing edges of the plate to be simply supported. The boundary conditions on the other two edges will be satisfied in the buckling formulation.

These displacement functions, when substituted into the equilibrium equations, yield the characteristic polynomial equation of eighth order. There will be a set of roots from this characteristic equation corresponding to each level of applied load. Each set of roots, along with the displacement equation, can be used to formulate the eight boundary conditions of the remaining two edges. This results in a set of eight homogeneous equations. The buckling load is obtained from these equations by determining the minimum values of the applied load for which the determinate of the coefficients matrix becomes zero.

The critical buckling loads of the plates established by test were compared with theoretical predictions. A summary of these comparisons is shown in table 12 and in figures 31 and 32. The error between theory and test averaged 13.2% for the plates tested with knife-edge side supports. The error between theory and test averaged 19.7% for plates tested with their sides free.

The above results are based on attaining perfect boundary conditions during tests. In actuality, the attainment of these perfect conditions is difficult to establish and undoubtedly represents a source of a portion of the error attained in the previous correlations. A study was made, therefore, in which the effective length of the plate specimens was modified to reflect nonattainment of perfect clamping at the ends during test. First, it was determined that, based on a perfect match between the test results obtained from the clamped-free specimens and theory, an average end-fixation factor of 3.48 was developed. This factor was then used to modify the effective length of the plates from 9.0 to 9.62 in. $[9(4.0/3.48)^{1/2} = 9.62]$. Based on this modified length, the errors of correlation were recalculated and showed significant improvement. The average errors for both symmetrical and

unsymmetrical clamped-simple specimens were reduced to 6.7%, for the unsymmetrical clamped-free specimens to 8.7%, and for the symmetrical clamped-free specimens 13.6%.

Conclusions

Clamped-clamped/simple-simple (CC/SS) plate buckling.—The average error in predicting the buckling load of the 12 test specimens of unsymmetrically laminated plates with CC/SS constraints is 12.7%. The average error for the 12 tests of the symmetrically laminated plates was 13.6%.

Clamped-clamped/free-free (CC/FF) plate buckling.—The average error of prediction for the 11 unsymmetrically laminated plates is 17.6% and for the 12 symmetrically laminated plates was 21.8%.

An analysis of the test data strongly indicates that a portion of the error between theory and test was due to nonattainment of perfect clamping at the ends of the plates. When modifications are used in the analysis, which reflect boundary conditions indicated by results are significantly improved. The effect of varying the metal thickness and degree of reinforcement was not significant, based on the small amount of test data.

TABLE 11.—PLATE ELEMENT SPECIMEN SIZES AND LAMINATIONS

Specimen	Layup type	Length in.	Length cm	Composite	Filler	Adhesive	Metal, in.	Adhesive	Filler	Composite
								Specimen layup sequence		
8A	Unsymmetrical	14.60	37.08	12-ply	BP-907	Epon 927 933	0.020 Ti	–	–	–
8B		13.80	35.05	10-ply	BP-907	Epon 927 933	0.032 Ti	–	–	–
8C		13.00	33.02	8-ply	BP-907	Epon 927 933	0.040 Ti	–	–	–
8D		12.20	30.98	6-ply	BP-907	Epon 927 933	0.050 Ti	–	–	–
8E	Symmetrical	12.20	30.98	6-ply	BP-907	Epon 927 933	0.020 Ti	Epon 927 933	BP-907	6-ply
8F		12.20	30.98	5-ply	BP-907	Epon 927 933	0.032 Ti	Epon 927 933	BP-907	5-ply
8G		11.40	28.95	4-ply	BP-907	Epon 927 933	0.040 Ti	Epon 927 933	BP-907	4-ply
8H		12.20	30.98	3-ply	BP-907	Epon 927 933	0.050 Ti	Epon 927 933	BP-907	3-ply

TABLE 12.—PLATE BUCKLING DATA

Specimen	Layer thicknesses, in.							CC/SS				CC/FF		
	Composite	Adhesive	Titanium	Adhesive	Composite	Total	Specimen	P(ult), lb	Pcr, lb	Error, %	Specimen	P(ult), lb	Error, %
							Unsymmetrical specimens[a]						
8A	—	—	0.0195	0.0185	0.0650	0.103	-1	24 000	11 700	- 0.1	-4	2010	-22.1
	—	—	0.0195	0.0195	0.0650	0.104	-2	21 900	11 750	- 1.7	-5	2065	-21.2
	—	—	0.0195	0.0125	0.0650	0.097	-3	15 900	9 000	-11.7	-6	2335	+ 6.5
8B	—	—	0.0317	0.0166	0.0557	0.104	-1	17 600	11 000	-14.6	-4	3150	+10.4
	—	—	0.0317	0.0176	0.0557	0.105	-2	16 400	11 475	-13.5	-5	3040	+11.4
	—	—	0.0317	0.0156	0.0557	0.103	-3	17 920	9 600	-22.5	-6		
8C	—	—	0.0340	0.020	0.047	0.101	-1	14 300	11 000	- 4.8	-4	2160	-18.1
	—	—	0.0340	0.019	0.047	0.100	-2	15 800	9 600	-14.3	-5	2120	-17.5
	—	—	0.0340	0.019	0.047	0.100	-3	11 520	8 200	-36.6	-6	2060	-20.9
8D	—	—	0.0504	0.0171	0.0375	0.105	-1	16 900	12 900	- 5.6	-4	2490	-20.1
	—	—	0.0504	0.0181	0.0375	0.106	-2	17 940	12 300	-13.4	-5	2525	-21.7
	—	—	0.0504	0.0181	0.0375	0.106	-3	18 000	12 300	-13.4	-6	2480	-29.0
							Symmetrical specimens[b]						
8E	0.0332	0.0107	0.0232	0.0107	0.0332	0.111	-1	12 260	11 490	-10.5	-4	5140	+11.9
	0.0332	0.0122	0.0232	0.0122	0.0332	0.114	-2	14 600	12 075	-12.6	-5	4340	-12.0
	0.0332	0.0122	0.0232	0.0122	0.0332	0.114	-3	13 080	10 680	-27.4	-6	3880	-25.3
8F	0.0274	0.01825	0.0327	0.01825	0.0274	0.124	-1	19 180	15 840	- 4.1	-4	3660	-53.7
	0.0274	0.01625	0.0327	0.01625	0.0274	0.120	-2	14 840	11 520	-32.8	-5	3900	-32.9
	0.0274	0.01575	0.0327	0.01575	0.0274	0.119	-3	15 880	12 210	-22.9	-6	4200	-21.0
8G	0.0232	0.02055	0.0395	0.02055	0.0232	0.127	-1	16 500	15 525	- 7.7	-4	4640	-18.4
	0.0232	0.01955	0.0395	0.01955	0.0232	0.125	-2	16 880	14 220	-13.6	-5	6360	+16.8
	0.0232	0.01605	0.0395	0.01605	0.0232	0.118	-3	16 080	13 410	- 6.3	-6	4600	- 0.1
8H	0.0168	0.0127	0.0530	0.0127	0.0168	0.112	-1	20 740	11 880	- 9.2	-4	2800	-26.8
	0.0168	0.0147	0.0530	0.0147	0.0168	0.116	-2	20 360	12 780	- 7.6	-5	2900	-31.9
	0.0168	0.0132	0.0530	0.0132	0.0168	0.113	-3	21 660	12 075	- 9.0	-6	3260	-11.1

[a]Unsymmetrical specimen average error: CC/SS = 12.7%; CC/FF = 17.6%

[b]Symmetrical specimen average error: CC/SS = 13.6%; CC/FF = 21.8%

Transitions

3.00 in. (7.62 cm)

9.00 in. (22.86 cm)

L

Plan View

Filler
Composite
Filler
Adhesive
Metal
Adhesive
Filler
Composite
Filler

Unsymmetrical specimen

Symmetrical specimen

Section View of Transition

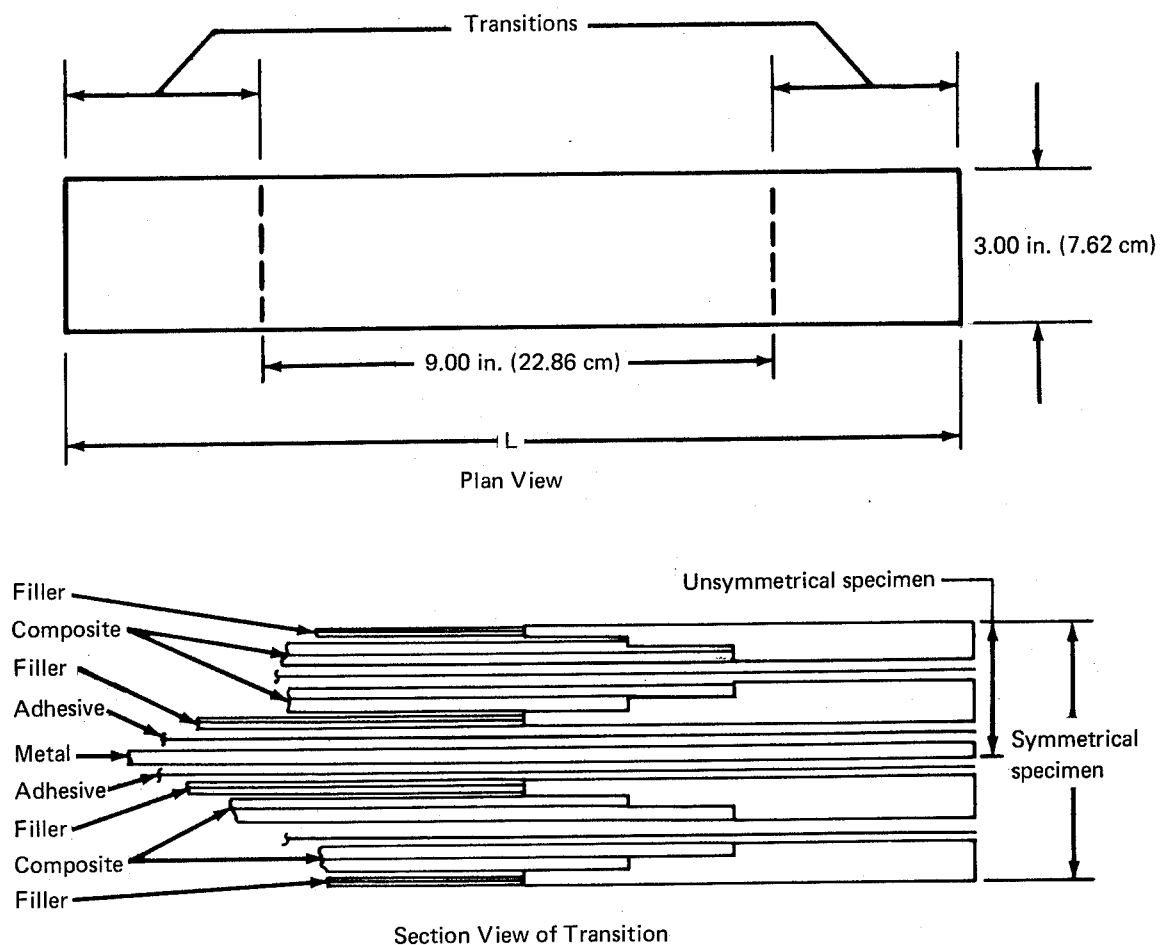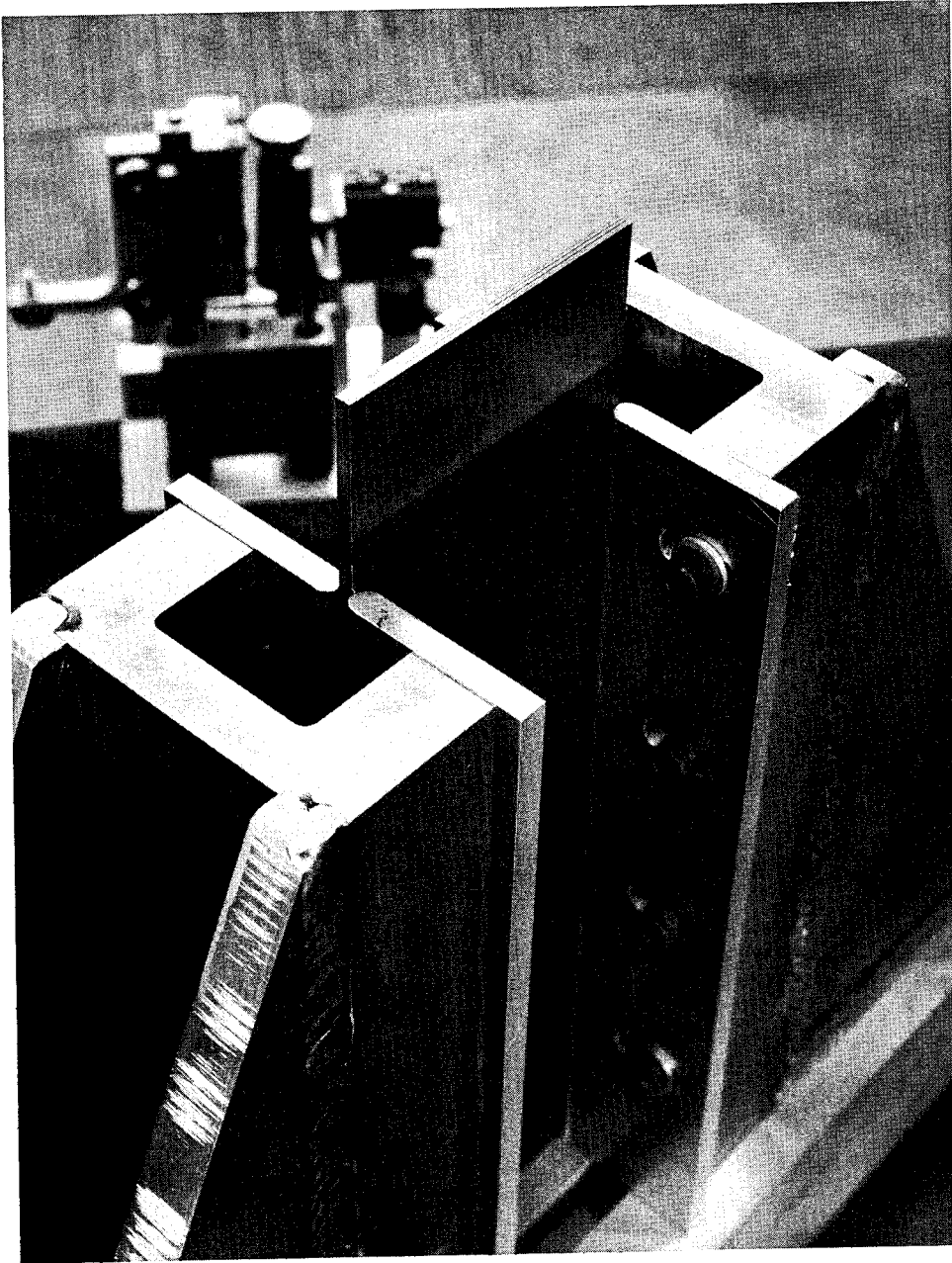FIGURE 28.—PLATE ELEMENT BUCKLING SPECIMENS

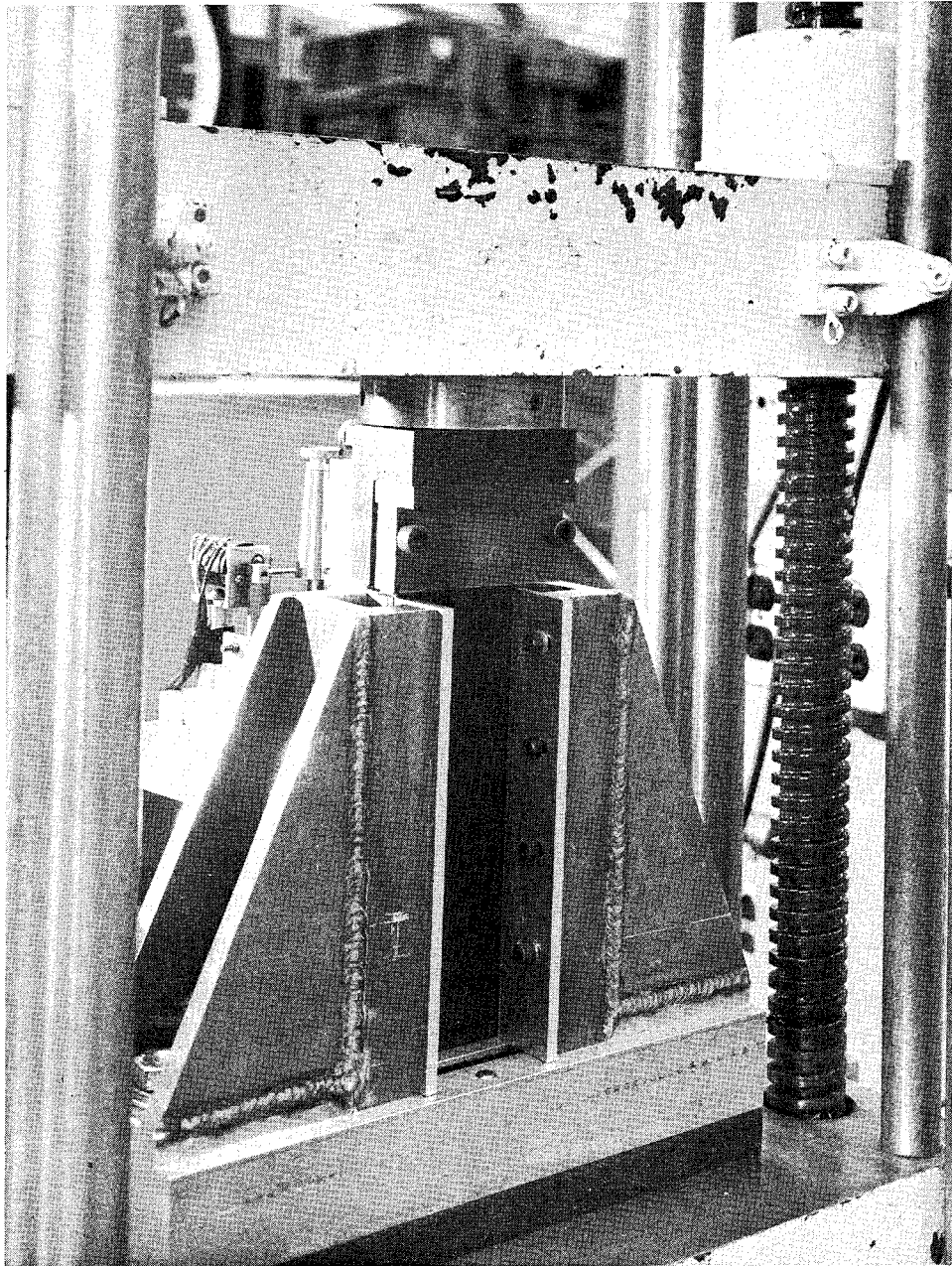FIGURE 29.—PLATE BUCKLING TEST FIXTURE
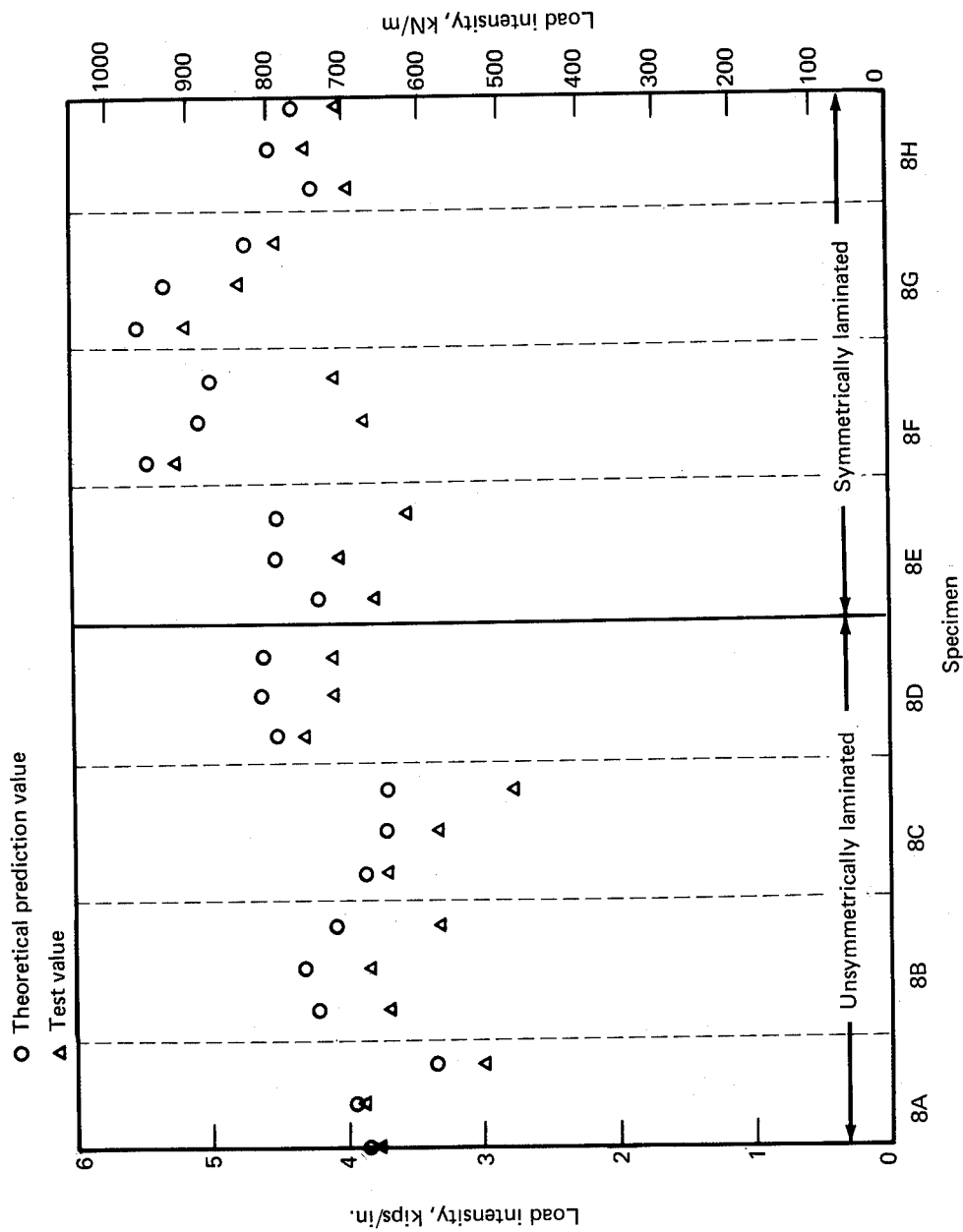
FIGURE 30.—PLATE BUCKLING SPECIMEN TEST SETUP

FIGURE 31.—COMPARISON OF THEORETICAL AND TEST BUCKLING LOADS FOR
COMPOSITE PLATES WITH CLAMPED, LOADED EDGES AND
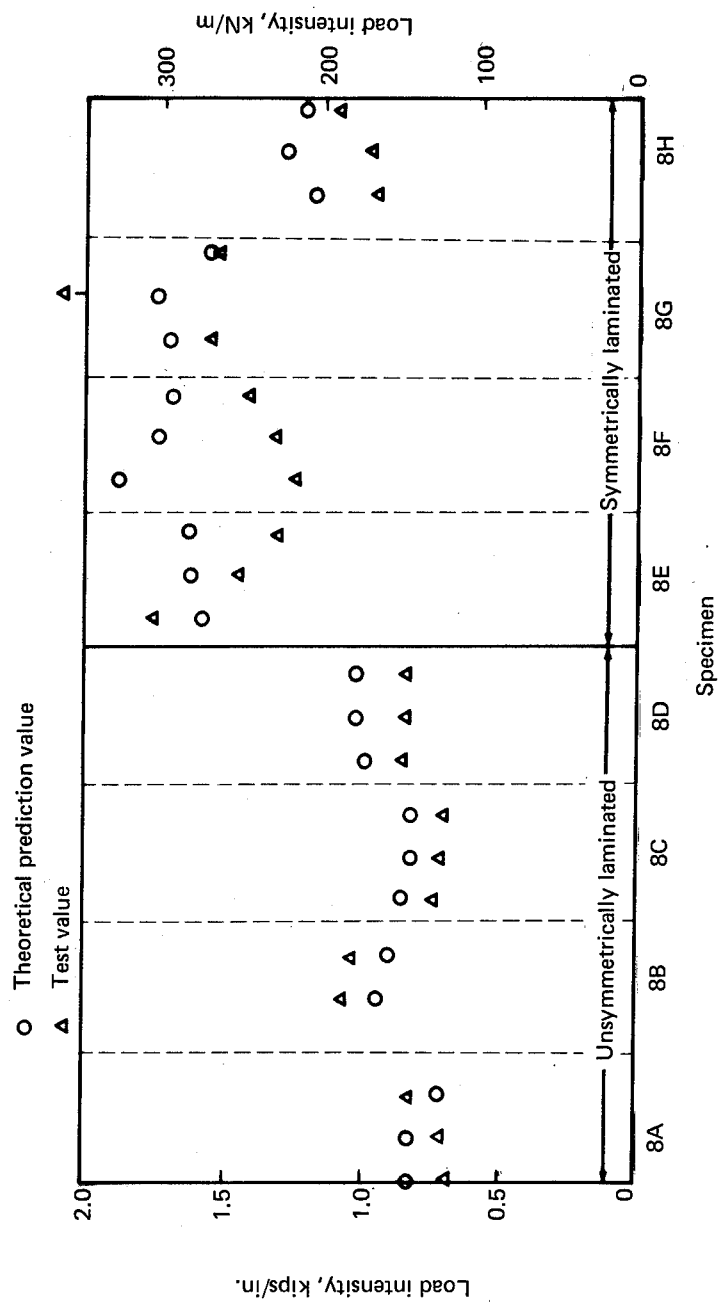SIMPLY SUPPORTED, UNLOADED EDGES

FIGURE 32.—COMPARISON OF THEORETICAL AND TEST BUCKLING LOADS FOR COMPOSITE PLATES WITH CLAMPED, LOADED EDGES AND FREE, UNLOADED EDGES

COLUMN CRIPPLING AND BUCKLING

Objective

The objective of this portion of the investigation was to establish the feasibility of reinforcing metal structural shapes with composites. The following represents a summary of the experimental investigations performed in this category. Under a contract modification, an analysis of the reinforcement of structural shapes is being developed. The experimental data presented in this report will establish a base for evaluating the analytical prediction techniques that will be published in final form under the contract modification (ref. 5).

Approach

Several composite-reinforced metal test specimens were fabricated and tested in compression to investigate various structural shapes with various degrees of reinforcement. These shapes included angles, zees, hats, and tees. The geometries, metal thicknesses, and amounts of composite reinforcement were varied to evaluate their impact on the structural capabilities of the reinforced structural shapes.

Three specimens of each type were tested in compression. The test data obtained included both the buckling load and the ultimate load for each specimen. Specimens of different lengths were tested to obtain both crippling and column buckling data.

The test data will also be used to determine the effectivity of predicting the column behavior using a new analysis being developed under a contract modification. These results will be published in final form in a separate report.

Test Specimens

The reinforced specimen configurations fabricated and tested consisted of angles, zees, hats, and tees. All of the specimens, except the formed tees, incorporated 6Al-4V titanium as the metal portion of the specimen. The formed tees incorporated 7075-T6 aluminum. All the reinforcements consisted of unidirectional boron BP-907 composites.

The reinforcements were flat laminates with titanium end fittings in all specimens except the formed tees. These laminates were made up as a single sheet adequate for providing the reinforcements for a complete set of specimens. This sheet was then machined into straps of the proper width as required by the specimens. The straps were then assembled to the titanium by bonding with an Epon 927/Epon 933 adhesive system that was cured at room temperature under vacuum for 48 hr and then postcured at 140° F (333° K) for 5 hr.

The reinforcement for the formed tee consisted of boron/BP-907 cylindrical rods. These rods were fabricated by rolling the uncured tape into a cylinder that was then encased in a shrink tube and cured. The rods were then assembled with the aluminum formed section by bonding with Epon 933 using the above cure cycle.

The specimen cross-section details are shown in figure 33. The lengths were varied to obtain both crippling and column buckling data and are summarized in table 13. Typical completed specimens are shown in figures 34, 35, and 36.

Testing and Results

The specimens were loaded in compression to failure in a Universal testing machine. During testing, a load-versus-specimen shortening curve was developed for each specimen. A theoretical slope line, based on the cross-sectional areas and properties of the materials used in each specimen, was superimposed on the elastic portion of the curves. The point at which the test curves changed slope significantly and deviated from the theoretical slope line was used to establish the crippling or buckling load (P_{cr}) for the specimens.

The results obtained from testing the composite-reinforced structural shapes are summarized in table 13.

Discussion

The composite-reinforced structural shapes failed in a manner similar to that observed in all-metal sections. In general, failures were initiated when one of the outstanding legs became unstable because of combined compression and torsional loads. The specimens attained ultimate when excessive deformations resulting from the instability caused debonding between the laminates and the metal portions of the sections.

A study performed under a contract modification on plate buckling illustrates the importance of using the unidirectional composites in a manner that will minimize the effect of its low torsional stiffness. In this work, the buckling loads of two plates of equal weight and having the same overall thickness were compared. The cross-sectional areas of both plates were equally divided between titanium and unidirectional composites. In the first plate, the titanium was sandwiched between composite laminates of equal thickness. In the second plate, the composite was sandwiched between two equal thicknesses of titanium.

The theoretical buckling loads were determined for plates with the above construction and boundary conditions approaching that of an outstanding leg of a structural shape. The ends of the plates were simply supported, one side was simply supported, and the other side was free.

The buckling load of the plate with the titanium on the outside was 69% greater than the plate with the composite on the outside. Also, when comparing the plate with the titanium on the outside with an all-titanium plate of the same thickness, its buckling load was within 94%. Since this plate was much lighter than the all-titanium plate, it proved to be 29% more efficient.

Conclusions

The relatively low torsional stiffness of unidirectional composites restricts their effective use as reinforcement for torsionally unstable configurations.

60

TABLE 13.—REINFORCED STRUCTURAL SHAPES—TEST RESULTS

Configuration	Specimen	Length		P_{ult} test		P_{cr} test		ϵ_{cr}, in./in. or cm/cm x 10^{-6}
		in.	cm	lb	kN	lb	kN	
Angle	9A-1	12.00	30.5	8 040	35.76	3 300	14.67	702
	9A-2	12.00		8 660	38.52	3 400	15.12	723
	9A-3	12.00		8 380	37.27	3 600	16.01	765
	9A-4	12.00		8 420	37.45	3 700	16.45	787
	9A-5	20.00	50.8	4 500	20.01	2 300	10.23	484
	9A-6	20.00		6 800	30.24	2 450	10.89	521
	9A-7	20.00		6 600	20.01	2 300	10.23	484
	9B-1	13.60	34.5	11 240	49.99	5 800	25.79	844
	9B-2	13.60		10 040	44.66	4 800	21.35	699
	9B-3	13.60		9 140	40.65	6 000	26.68	874
	[a]9B-4	8.85	22.5	26 200	116.54	26 200	116.54	3814
	[a]9B-5	3.34	8.45	16 300	72.50	16 300	72.50	2373
Zee	9C-1	13.60	34.5	27 700	123.21	20 500	91.18	2232
	9C-2	13.60		27 500	122.32	17 000	75.61	1851
	9C-3	13.60		26 800	119.21	22 000	97.86	2395
	9D-1	12.00	30.5	11 240	49.99	5 800	25.79	938
	9D-2	12.00		10 040	44.66	4 600	20.46	744
	9D-3	12.00		9 140	40.65	5 850	26.02	946
	9D-4	12.00		9 260	41.19	5 600	24.91	906
	9D-5	20.00	50.8	12 200	54.26	4 700	20.90	760
	9D-6	20.00		11 300	50.26	5 200	23.13	841
	9D-7	20.00		11 480	51.06	5 100	22.68	825
Hat	9E-1	13.60	34.5	32 200	143.23	29 000	128.99	4707
	9E-2	13.60		30 500	135.67	25 000	111.20	4058
	9E-3	13.60		33 300	148.12	30 500	135.67	4951
	9F-1	12.80	32.5	3 840	17.08	2 600	11.56	939
	9F-2	12.80		3 700	16.45	3 400	15.12	1227
	9F-3	12.80		6 900	30.69	4 300	19.12	1552
Formed T	9G-1	6.00	15.2	20 300	90.29	16 500	73.39	3005
	9G-2	6.00		19 080	84.87	18 200	80.95	3315
	9G-3	6.00		20 120	89.49	13 000	57.82	2367
	9H-1	6.00	15.2	20 940	93.14	18 000	80.06	2898
	9H-2	6.00		21 300	94.74	19 200	85.40	3091
	9H-3	6.00		22 320	99.28	19 800	88.07	3188
Machined T	9I-1	10.00	25.4	38 000	169.03	31 000	13.78	4592
	9I-2	10.00		37 200	165.47	37 000	164.58	5481
	9I-3	10.00		38 600	171.70	37 250	165.69	5518
	9I-4	10.00		38 250	170.14	37 000	164.58	5481
	9J-1	9.20	23.4	11 040	49.10	3 100	13.78	1845
	9J-2	9.20		11 440	50.88	3 200	14.23	1904
	9J-3	9.20		10 260	45.63	3 200	14.23	1904

[a]Ends potted

			t	b	r
(9A)	8-ply,	in.	0.040	1.16	0.03
		cm	0.101	2.95	0.08
(9B)	12-ply,	in.	0.063	1.10	0.12
		cm	0.160	2.80	0.30

			t	b	r
(9C)	12-ply,	in.	0.063	1.10	0.12
		cm	0.160	2.80	0.30
(9D)	8-ply,	in.	0.040	1.16	0.08
		cm	0.101	2.95	0.20

			t	b_2	b_3	r
(9E)	12-ply,	in.	0.063	0.43	0.28	0.125
		cm	0.160	1.09	0.71	0.318
(9F)	5-ply,	in.	0.025	0.50	0.50	0.050
		cm	0.064	1.27	1.27	0.127

			t_1	t_2
(9I)	8-ply,	in.	0.063	0.125
		cm	0.160	0.308
(9J)	3-ply,	in.	0.025	0.050
		cm	0.064	0.127

(9G)   t = 0.012 (0.030 cm)
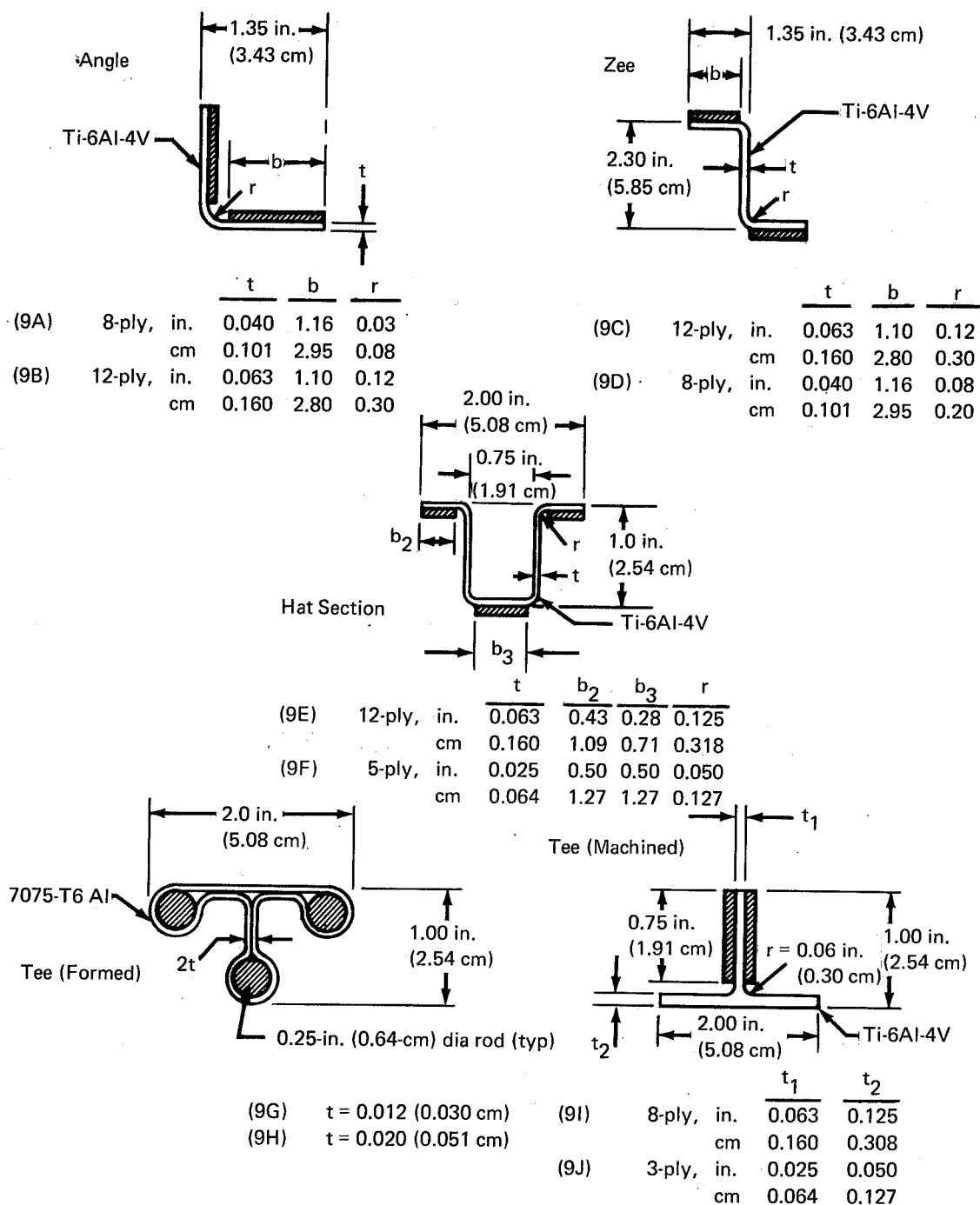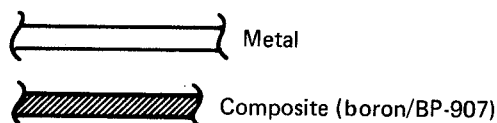
(9H)   t = 0.020 (0.051 cm)

FIGURE 33.—CROSS-SECTION GEOMETRIES OF COMPOSITE-REINFORCED STRUCTURAL SHAPES
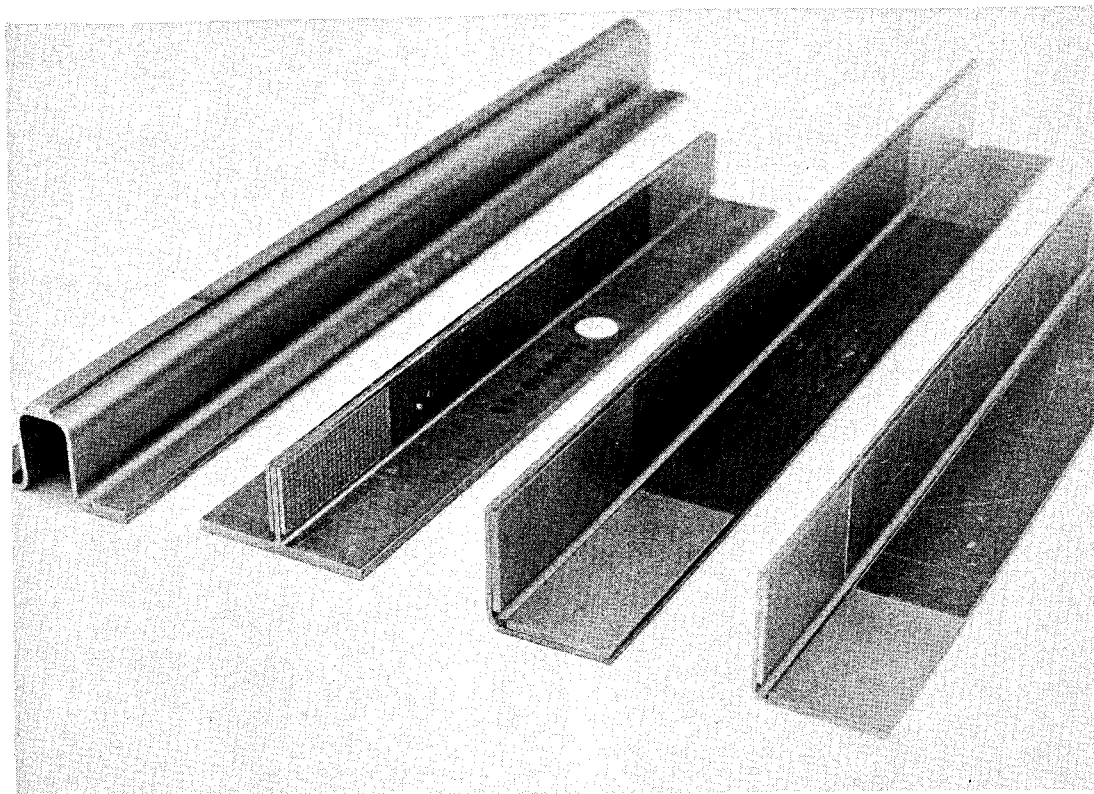
62

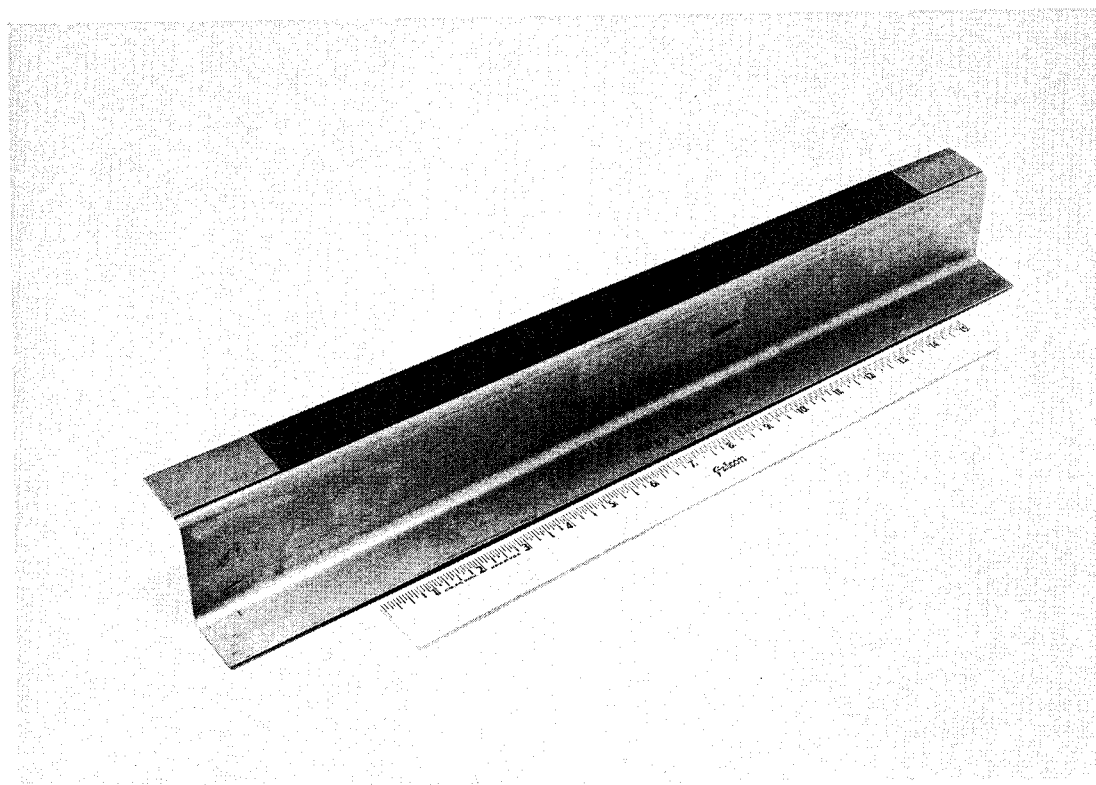FIGURE 34.—TYPICAL COMPOSITE-REINFORCED HAT, TEE, AND ANGLE SECTIONS

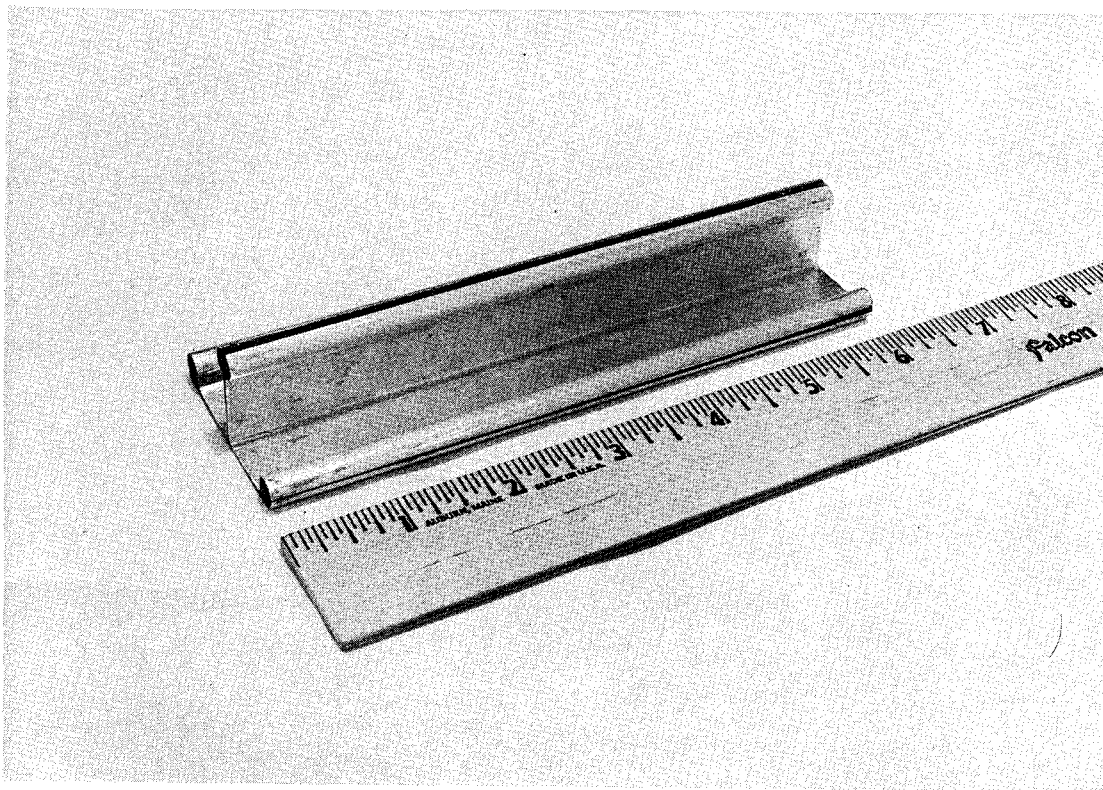FIGURE 35.—TYPICAL COMPOSITE-REINFORCED ZEE SECTION

FIGURE 36.—COMPOSITE ROD AND ALUMINUM TEE SECTION

SANDWICH WRINKLING AND BUCKLING

Objective

The objective of this portion of the program was to evaluate the compression capabilities of honeycomb sandwich assemblies incorporating boron-composite-reinforced metal skins.

Approach

Sandwich wrinkling and buckling specimens that incorporated several composite skin reinforcement concepts and a range of L/r values were fabricated and tested. The specimens having the larger L/r values were analyzed using conventional column equations. These analyses were compared with specimen test data to evaluate their capability for predicting the compressive structural behavior for this type of construction.

Test Specimens

Several test specimens were fabricated with various geometries and reinforcement concepts. The metal skins were reinforced uniformly with composite face plies, locally with composite straps, and with combinations of the two.

Test specimen descriptions are detailed in figure 37 and table 14. Typical fabricated wrinkling and buckling specimens are shown in figures 38 and 39, respectively.

Testing and Results

All of the sandwich panel specimens were tested in compression in a Baldwin Southwark test machine. The average cross-head motion rate was 0.02 in./min (0.051 cm/min). The test data recorded consisted of specimen shortening versus load to failure.

Table 15 summarizes the sandwich wrinkling test results. The ultimate strain was computed with an area that included transforming all reinforcing material to equivalent titanium. (See app. D.) The maximum step stresses, which were the primary cause of failure, occurred in the last step in the load transition region (see fig. 40 and table 15). Specimens 10C-1 and 10C-2 were initially rejected because of poor manufacturing quality. They were tested, however, and the failure mode consisted of the skin crippling at the ends of the specimens, well away from the poorly bonded area. It was concluded that the skins were not adequately supported at the specimen ends due to partial removal of the honeycomb cell walls during specimen machining. The replacement specimens, 10C-4 and 10C-5, had a small depth of core removed at the ends and replaced with a potting compound. These specimens failed at a higher load than those they replaced and in a mode consistent with the other specimen failures.

Table 16 summarizes the sandwich panel buckling tests. The ultimate loads shown were the maximum loads that the panels were able to sustain. The critical loads were obtained from the in-plane shortening versus load curves by selecting the load at which the curves deviated from a slope line established from the equivalent face sheet modulus.

Discussion

The 10A specimens represent a sandwich skin reinforcement concept in which the composite was uniformly distributed over the complete skin surface. These specimens failed at boron fiber stresses ranging from 384 ksi (2640 MN/m^2) to 395 ksi (2720 MN/m^2). These fiber stresses represent strain levels well beyond the magnitude that would have failed the 0.01-in. (0.025-cm) titanium metal skins themselves due to skin wrinkling. As little as two plies of boron-epoxy reinforcement would have prevented this mode of failure and permitted the 10-mil titanium skins to be stressed to yield.

Specimen failure initiated in the maximum stressed area in the last step of the transition fitting (see fig. 40). This location is critical because it represents the minimum effective cross-sectional area of structural material that carries the full specimen load. Stresses in this region attained levels of 155 to 160 ksi (1070 to 1100 MN/m^2), which are well beyond the 132-ksi (910-MN/m^2) compression yield of the titanium.

The 10B specimens incorporated the same uniform reinforcement as the 10A specimens, but, in addition, two 90° plies were added to each skin. This construction typified composite reinforcement for aircraft structure designed to carry biaxial loads. The metal transition region was thickened to accommodate the additional 90° plies thereby lowering the metal transition stresses at the same fiber stress levels attained in the 10A specimens. The 10B specimens reached maximum fiber stress between 453 ksi (3120 MN/m^2) and 487 ksi (3350 MN/m^2). The critical metal stresses attained in the steps were on the order of those attained in the 10A group.

The 10C specimens represented a configuration in which all the reinforcement was concentrated into discrete load paths. The failure modes shown in figure 41 indicated that the skins were not properly stabilized at the ends resulting in local crippling. The design was changed to incorporate potting compound in the ends to stabilize the skins. Specimens that incorporated this change, 10C-4 and 10C-5, tested higher than those they replaced and failed in a mode consistent with the bulk of the sandwich specimens.

The 10D specimens represented a concept that was a combination of 10A and 10C. In these 10D specimens, the reinforcement was evenly distributed, and some were placed in discrete load paths. Fiber stress levels ranged between 463 ksi (3190 MN/m^2) and 467 ksi (3210 MN/m^2). These specimens failed in the step transition region used in conjunction with the uniform reinforcement of the skin at a level beyond the compression yield of the titanium.

Specimens 10E through 10H represent sandwich compression concepts having L/r values in excess of 97.5. All of these specimens exhibited column behavior and failed elastically. A summary of the test data is shown in table 16 as are the predicted critical loads. The theoretical predictions were made using $\epsilon_{cr} = c\pi^2/(L/r)^2$ with a fixity factor of c = 3.5.

The critical strain versus L/r is plotted in figure 42. The test data correlate well with the theoretical predictions.

Conclusions

Stable concepts (wrinkling specimens) were investigated that developed fiber stress levels as high as 487 ksi (3350 MN/m^2). The full potential of each concept was limited by

the ultimate metal strain in the load transition areas. The reinforcement concept could be improved further by using a thicker stepped transition or a higher strength material in the load transfer region.

Analytical techniques are available for predicting buckling behavior of sandwich panels incorporating composite-reinforced metal concepts. The procedure used classic column equations in conjunction with transformed area techniques (app. D).

TABLE 14.—SANDWICH WRINKLING AND BUCKLING SPECIMEN DATA

Specimen	Reinforcing	Length		Width		Thickness		Composite face skin plies (each surface)	Strap plies (each strap)
		in.	cm	in.	cm	in.	cm		
10A	Skin	17.00	43.2	3.00	7.60	1.06	2.68	5 at 0°	
10B	Skin	17.00	43.2	3.00	7.60	1.09	2.76	5 at 0° 2 at 90°	
10C	Strap	22.00	55.8	6.00	15.20	1.02	2.58		10 at 0°
10D	Strap and skin	17.00	43.2	6.00	15.20	1.02	2.58	2 at 0°	5 at 0°
10E	Skin	27.00	68.5	3.00	7.60	0.56	1.43	5 at 0°	
10F	Skin	27.00	68.5	3.00	7.60	0.59	1.49	5 at 0° 2 at 90°	
10G	Strap	32.00	82.2	6.00	15.20	0.52	1.32		10 at 0°
10H	Strap and skin	32.00	82.2	6.00	15.20	0.52	1.32	2 at 0°	5 at 0°

TABLE 15.—SANDWICH WRINKLING TEST DATA

Specimen	Ultimate load		Ultimate strain, in./in. or cm/cm × 10^-6	Titanium stress		Boron stress		Max step stress		Remarks
	kips	kN		ksi	MN/m²	ksi	MN/m²	ksi	MN/m²	
10A-1	37.7	167	6450	105.7	728	387	2660	157.1	1080	Buckled at last step
10A-2	38.5	171	6583	108.0	744	395	2720	160.4	1100	Buckled at last step
10A-3	37.4	166	6400	104.9	722	384	2640	155.8	1070	Buckled at last step
10B-1	47.8	212	8122	133.1	917	487	3350	156.0	1070	Buckled at last step
10B-2	44.4	197	7544	123.7	852	453	3120	145.0	999	Buckled at last step
10C-1	36.2	160	5366	88.1	607	322	2210	100.8	694	Skin failed at end[a]
10C-2	39.2	174	5815	95.3	656	348	2390	109.2	752	Skin failed at end[a]
10C-3	34.0	150	5045	82.7	569	303	2080	94.7	650	Skin failed at end
10C-4	41.4	183	6136	100.7	692	368	2530	115.3	794	Buckled at last step[b]
10C-5	42.0	186	6226	102.2	704	373	2560	116.9	805	Buckled at last step[b]
10D-1	63.2	280	7710	126.4	870	463	3190	141.3	973	Failed at step in skin
10D-2	63.8	283	7783	127.6	879	467	3210	142.5	981	Failed at step in skin

[a]10C-1 and 10C-2 were rejected because of unacceptable quality; 10C-3, 10C-4, and 10C-5 were their replacements.

[b]Specimens had 0.5 in. of the core removed at the ends and replaced with potting to stabilize the skins.

TABLE 16.—SANDWICH BUCKLING TEST DATA

Specimen	Critical strain (test), in./in. or cm/cm x 10^{-6}	Critical load				Ultimate load (test)		Remarks
		Test		Calculated				
		kips	kN	kips	kN	kips	kN	
10E-1	2975	17.4	77.2	18.8	83.4	18.8	83.4	Elastic failure
10E-2	3129	18.3	81.2	18.8	83.4	18.5	82.1	Elastic failure
10E-3	3180	18.6	82.5	18.8	83.4	18.9	83.9	Elastic failure
10F-1	3655	21.5	95.4	21.6	95.9	22.5	99.9	Initial elastic failure—core failed during springback
10F-2	4003	23.5	104.3	21.6	95.9	23.8	105.6	Initial elastic failure—core failed during springback
10F-3	3825	22.5	99.9	21.6	95.9	23.7	105.2	Initial elastic failure—core failed during springback
10G-1	1761	11.9	52.8	11.9	52.8	12.1	53.7	Elastic failure
10G-2	1687	11.4	50.6	11.9	52.8	11.6	51.5	Elastic failure
10G-3	1732	11.7	51.9	11.9	52.8	12.0	53.2	Elastic failure
10H-1	3172	26.0	115.4	26.2	116.3	27.0	119.8	Elastic failure
10H-2	3074	25.2	111.8	26.2	116.3	26.9	119.4	Elastic failure
10H-3	3514	28.8	127.8	26.2	116.3	29.2	129.6	Elastic failure
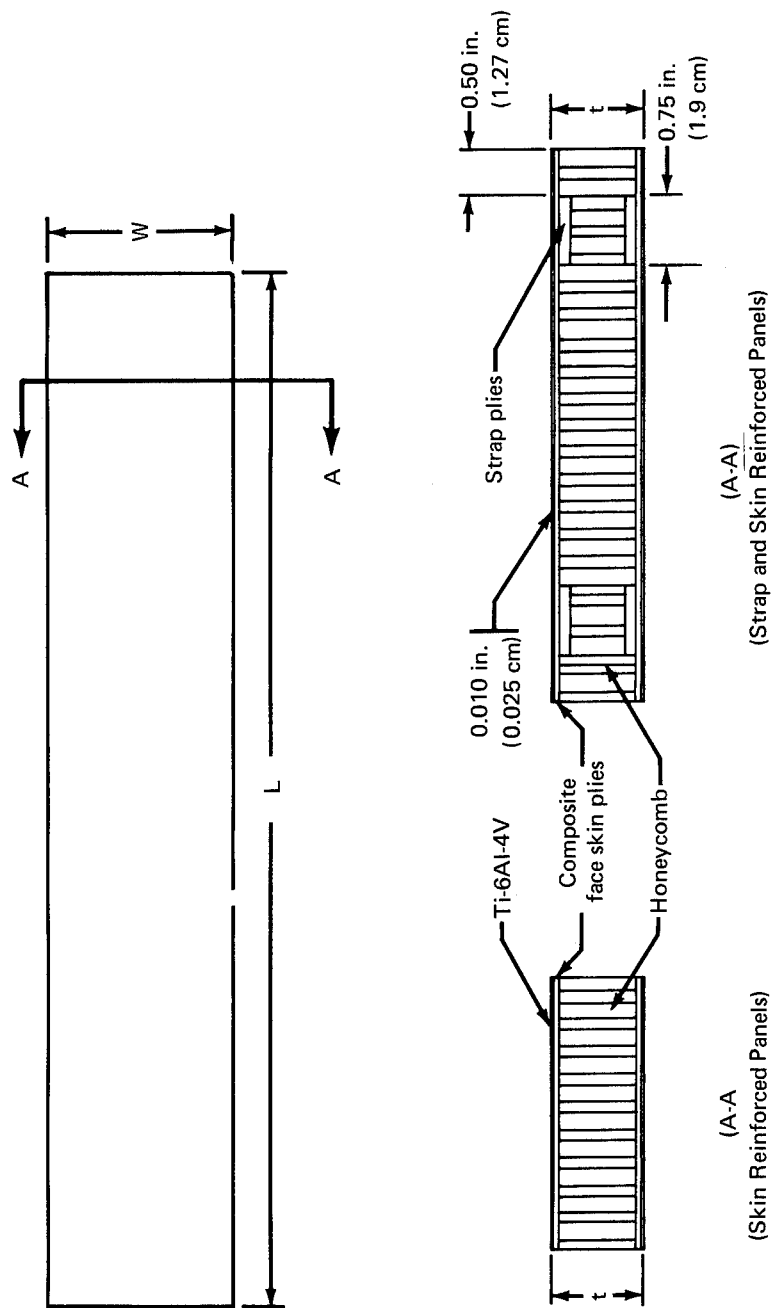
FIGURE 37.—HONEYCOMB SANDWICH PANEL CONFIGURATIONS

71
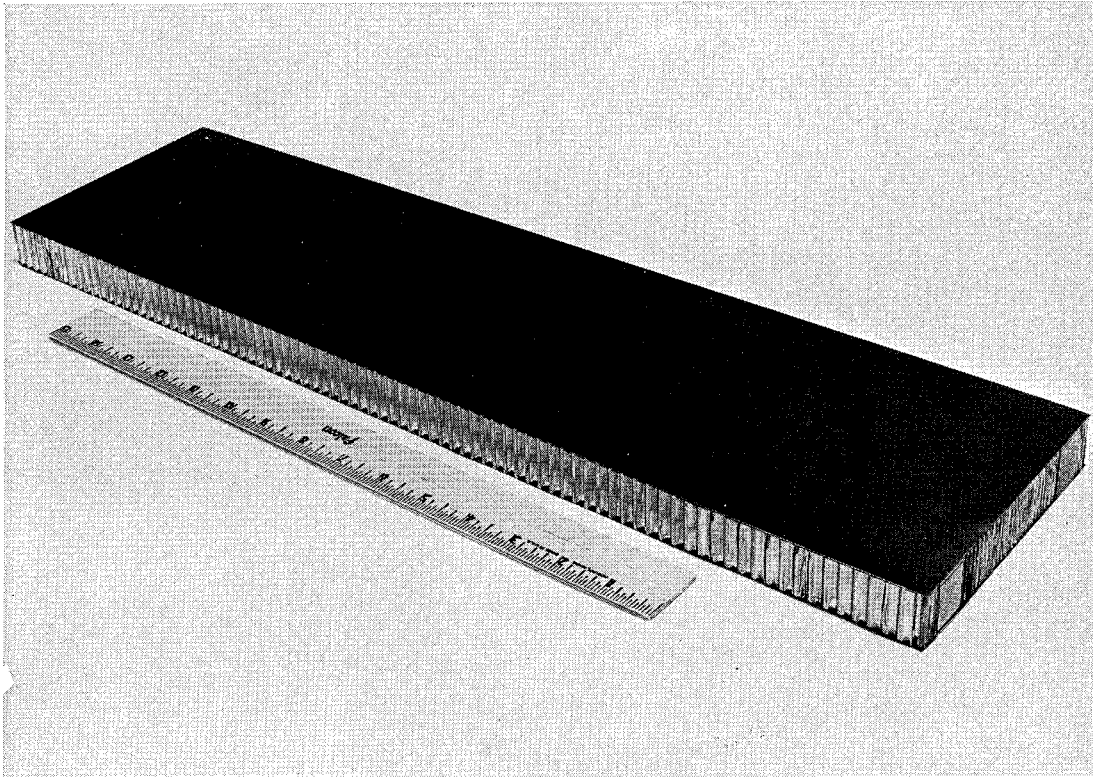
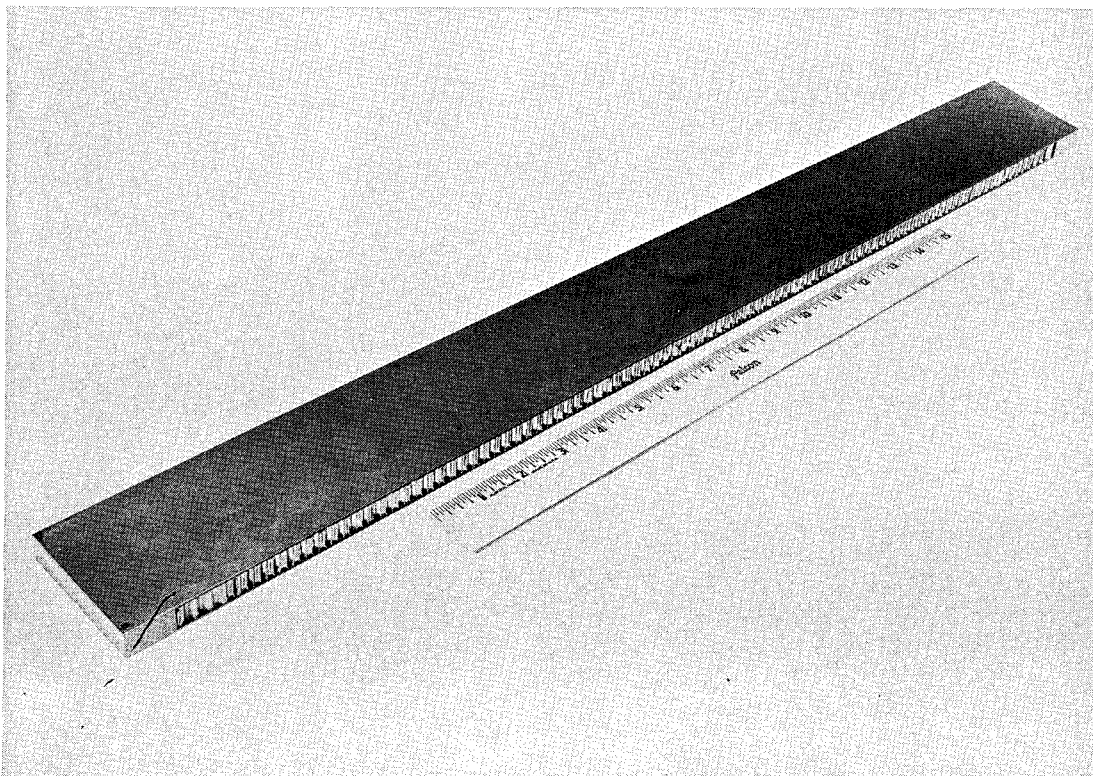FIGURE 38.—TYPICAL SANDWICH WRINKLING SPECIMEN
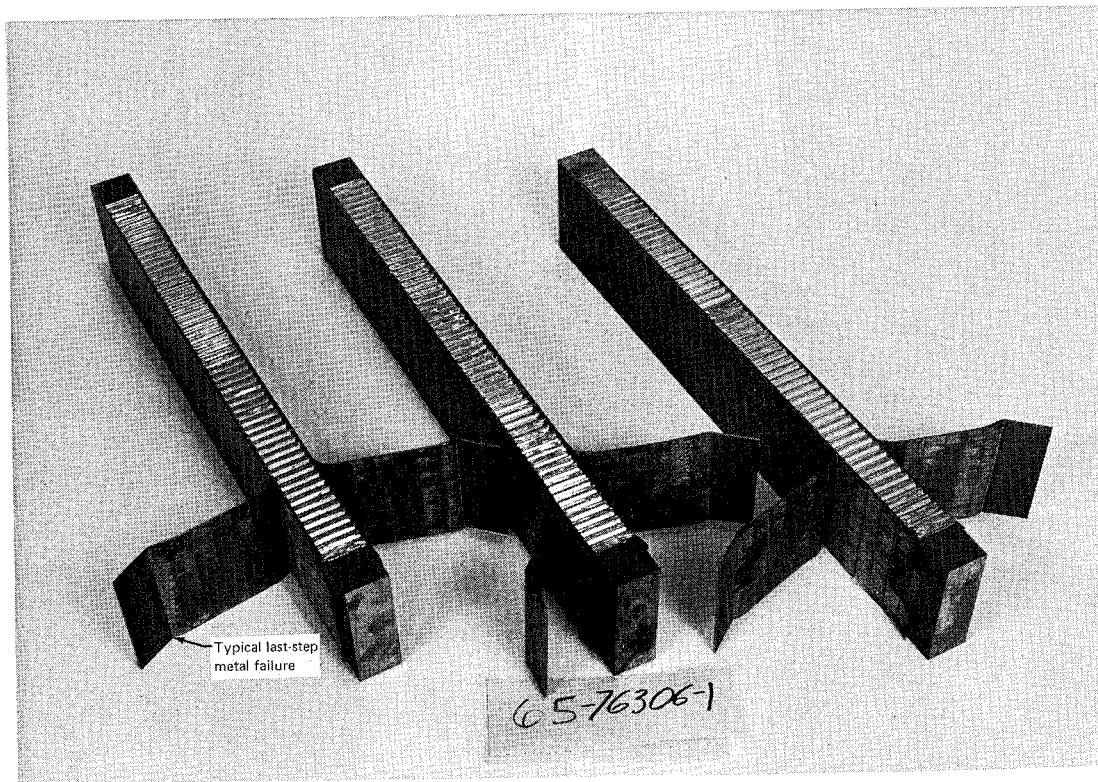

FIGURE 39.—TYPICAL SANDWICH BUCKLING SPECIMEN

Typical last-step
metal failure

65-76306-1

FIGURE 40.–TYPICAL SKIN-REINFORCED SANDWICH WRINKLING SPECIMEN FAILURE

65-76306-3
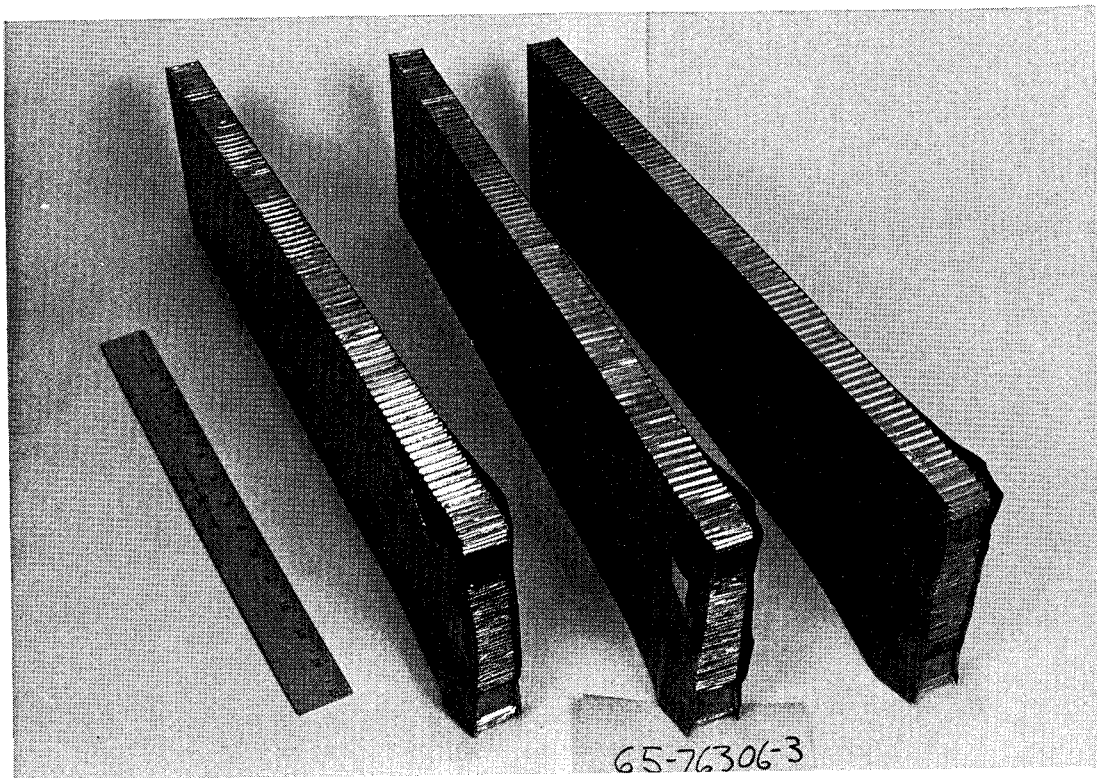
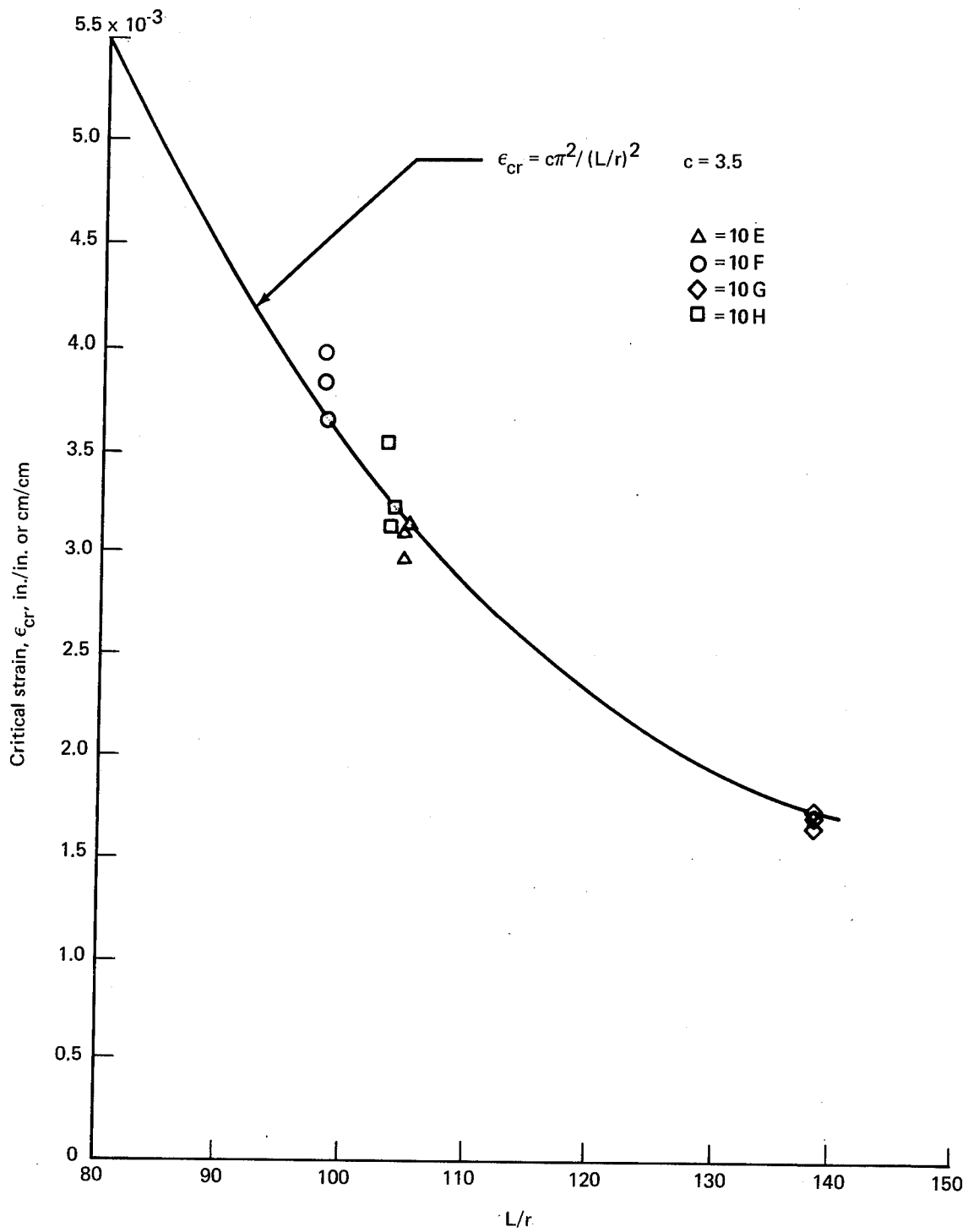FIGURE 41.–STRAP-REINFORCED SANDWICH WRINKLING SPECIMEN FAILURE

FIGURE 42.—SANDWICH BUCKLING TEST DATA

In the figure:

$$\epsilon_{cr} = c\pi^2 / (L/r)^2 \qquad c = 3.5$$

$\triangle$ = 10 E
$\bigcirc$ = 10 F
$\diamond$ = 10 G
$\square$ = 10 H

Axis labels: Critical strain, ϵ_{cr}, in./in. or cm/cm (vertical), L/r (horizontal)

CONCEPT VERIFICATION PANELS

Objective

The objective of this portion of the program was to demonstrate the structural feasibility of compression-critical composite-reinforced metal aircraft structure.

Approach

To determine the feasibility of using composite-reinforced metal for compression-critical structure, several stiffened-panel concepts were evaluated. These panels were designed to the same constraints and with the same compression load carrying capability as either the Boeing 707 or proposed supersonic transport fuselage structure (fig. 43). Four panel designs were fabricated and tested. The results obtained were compared with the structural capabilities of the equivalent all-metal structure to determine their weight-savings potential.

Test Specimens

Each design was incorporated into two panels of different lengths to investigate both compression crippling and column behavior. The shorter panels were 15.00 in. (38.2 cm) long and were used to study local crippling or strength failure modes. The longer panels were 33.7 in. (85.6 cm) long. This length, used in conjunction with the end fixity of c = 3.5 established during test, is equivalent to fuselage structure supported with frames spaced at 18.00 in. (45.7 cm).

Details of three reinforcement concepts, applicable to 707 fuselage panel designs, are shown in figures 44, 45, and 46. The 707 fuselage shell structure experiences compressive load intensities up to 8 kips/in. (1400 kN/m) at temperatures ranging from -67° F to 160° F (219° K to 344° K). Completed reinforced panels designed to these loads are shown in figures 47 and 48.

A reinforcement concept representative of supersonic transport applications is shown in figure 49. The proposed supersonic transport fuselage structure experiences load intensities up to 18 kips/in. (3152 kN/m). Flight temperatures range from -65° F to 450° F (219° K to 505° K). A completed reinforced panel designed to these requirements is shown in figure 50.

All concepts incorporated stepped titanium load-transfer regions to introduce load into the composites.

Most of the panel ends were stabilized with cast epoxy to prevent delamination during machining. The final preparation for test consisted of machining the ends flat and parallel while the panels were clamped flat.

Testing and Results

All of the long panels tested at room temperature were instrumented with strain gages. Gages were placed at one end of each stiffener to establish load distribution along the panel width. Strain gages were placed back to back along one stiffener centerline to establish

column behavior. The skin between stiffeners was instrumented to determine when skin buckling occurred. Gages were either read continuously, or at approximately 5% load increments. In all tests, both crippling and column, the load versus in-plane shortening was continuously recorded. The test results obtained from the panel tests and panel weights are summarized in table 17. The panel weights represent the total weight of the panel (without end reinforcements such as stepped titanium fittings) divided by the panel area.

In addition to the concept panel tests, several single stiffeners were also tested to obtain preliminary design and manufacturing data. These results are also summarized in table 17.

A typical room temperature test setup is shown in figure 51. The strain gage instrumentation is shown as well as the deflectometer used to measure head travel. A typical test setup for a 450° F (505° K) test is shown in figure 52.

Discussion

The longer panels were treated as columns. Two relationships were used: the Euler column formula and the Johnson parabola. The expression $w_{effective} = 0.85t\sqrt{E/Fc}$ was used in conjunction with these relationships to account for the effective skin after it had buckled. To establish the plate crippling strength required by the Johnson parabola, crippling was assumed to occur at a panel strain of 0.007 in./in. (See fig. 53.)

A comparison of the test results and theoretical predictions is shown in figure 53. The maximum achieved strains generally fell short of their predictions, when based on an assumed maximum strain equal to 0.007 in./in. (cm/cm). When using a critical strain equal to 0.006, as indicated by the shorter crippling panels, the test data correlated well with the Johnson parabola, as shown by the dashed curve in figure 53.

Skin buckling took place well before several of the long panels failed. This placed large peel loads on the stiffener-skin bond causing it to separate and initiate panel failure. Figures 54, 55, and 56 show this debonded condition in the failure area of several tested panels. The single stiffener hat specimens, which did not have to contend with buckled intermediate skins, attained higher strains than the multiple-hat-stiffened panel. This also indicated that the buckled skin contributed to failure initiation.

Strain gage data showed that eccentric column loading was experienced by most of the panels during test. A portion of the load-versus-strain data for the reinforced titanium angle concept is shown plotted in figure 57. These data show that some bending was experienced throughout loading and was increased after the skin buckled. As shown in figure 58, the neutral axis of the panel cross section shifts as the section changes from all-composite reinforcement to all-metal in the transition region. An additional shift is also experienced as effective material is lost in the center of the panel due to skin buckling.

The poor performance of the reinforced honeycomb panels, figure 59, was attributed to a manufacturing error. Because of a core identification mistake, both panels were manufactured with incorrect core density (lighter) between the composite straps. This resulted in inadequate core shear stiffness causing the crippling specimen 11F to fail prematurely. The core of column panel 11E was crushed in the strap area by bonding pressure. This was verified by sectioning the panel away from the failure area after test. The resulting specimen,

therefore, had the boron reinforcement closer to the neutral axis than desired and was less stable than required. Although incorrectly fabricated, the capability of manufacturing a composite-reinforced honeycomb assembly with the degree of complexity required in aircraft was demonstrated. The analysis and structural capability of composite-reinforced sandwich was demonstrated in the section on sandwich wrinkling and buckling.

The residual thermal stresses in the composite-reinforced titanium assemblies bonded with AF 126 adhesive were calculated to determine their significance. The stress-free temperature used was 250° F (393° K) (see fig. 10). The titanium residual thermal stress at test temperature was less than 5 ksi tension (34.47 MN/m^2) (see fig. 12) and was assumed insignificant.

Before testing the five-stringer aluminum-boron-epoxy panel (11A), a typical single stiffener of the same design was fabricated and tested. This specimen, 11K failed at a load of 33.3 kips (149 kN). Figure 60 shows the failed stiffener. The failure load was high enough to demonstrate the feasibility of the design concept and also met the load intensity requirement of 8 kips/in. It was slightly lower than the equivalent load developed in the five-stringer panel 11A. This was attributed to the relative instability of the outstanding aluminum flanges when compared with the additional support provided by the continuity of the skin in a multistiffener panel.

Two reinforced-hat stiffeners were also fabricated and tested. The first stiffener, 11L, used a room-temperature bond for assembling the composite to the titanium hat. It failed at 46.8 kips (210 kN). The second stiffener, 11M, used an elevated-temperature adhesive for assembling the composite to the hat. It failed at 43.9 kips (197 kN) and is shown in figure 61 after test. The magnitude of the failure loads demonstrated an excellent potential for carrying proposed design loads. They were equivalent to intensities of 8.5 kips/in. (1.49 MN/m) and 8.0 kips/in. (1.40 MN/m) when used in a panel design incorporating this concept. These loading intensities were higher than the corresponding loads obtained in the panel tests. It is felt that initiation of panel failure was in part caused by the high peel loads developed in the stiffener-skin bonds. The individual stiffeners did not have to contend with the buckled intermediate skins that caused these peel loads.

The first, short, titanium, angle-stiffened panel (11J) incorporating boron-polyimide composites failed at 232.5 kips (1.04 MN). When testing was stopped, two of the five stiffeners failed (fig. 62). Two of the undamaged stiffeners were sawed off of the panel and tested separately. One failed at 60 kips (267 kN). The composite in this stiffener was made of seven 10-ply laminates. The matrix was used as an adhesive in the center of each of the 10-ply laminates. The second stiffener incorporated 14 five-ply laminates. They were assembled with FM 34 adhesive. This construction was used in the balance of the boron-polyimide panels tested. The second stiffener failed at 90 kips (400 kN), which was equivalent to the load intensity attained in the short panel incorporating this design with boron-epoxy composites.

A second, short, five-stiffener, boron-polyimide panel was tested at 450° F (505° K) (fig. 63). This panel failed at a load of 235.0 kips (1.046 MN). The failure mode was similar to the initial failure experienced in the room temperature tests, which consisted of composite peel, as shown in figure 64.

Because of the failure modes experienced in the tests of the short panels, it was concluded that the titanium angle stiffener concept is not suitable for incorporating boron-polyimide composites. Buckling of the intermediate skin imposes large peel loads on the

composite and/or the adhesives. Polyimide does not have good resistance to this type of loading. To permit the long panels to be tested to obtain column behavior modes, these panels were reinforced to negate peel load failures. Steel plates 0.25-in. thick straddled each of the stiffeners and were held in place with clamps. A Teflon strip was placed between the steel plates and the stiffeners to permit the latter to act unrestricted as columns and to ensure that the steel did not pick up the load. One of the steel plates was strain gaged, and the readings taken showed that the load was not picked up by the steel during test. The room temperature long panel failed at a load of 349.5 kips (1.55 MN), which was approximately the same level obtained with the titanium-boron-epoxy angle panel. The long panel tested at 450° F (505° K) attained an ultimate load of 247.0 kips (1.10 MN). This was significantly lower than expected. The failure mode consisted of a typical column failure (fig. 65).

Because of differential thermal expansion between the composite and metal, moments were introduced during the test. A beam column analysis was used to determine the magnitude of added stress caused by these moments. It showed that bending increased the compression stresses by 7.5%.

Most of the panels designed to carry 8 kips/in. achieved this load intensity. These results are plotted as a function of weight-effective stress in figure 66. The weight-effective stress was determined by dividing the panel maximum test load intensity by a weight-equivalent area. The area was developed by dividing the typical panel section weight by the density of the material used in competing all-metal panels. Also included is a curve that shows the efficiency (weight-effective stress) of comparable 707 aircraft construction. These data are replotted in figure 67 to show the relative efficiency of the reinforcement concepts when compared with conventional all-metal construction.

The design intesity of 8 kips/in. (1.40 MN/m) was achieved by both the single stiffener and the panel incorporating the reinforced aluminum angle concept. The potential weight saving of this concept is approximately 21% at 8 kips/in. and 29% at 9 kips/in. The titanium hat concept tests indicated a weight saving of about 24% is possible at N_x = 8 kips/in. (1.40 MN/m). While the reinforced honeycomb concept failed below ultimate design intensity, this test showed a potential weight saving of 33% at N_x = 5.6 kips/in. (980 kN/m).

A load intensity of 17.8 kips/in. (3.12 MN/m) was achieved in the room temperature test of the reinforced titanium angle concept incorporating boron-epoxy composites. When compared with all-titanium supersonic transport designs, this indicated potential weight savings of 14%. The room-temperature test of this same concept incorporating boron-polyimide composites showed approximately the same results. The latter was stabilized, as discussed earlier, to obtain a column failure because short panel tests showed this concept subjected the composite to high peel loads and should not be used with boron-polyimide composites. This concept, when tested at 450° F (505° K), fell well below its design ultimate but still showed a weight saving of 9% at the achieved load intensity of 13.3 kips/in. (2.33 MN/m). A summary of the above results is shown in figures 68 and 69.

Cost is one of the major items considered when implementing the use of composites in aircraft structural components. Care must be exercised in selecting the manner and application in which composites are used because of their relatively high cost to accomplish structural weight savings in a cost-effective manner. The composite reinforcement of metal structure provides a concept for accomplishing cost-effective weight savings. Several of the panels fabricated and tested in this program developed significant weight savings while using relatively small amounts of composites.

A study was performed to evaluate the cost effectiveness of the panels evaluated in this program. A cost-effectiveness factor (CEF) was developed for each panel, based on the weight saved divided by the weight of the composite used. A summary of these results is shown in table 18.

An acceptable CEF for typical aircraft structure at today's composite prices should be approximately 1.5 or greater. As shown by their CEF numbers in table 18, the aluminum angle and titanium hat configurations indicated cost-effective weight savings. The CEF numbers are appreciably greater than can be expected on all composite construction. As a comparison, a study performed in-house on an all-composite wing box showed a CEF of less than 1.0. The sandwich design (11E) would have fared much better if premature failure due to a manufacturing error had not occurred. Based on the above, the reinforced titanium angle concepts (11G and 11I) would not be recommended for implementation because of cost.

Conclusions

Compression panel tests of composite-reinforced metal structure have demonstrated weight savings of 30% when compared to equivalent all-metal aircraft structure. Composite-reinforced metal concepts provide configurations that permit weight savings to be made in a cost-effective manner.

TABLE 17.—PANEL AND STIFFENER TEST DATA SUMMARY

Specimen	Description	Length (in.)	Length (cm)	Test temperature (°F)	Test temperature (°K)	Ultimate load (kips)	Ultimate load (N × 10⁵)	Intermediate skin buckle (kips)	Intermediate skin buckle (N × 10⁵)	N_x (kips/in.)	N_x (MN/m)	Weight (lb/ft²)	Weight (kg/m²)	Maximum strain (in./in. or cm/cm)	Comments
11A	Reinforced aluminum angle column	33.7	85.5	70	294	180	8.0	120-130	5.3-5.8	9.0	1.57	2.189	10.69	0.0048	Skin-stringer debond (fig. 54)
11B	Reinforced aluminum angle crippling	15.0	38.1	70	294	210	9.3	–	–	–	–	2.189	10.69	0.0056	
11C	Reinforced titanium hat column	33.7	85.5	70	294	155	6.9	25-50	1.1-2.2	7.05	1.23	2.102	10.26	0.0052	Skin-stringer debond (fig. 55)
11D	Reinforced titanium hat crippling	15.0	38.1	70	294	181	8.0	–	–	–	–	2.102	10.26	0.0061	
11E	Reinforced honeycomb sandwich column	15.0	38.1	70	294	211	9.4	–	–	5.6	0.96	1.426	6.96	0.0028	Column instability (fig. 59)
11F	Reinforced honeycomb sandwich crippling	15.0	38.1	70	294	211	9.4	–	–	–	–	1.426	6.96	0.0056	Core shear failure (fig. 56)
11G	Reinforced titanium angle column	33.7	85.5	70	294	356	15.8	250	11.1	17.8	3.12	3.888	18.98	0.0043	Skin/stringer debond (fig. 5G)
11H	Reinforced titanium angle crippling	15.0	38.1	70	294	461	20.5	–	–	–	–	3.888	18.98	0.0056	
11I	Reinforced titanium angle column (polyimide)	33.7	85.5	70 and 450	294 and 505	350 / ᵃ266	15.5 / 11.8	325	14.4	17.5 / 13.3	3.06 / 2.33	3.888	18.98	0.0042 / 0.0031	Stiffener riveted to skin. Steel plates and clamps were used to counter peel loads. (fig. 65)
11J	Reinforced titanium angle crippling (polyimide)	15.0	38.1	70 and 450	294 and 505	232.5 / 235	10.3 / 10.4					3.888	18.98	0.0028 / 0.0028	Stiffeners were riveted to skin (fig. 62) (fig. 64)
11K	Reinforced aluminum angle single stiffener	33.7	85.5	70	294	33.3	1.5	–	–	8.3	1.45			0.0044	Failure perpendicular to skin plane (fig. 60)
11L	Reinforced titanium hat single stiffener	33.7	85.5	70	294	46.8	2.1	–	–	8.5	1.49			0.0063	
11M	Reinforced titanium hat single stiffener	33.7	85.5	70	294	43.9	1.9	–	–	8.0	1.40			0.0059	(fig. 61)
11N	Reinforced titanium angle (PI) single stiffener	15.0	38.1	70	294	60.0	2.66							0.0039	Matrix used as adhesive in center of composite
11O	Reinforced titanium angle (PI) single stiffener	15.0	38.1	70	294	90	4.0							0.0054	FM 34 used as adhesive in center of composite

ᵃUltimate test load (247 kips) increased to reflect beam column effect.

TABLE 18.—CONFIGURATION COST EFFECTIVENESS

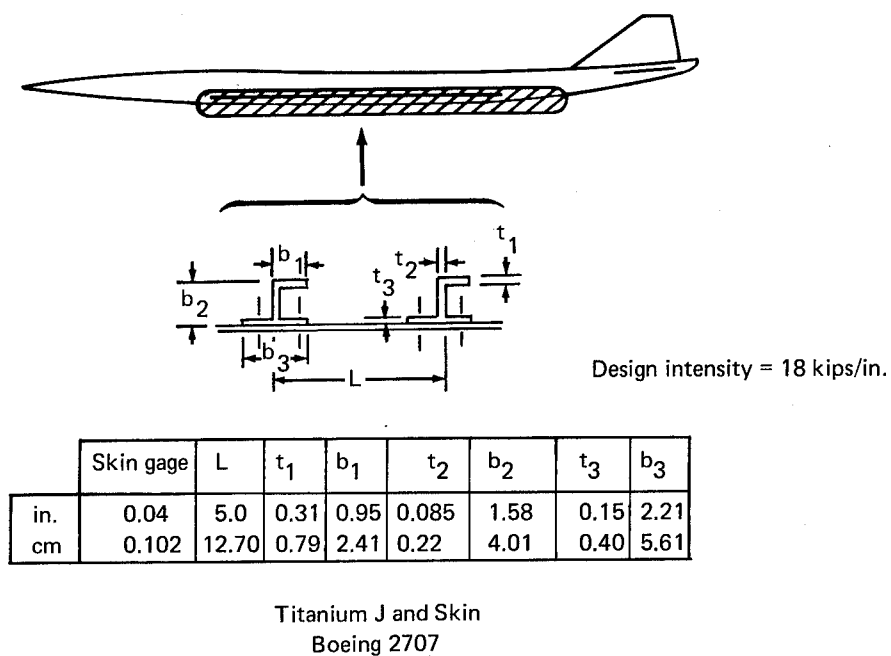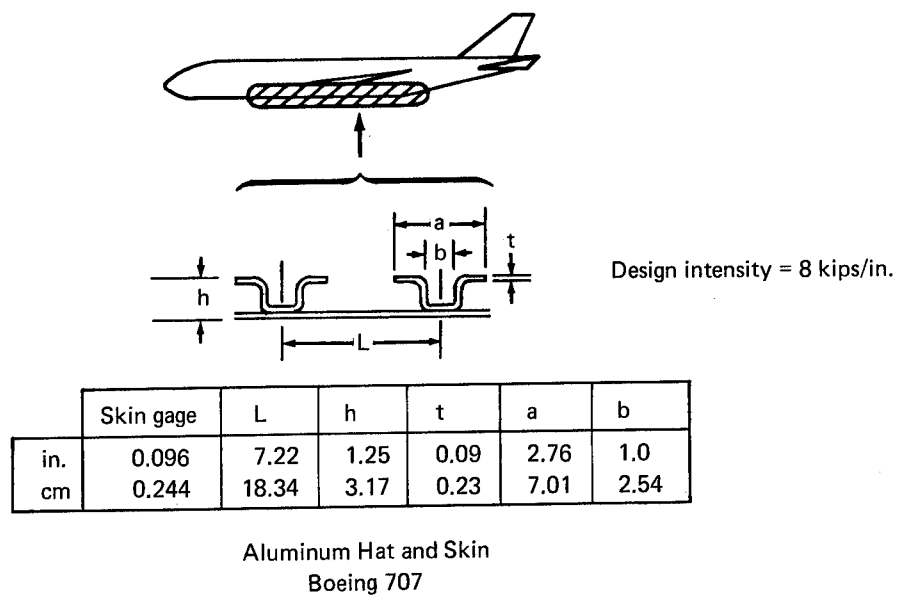| Specimen	11A	11C	11E	11G	11I
Panel configuration	Aluminum angle	Titanium hat	Sandwich	Titanium angle (epoxy)	Titanium angle (polyimide)
Cost-effectiveness factor	1.45	1.73	1.12	0.57	0.53

Design intensity = 8 kips/in.

	Skin gage	L	h	t	a	b
in.	0.096	7.22	1.25	0.09	2.76	1.0
cm	0.244	18.34	3.17	0.23	7.01	2.54

Aluminum Hat and Skin
Boeing 707

Design intensity = 18 kips/in.

	Skin gage	L	t_1	b_1	t_2	b_2	t_3	b_3
in.	0.04	5.0	0.31	0.95	0.085	1.58	0.15	2.21
cm	0.102	12.70	0.79	2.41	0.22	4.01	0.40	5.61

Titanium J and Skin
Boeing 2707

FIGURE 43.—CONVENTIONAL LOWER LOBE FUSELAGE STRUCTURE

Boron composite
(30 layers)

1.35 in.
(3.43 cm)

1.00 in.
(2.54 cm)

1.35 in.
(3.43 cm)

Bond

4.00 in.
(10.16 cm)

Matrix: BP-907
Skin: 0.040 7075-T6 aluminum
Angle: 0.050 7075-T6 aluminum
Bond:·   Epon 927/933
Length   11A, 33.7 in. (85.8 cm)
                  11B, 15.0 in.
Design intensity: N_x = 8 kips/in. at room temperature
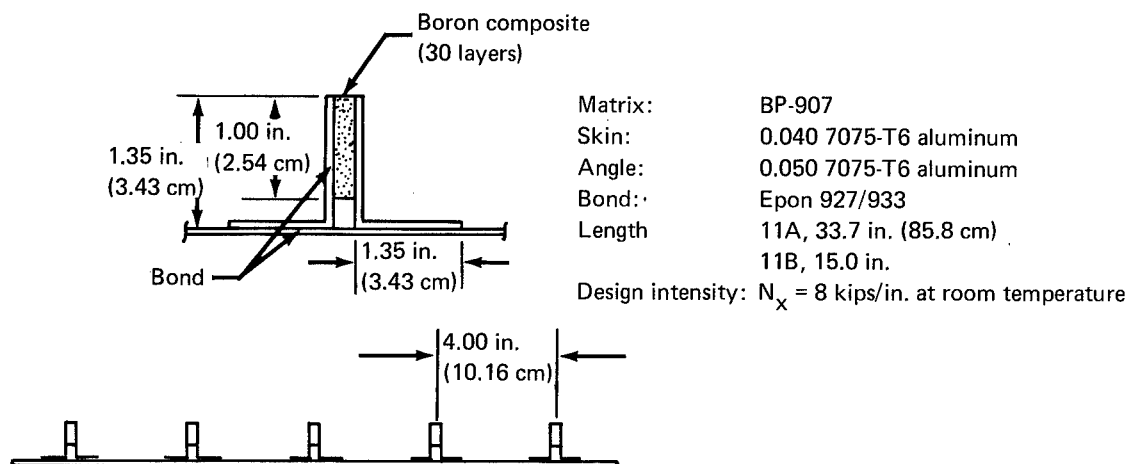
FIGURE 44.—REINFORCED ALUMINUM ANGLE CONCEPT (11A AND 11B)

1.10 in.
(2.79 cm)

0.75 in.
(1.90 cm)

Boron composite
(20 layers)

Bond

1.10 in.
(2.79 cm)

0.75 in. (1.90 cm)

5.50 in.
(13.97 cm)

Matrix: BP-907
Skin: 0.040 Ti-6Al-4V
Formed hat: 0.050 Ti-6Al-4V
Bond: AF 126
Length: 11C, 33.7 in. (85.8 cm)
                  11D, 15.0 in. (38.10 cm)
Design intensity: N_x = 8 kips/in. at room temperature
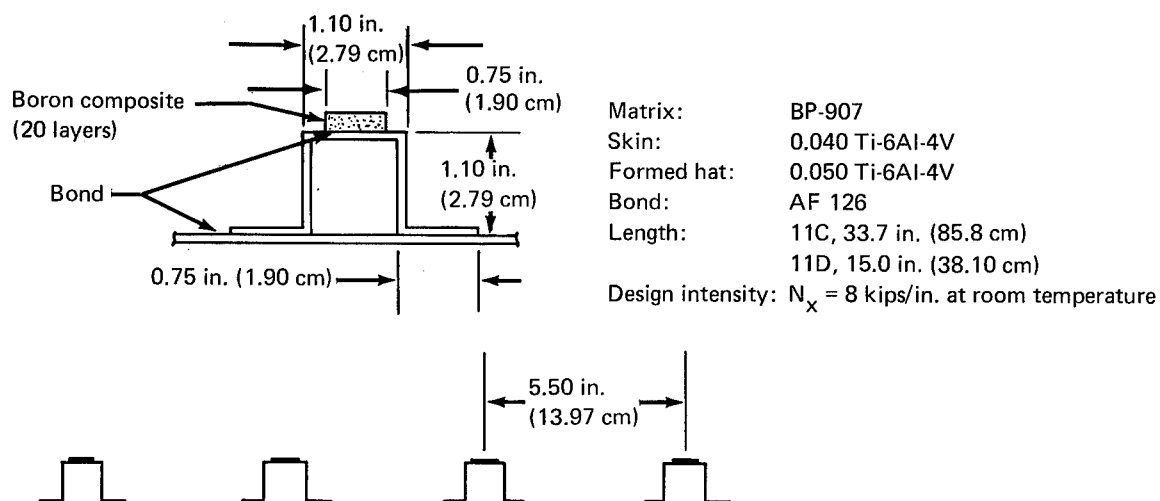
FIGURE 45.—REINFORCED TITANIUM HAT CONCEPT (11C AND 11D)

Matrix: BP-907
Skin: 0.013 Ti-6Al-4V
Bond: AF 126
Length: 11E, 33.7 in. (85.8 cm)
                  11F, 15.0 in. (38.10 cm)
Design intensity: N_x = 8.0 kips/in.

1.00 in.
(2.54 cm)

0.826 in.
(2.10 cm)

Boron composite
(20 layers/strap)
(typical)

Aluminum honeycomb
core (3.1 lb/ft^3)

4.00 in.
(10.16 cm)
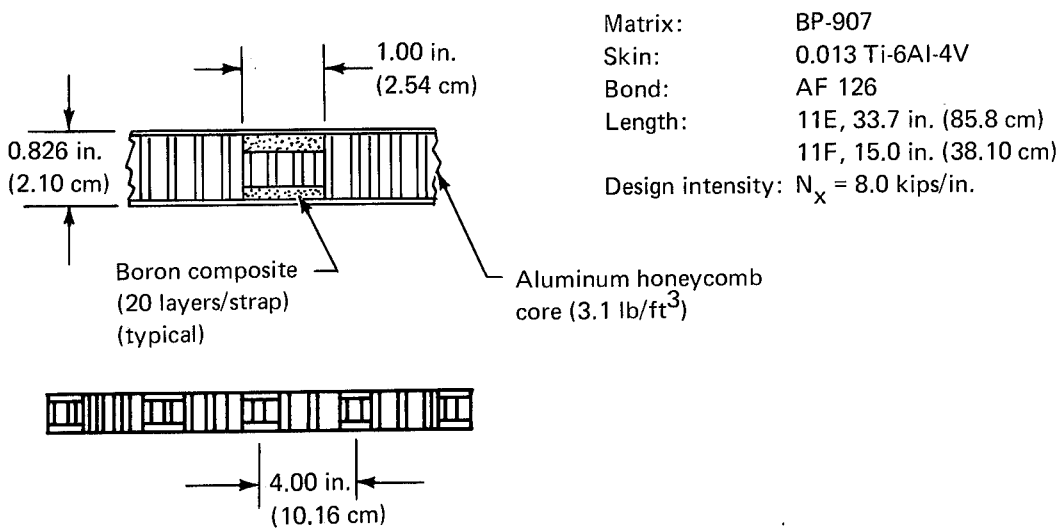
FIGURE 46.—REINFORCED HONEYCOMB SANDWICH CONCEPT (11E AND 11F)
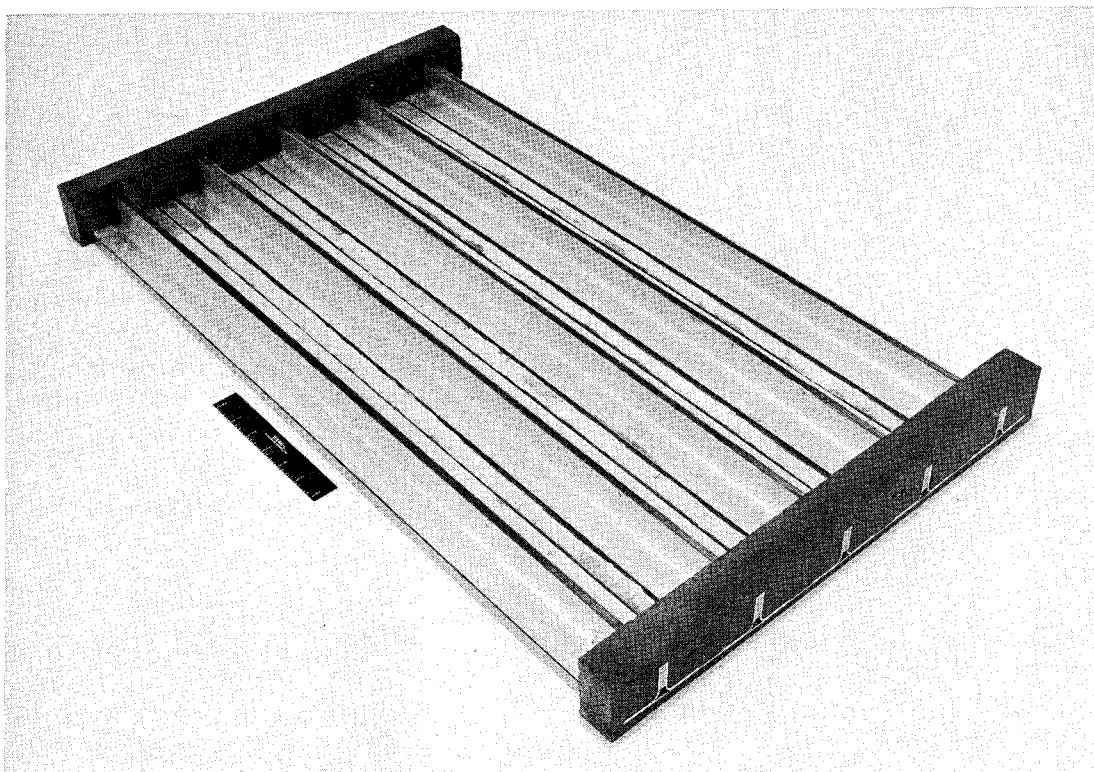
FIGURE 47.—REINFORCED ALUMINUM ANGLE CONCEPT
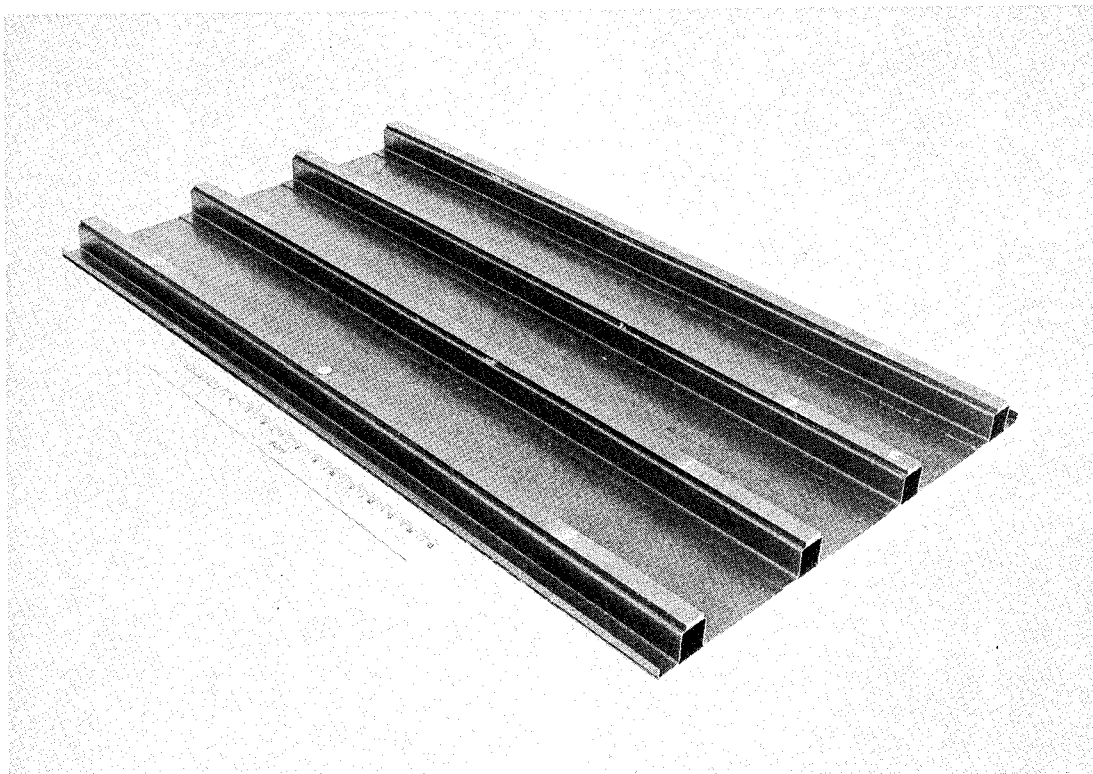
FIGURE 48.—REINFORCED TITANIUM HAT CONCEPT
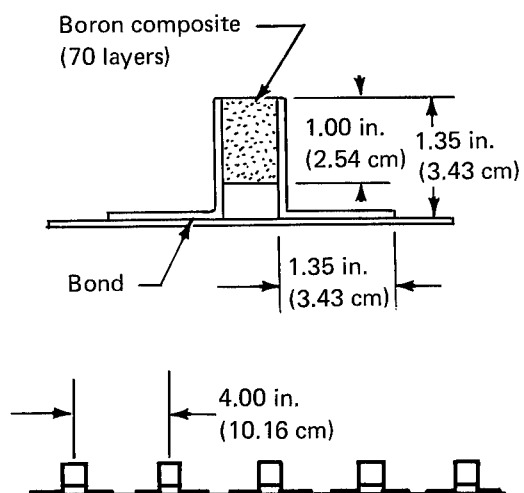
Specimen	Length		Matrix	Bond
	in.	cm		
11G	33.7	85.8	BP-907	AF 126
11H	15.0	38.10	BP-907	AF 126
11I	33.7	85.8	35-520	FM 34
11J	15.0	38.10	35-520	FM 34

Skin: 0.040 Ti-6Al-4V
Angle: 0.050 Ti-6Al-4V
Design intensity: 11G, N_x = 18 kips/in.
at room temperature
11I, N_x = 18 kips/in.
at 450° F (506° K)

FIGURE 49.—REINFORCED TITANIUM ANGLE CONCEPT (11G, 11H, 11I, AND 11J)
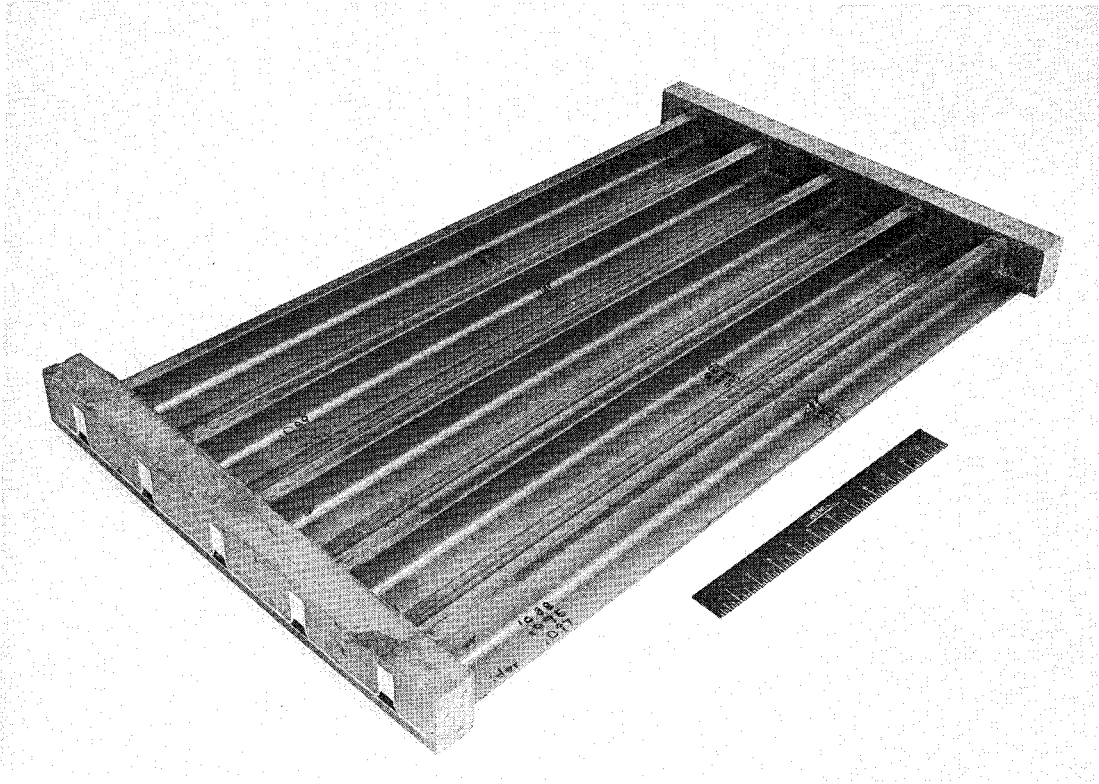
FIGURE 50.—REINFORCED TITANIUM ANGLE CONCEPT
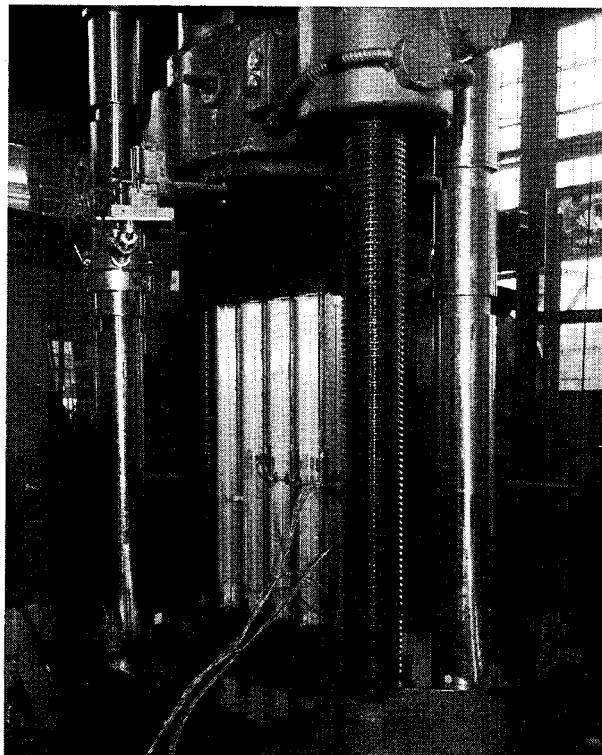
FIGURE 51.—TYPICAL PANEL TEST SETUP
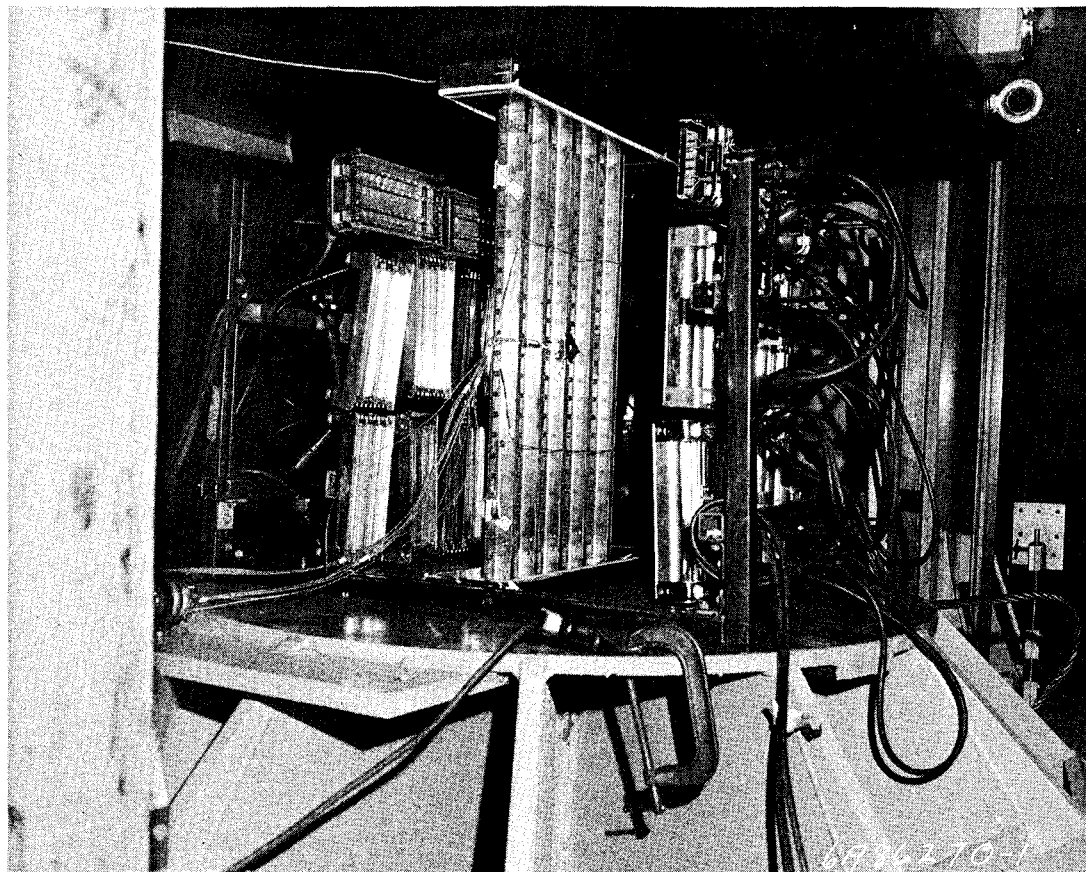
FIGURE 52.—TYPICAL TEST SETUP FOR 450° F TEST
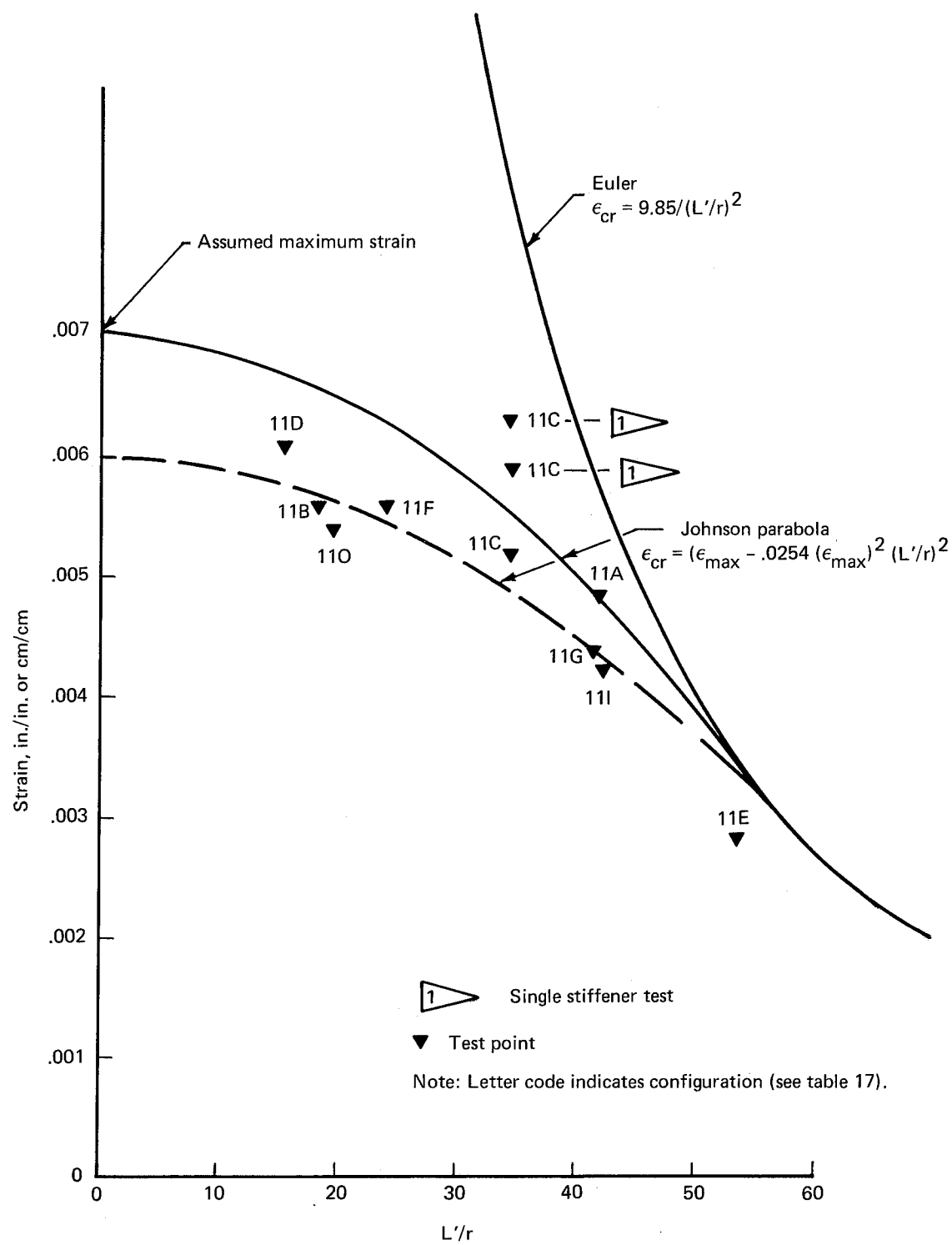
FIGURE 53.—COMPARISON OF TEST RESULTS AND THEORETICAL PREDICTIONS

The figure shows a plot of Strain, in./in. or cm/cm (vertical axis, from 0 to .007) versus L'/r (horizontal axis, from 0 to 60).

Curves and labels:
- Euler: $\epsilon_{cr} = 9.85/(L'/r)^2$
- Assumed maximum strain
- Johnson parabola: $\epsilon_{cr} = (\epsilon_{max} - .0254 \, (\epsilon_{max})^2 \, (L'/r)^2$

Test points labeled: 11D, 11B, 11O, 11F, 11C, 11A, 11G, 11I, 11E, 11C, 11C

Legend:
- ▷1 Single stiffener test
- ▼ Test point

Note: Letter code indicates configuration (see table 17).
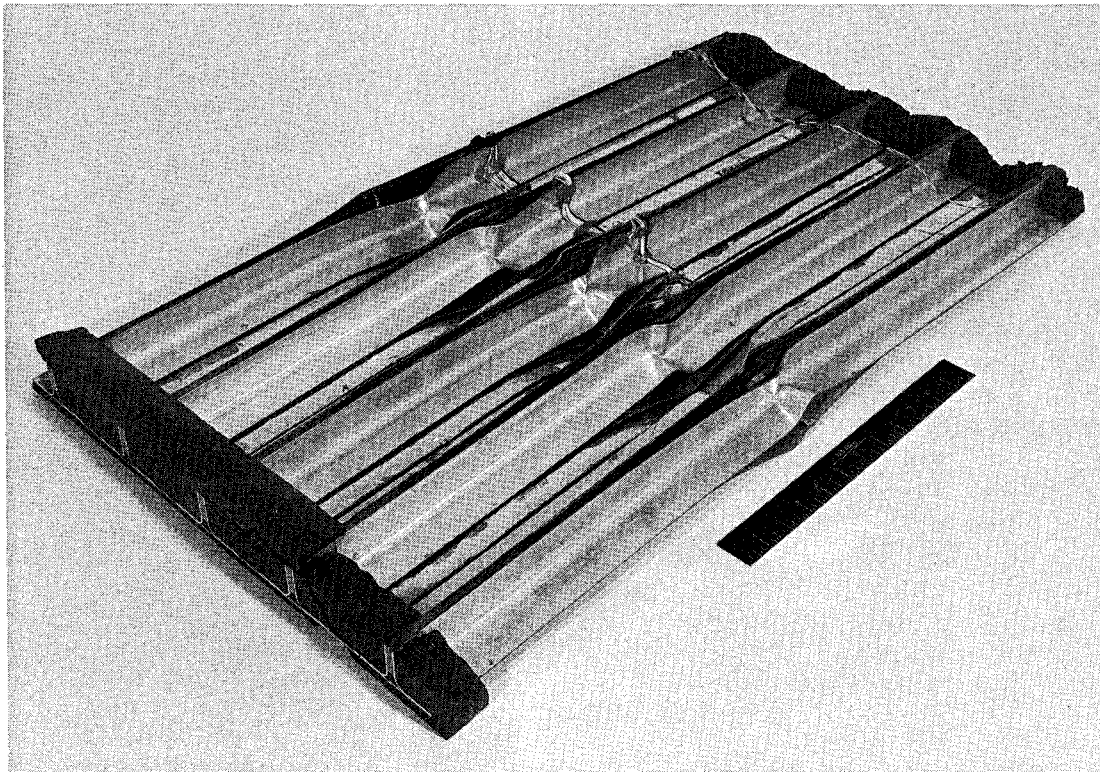
FIGURE 54.—REINFORCED ALUMINUM ANGLE COLUMN
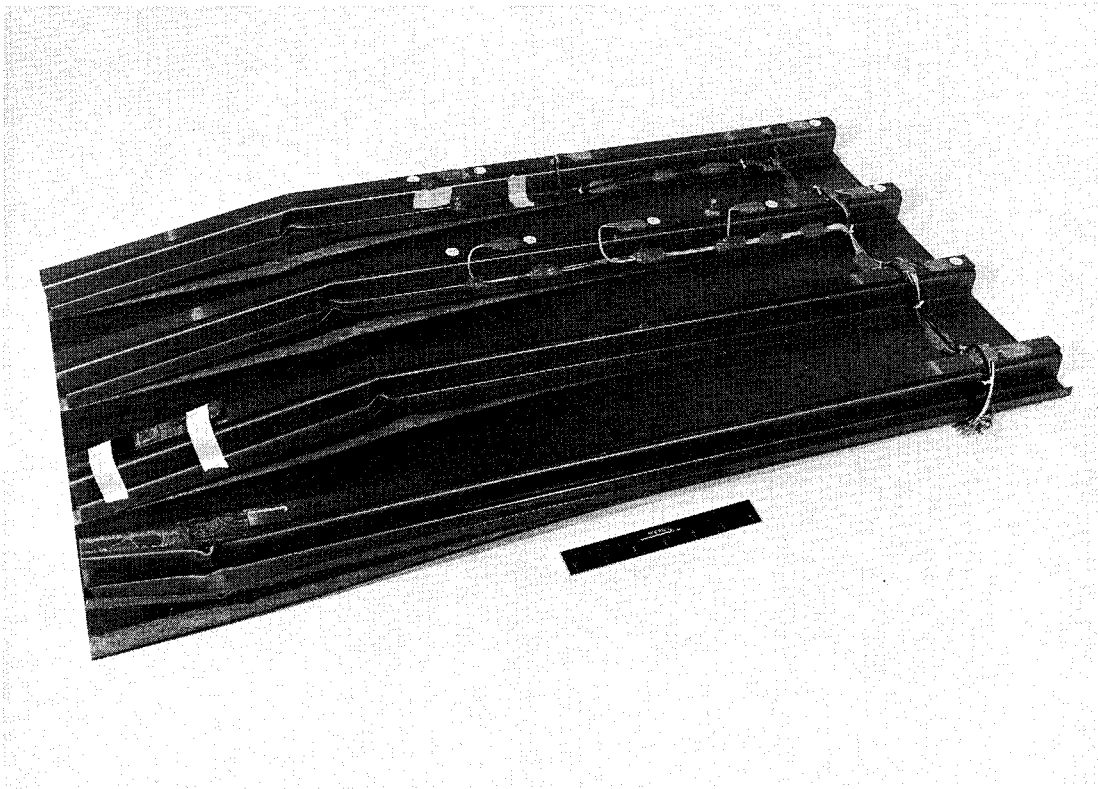
FIGURE 55.—REINFORCED TITANIUM HAT COLUMN
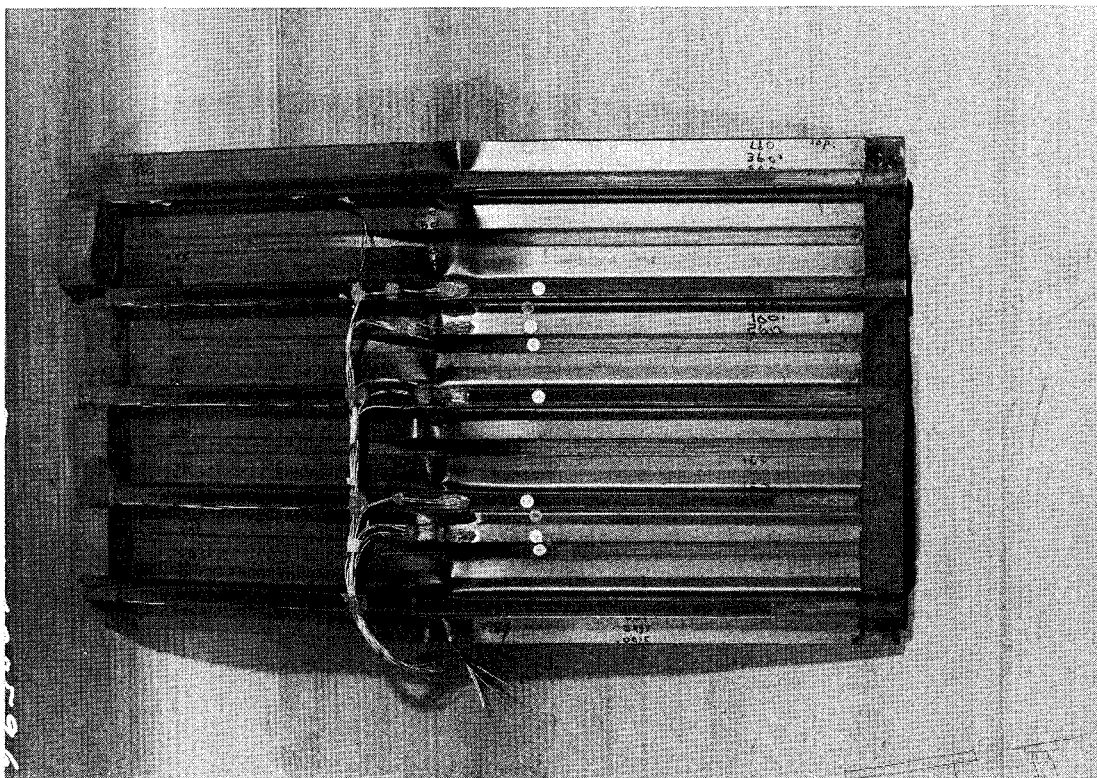
FIGURE 56.—REINFORCED TITANIUM ANGLE COLUMN
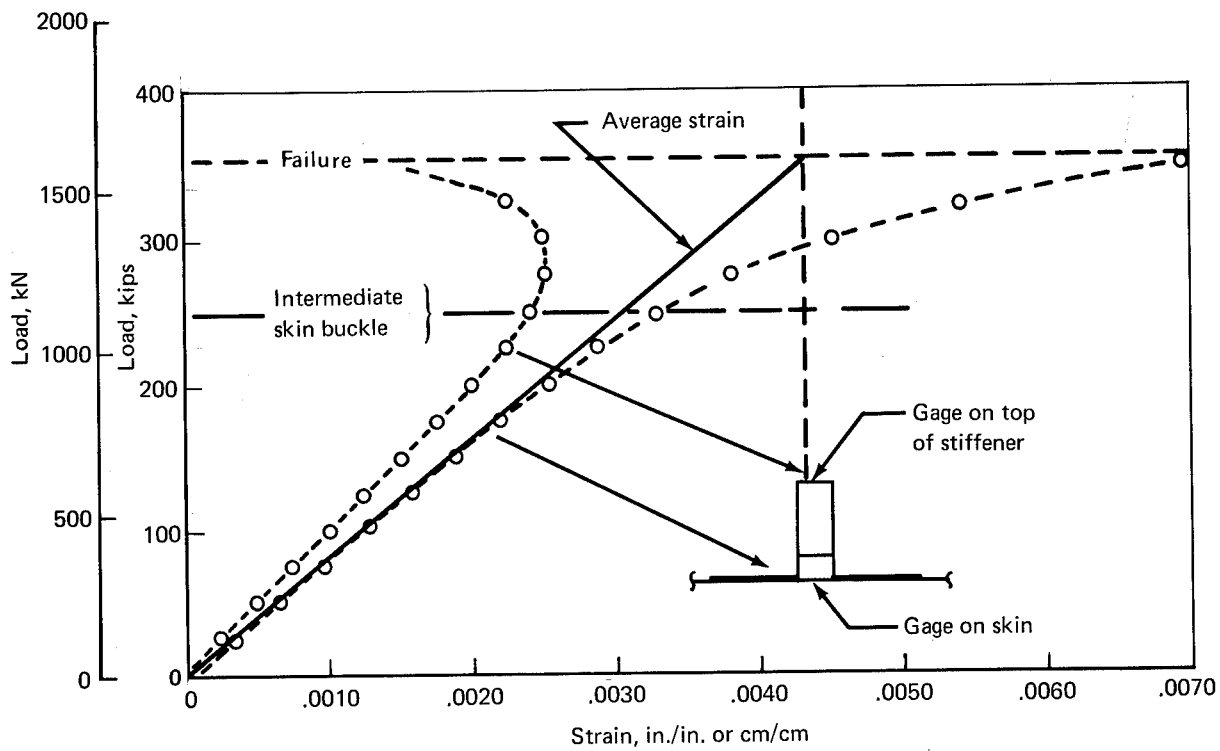
FIGURE 57.—BACK-TO-BACK STRAIN GAGE TEST DATA—SPECIMEN 11G
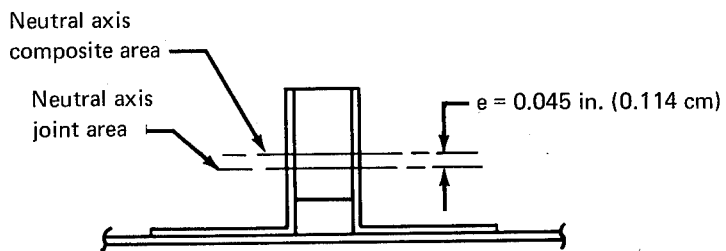
*FIGURE 58.—NEUTRAL AXIS SHIFT BETWEEN PANEL CENTER
AND JOINT AREA—SPECIMEN 11G*
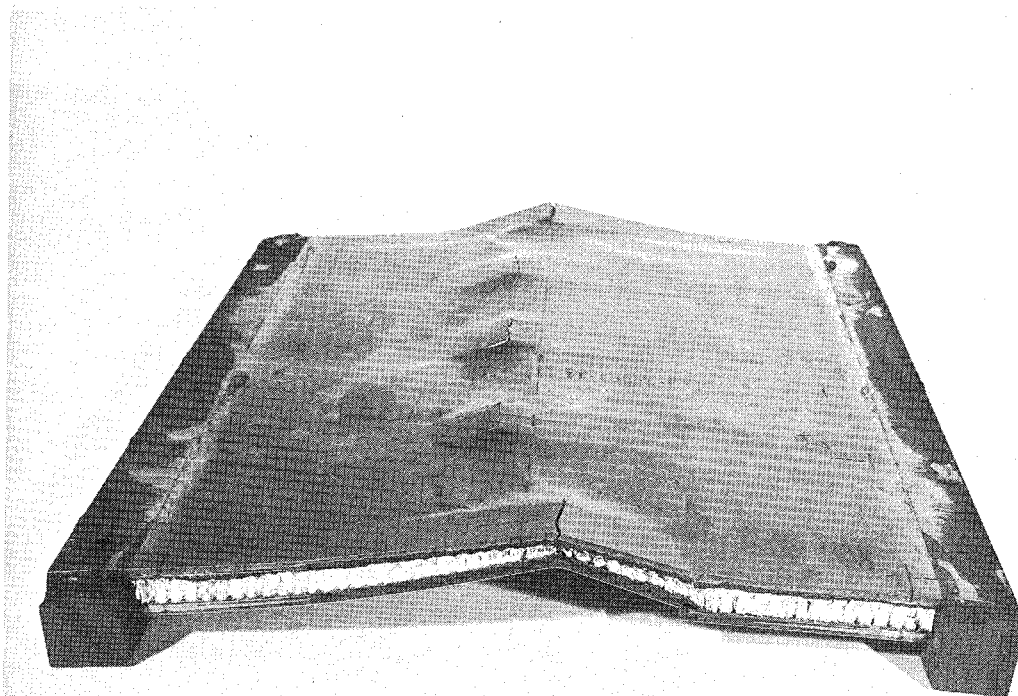
FIGURE 59.—REINFORCED HONEYCOMB SANDWICH
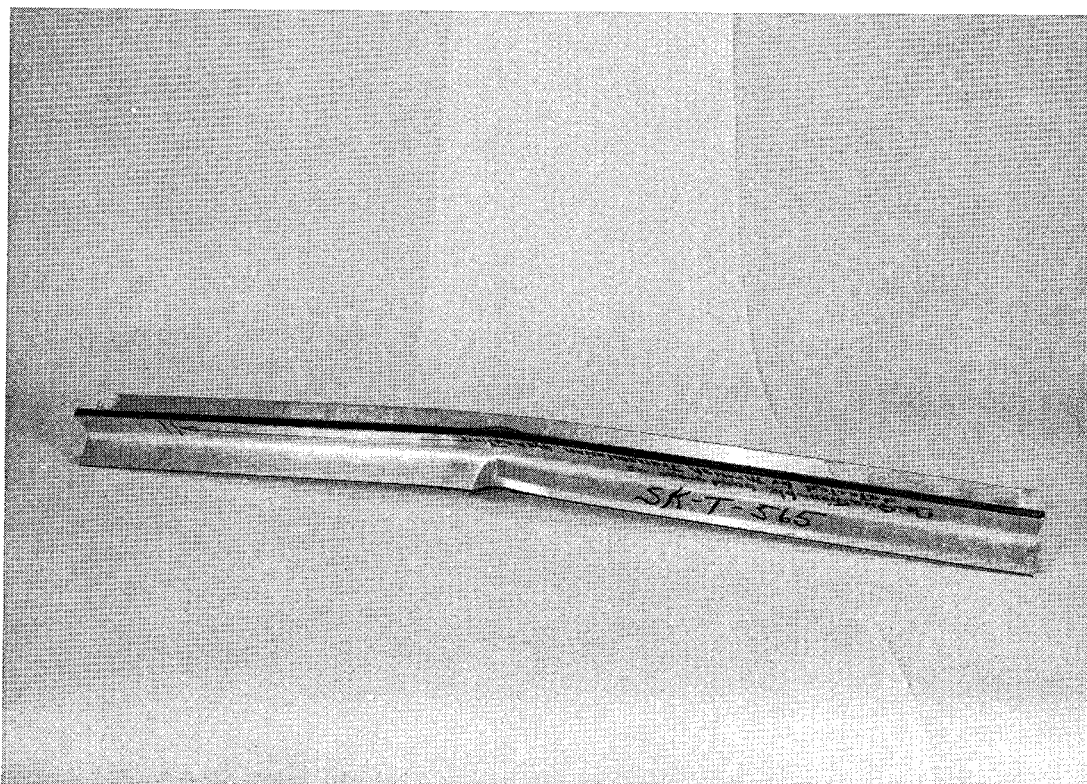
FIGURE 60.—REINFORCED ALUMINUM ANGLE SINGLE STRINGER
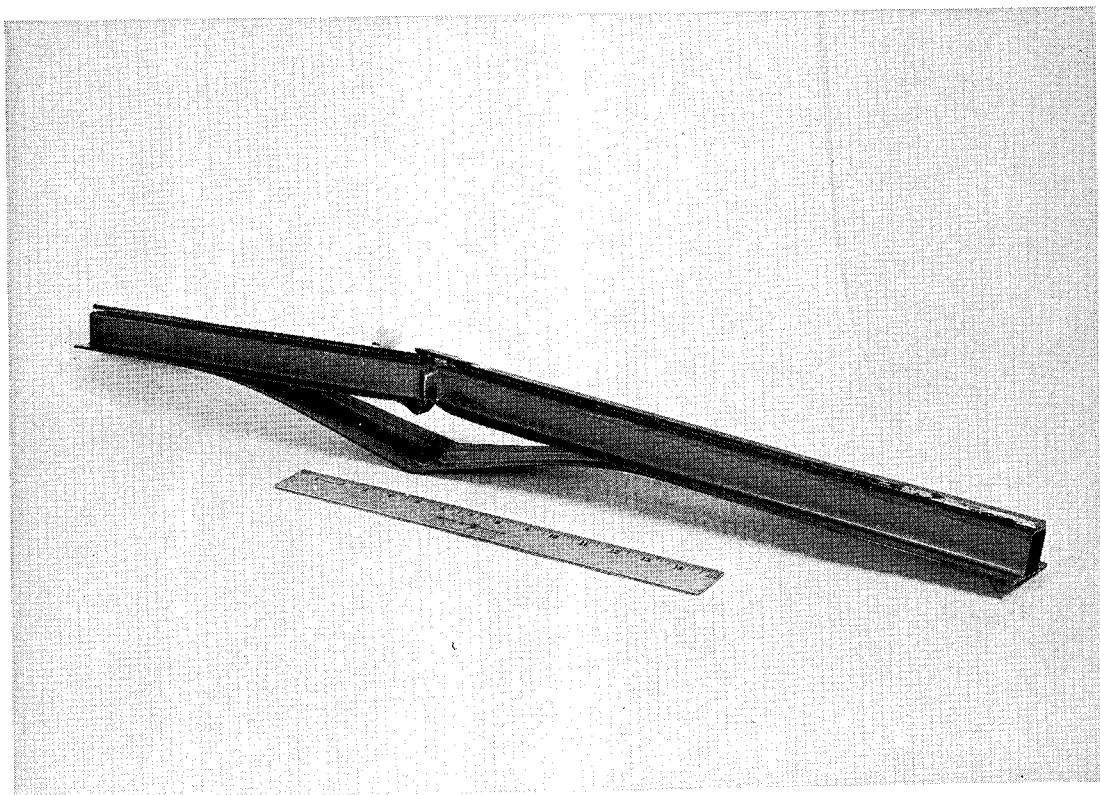
FIGURE 61.—REINFORCED TITANIUM HAT SINGLE STRINGER
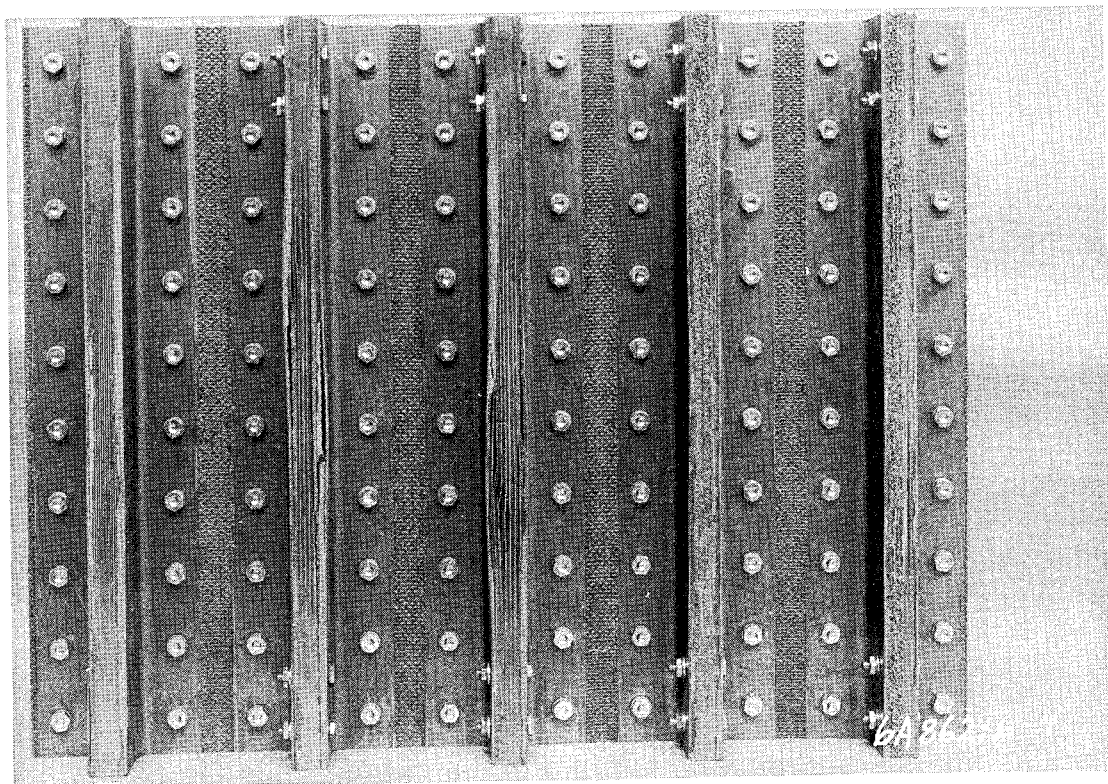
FIGURE 62.—BORON-POLYIMIDE TITANIUM ANGLE STIFFENED PANEL

93
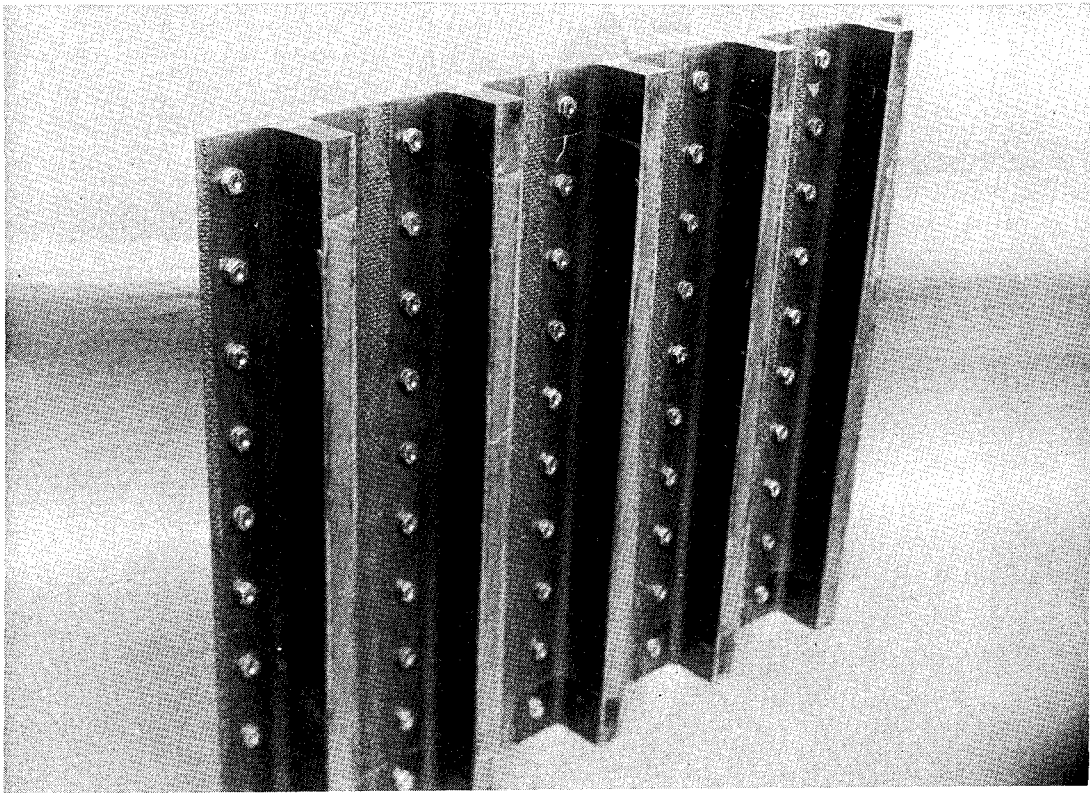
FIGURE 63.—BORON-POLYIMIDE CRIPPLING PANEL
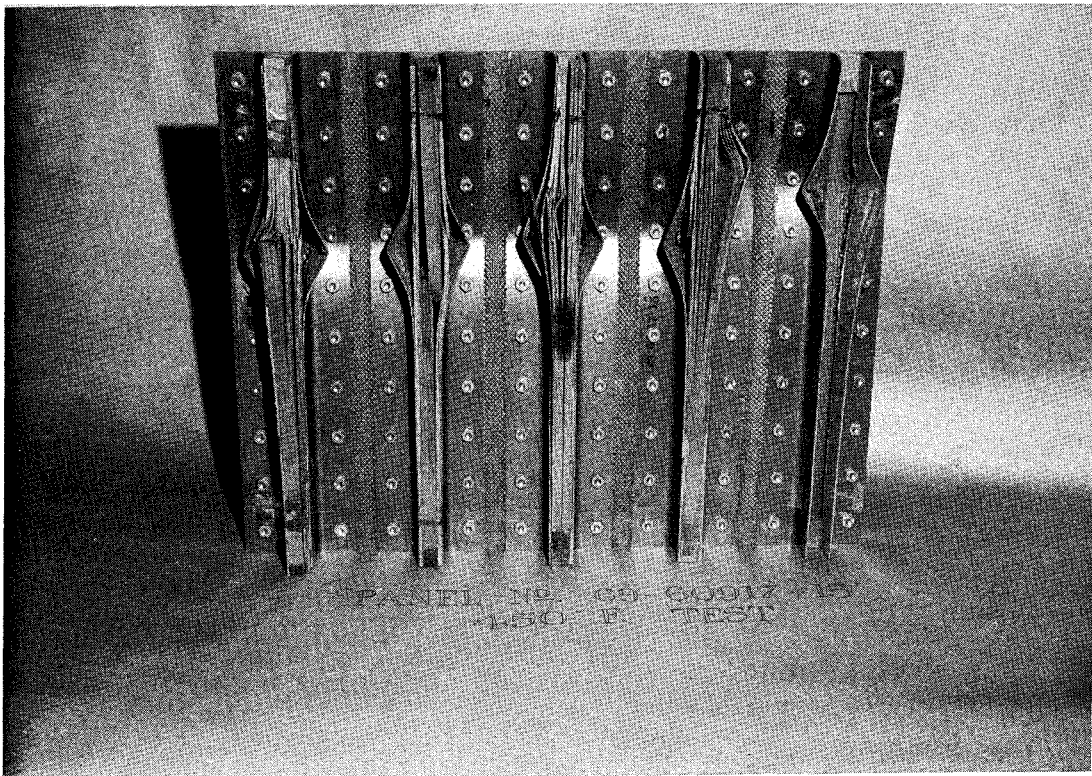
FIGURE 64.—BORON-POLYIMIDE CRIPPLING PANEL—450° F TEST
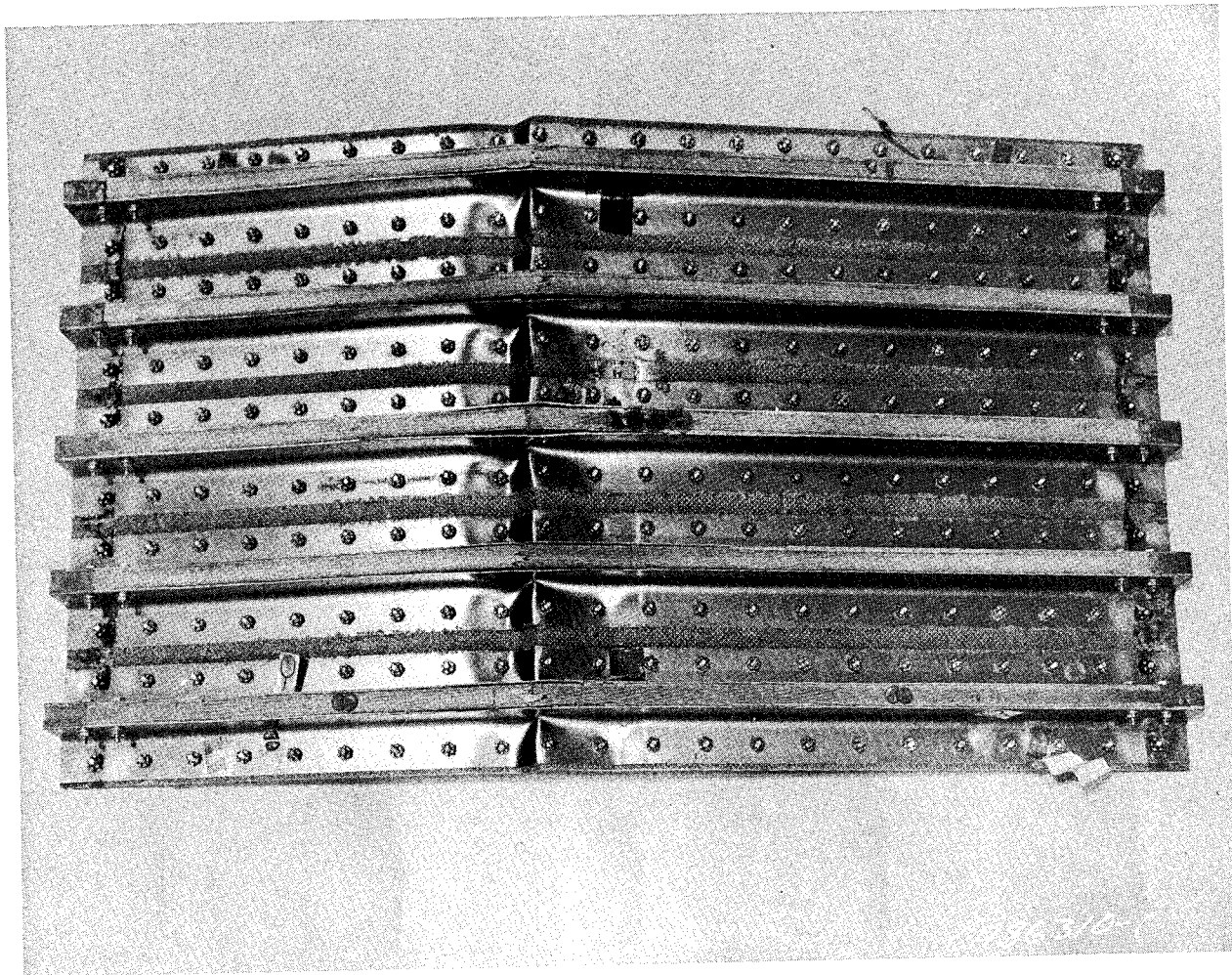
FIGURE 65.—FAILED BORON-POLYIMIDE STIFFENED PANEL

● 11A, reinforced aluminum angle column

○ 11K, reinforced aluminum angle single stiffener

▲ 11C, reinforced titanium hat column

△ 11L and 11M, reinforced titanium hat single stiffener
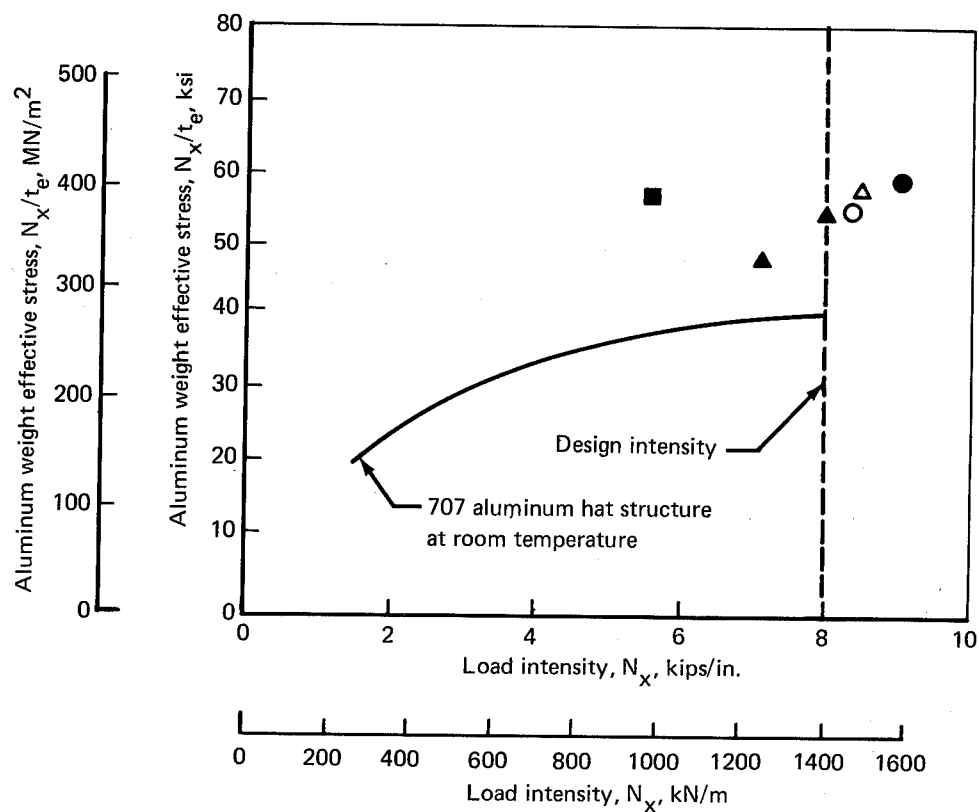
■ 11E, reinforced honeycomb sandwich column

FIGURE 66.—PANEL EFFICIENCY—SUBSONIC AIRCRAFT

● 11A, reinforced aluminum angle column

○ 11K, reinforced aluminum angle single stiffener

▲ 11C, reinforced titanium hat column

△ 11L and 11M, reinforced titanium hat single stiffener
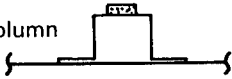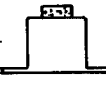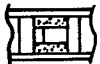
■ 11E, reinforced honeycomb sandwich column
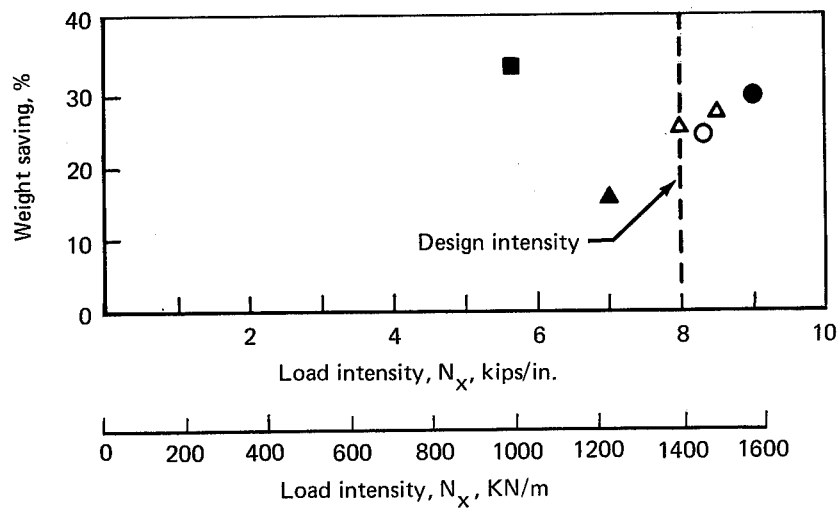
FIGURE 67.—WEIGHT SAVING—SUBSONIC AIRCRAFT
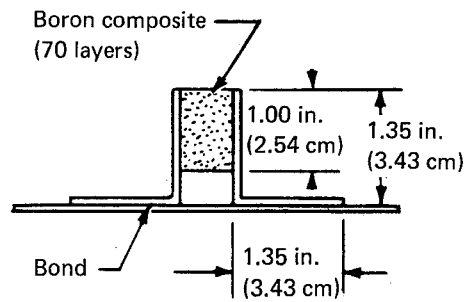
Reinforced Panel Stiffener Configuration
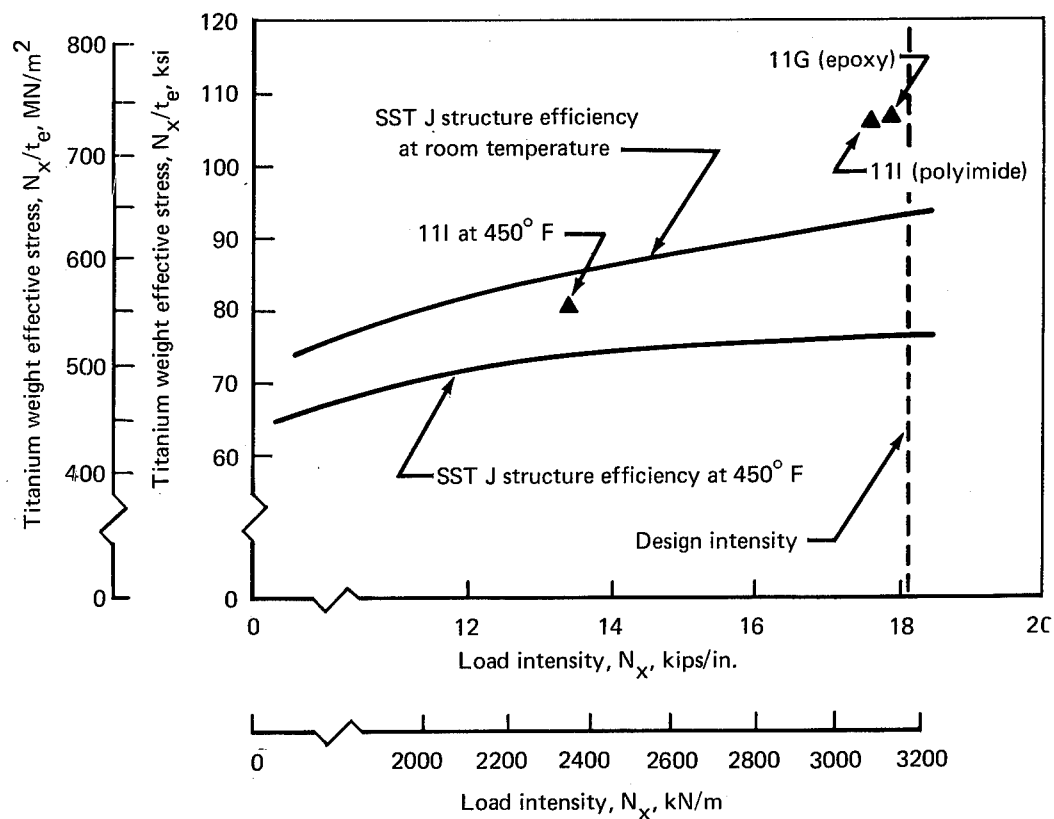
FIGURE 68.—PANEL EFFICIENCY—SUPERSONIC AIRCRAFT

Boron composite
(70 layers)

1.00 in.
(2.54 cm)

1.35 in.
(3.43 cm)

Bond

1.35 in.
(3.43 cm)

Reinforced Panel Stiffener Configuration

Weight saving at room temperature

Weight saving at 450° F

11I

11G

11I

Load intensity, N$_x$ Kips/in.

Load intensity, N$_x$, kN/m
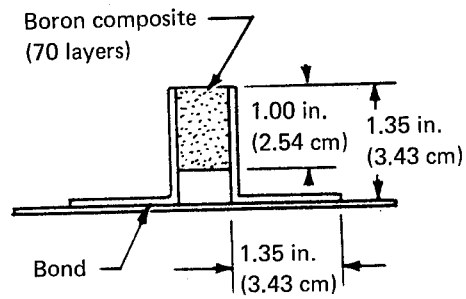
FIGURE 69.—WEIGHT SAVING—SUPERSONIC AIRCRAFT

SUMMARY OF CONCLUSIONS AND RECOMMENDATIONS

Bonding Development

The bonding of boron-epoxy composite to aluminum was successfully accomplished. The combination of Epon 927 adhesive film with Epon 933 was selected for assembling boron-epoxy laminates to aluminum for use-temperatures consistent with subsonic aircraft.

AF 126 was selected as the primary adhesive to be used for bonding boron-epoxy composites to titanium. Pasa Jel and phosphate fluoride conversion coating of titanium were both satisfactory.

The FM 34 adhesive and 35-520 Pyralin laminating resin systems were selected for assembling boron-polyimide composites to titanium. These system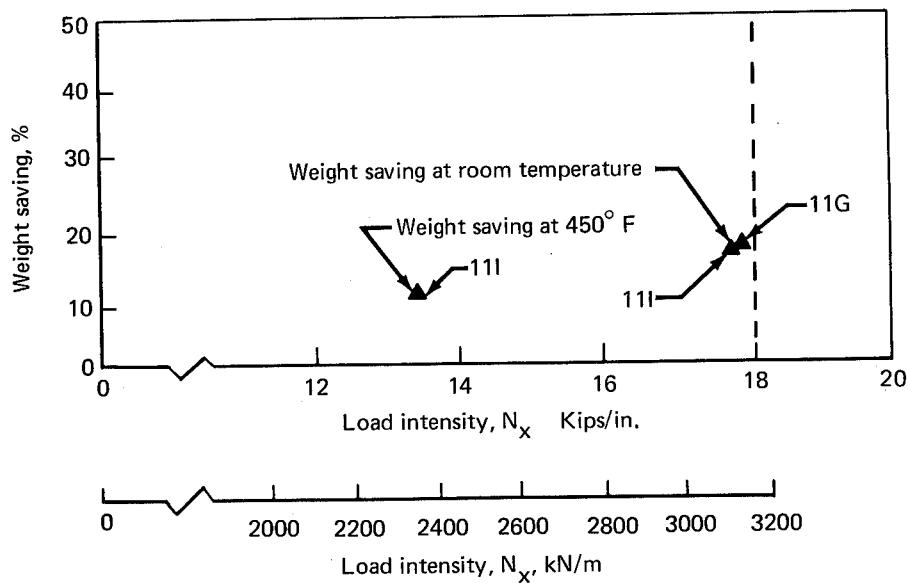s required rigid adherence to process procedures to obtain satisfactory results. In general, the polyimide's performance was inconsistent in this program. The systems proved highly sensitive to tooling and processing techniques.

Further work on low-temperature-curing adhesives is recommended. Emphasis should be placed on locking the constituent material systems together to reduce residual thermal stresses and then postcuring to increase strength.

Further development of polyimide adhesives is recommended. A larger number of systems should be investigated to provide a better selection for various applications. Emphasis should be placed on ease of processing, consistency of performance, and strength retention at elevated temperatures.

Residual Thermal Stress

The stress-free temperatures computed from observed curvature of structural laminates were in good agreement with values determined experimentally by reheating. These calculations use the difference in coefficient of thermal expansion of the constituent materials and may be highly sensitive to their absolute values.

Further work is recommended to develop more extensive data on the thermal physical properties of composite constituent materials and composites. Further work is also recommended to establish techniques for reducing the magnitude of the residual stresses resulting from bonding composites to metals.

Composite Load Transfer

Boron-epoxy composite-to-metal load transfer designs are available that permit 360-ksi (2482-MN/m^2) fiber stresses to be developed in the composite at room temperature. Boron-polyimide composites are capable of developing 310-ksi (2137-MN/m^2) fiber stresses with this design. The basic design consisted of bonding a single ply of composite on each step of a chemically milled titanium fitting. The length of the steps in the 0.30- to 0.50-in. (0.76- to 1.27-cm) range did not significantly affect the strength of this region. Phosphate fluoride was superior to pasa jel for preparing the stepped titanium surfaces for bonding using BP-907 matrix as the adhesive.

Investigation of higher strength materials for metal transition fittings is recommended.

Compression Stress-Strain

The elastic compression stress-strain response of boron-composite-metal systems was predicted within 7% to 10% using a simple transformed-area approach and typical material properties.

Measured Poisson's ratios were somewhat higher than anticipated. The honeycomb core in the test specimens apparently contributed to this behavior.

Several of the specimens incorporating boron-polyimide composites failed prematurely. The large amount of volatiles released by the polyimides prevented good consistent bonding in the metal-to-metal fitting areas.

A broader study of composite-metal ratios is recommended. The effect of core on the skin's Poisson's ratio should be further investigated.

Plate Bending

The bending stiffness of composite-reinforced metal plates was accurately predicted. The specimen section was transformed to an equivalent one-material plate by using a transformed-area technique. After transformation, simple beam relationships were used to accurately predict bending deflections.

Further work is recommended to investigate effects of composite-metal ratios in a greater range of thicknesses.

Plate Buckling

A buckling analysis for anisotropic layered plates is being developed under a contract modification, and the final results are expected to be published in a separate document. The results reported here are preliminary.

The average error made in predicting the buckling load of 12 test plates with unsymmetrical laminate distribution and clamped-clamped/simple-simple boundary conditions was 12.7%. The average error for 12 tests of symmetrically laminated plates with the same boundary conditions was 13.6%. The average error made in predicting the buckling load for 11 test plates with unsymmetrical laminate distribution and clamped-clamped/free-free boundary conditions was 17.6%; the average error was 21.8% for 12 symmetrically laminated plates with the same boundary constraints. Significant improvements were made to the above correlations when adjustments were made to the boundary conditions to reflect potential testing errors.

Column Crippling and Buckling

The reinforcement of structural shapes reinforced with unidirectional composites must be restricted to configurations not subject to torsional failure modes. The relatively low torsional stiffness of unidirectional composites does not permit them to be used effectively for reinforcing torsionally unstable sections, when compared with equivalent (equal weight) all-metal sections.

Sandwich Wrinkling and Buckling

Sandwich crippling specimens were tested that attained fiber stress levels as high as 487 ksi (3350 MN/m^2). The full potential was limited by the ultimate metal strain in the load transition areas. The reinforcement concept could be improved by using a thicker stepped transition or a higher strength material in the load transfer region.

Sandwich buckling was accurately predicted by using classic column equations in conjunction with transformed areas.

Further work is recommended to improve the transfer regions, to better understand the weight effect of a wide range of reinforced-skin strap configurations, and to understand the weight effect of core thickness in combination with skin and strap configurations.

Concept Verification Panels

The design intensity of 8 kips/in. (1.4 MN/m) was achieved by both the single stiffener and the panel incorporating the reinforced aluminum angle concept. The potential weight saving of this concept is approximately 21% at 8 kips/in. (1.4 MN/m) and 29% at 9 kips/in. (1.57 MN/m). The titanium hat concept tests indicated a weight saving of 24% is possible at 8 kips/in. (1.4 MN/m). While the reinforced honeycomb concept failed below the design intensity due to a manufacturing error, tests of this concept showed a potential weight saving of 33% at N_x = 5.6 kips/in. (0.98 MN/m).

A load intensity of 17.8 kips/in. (3.12 MN/m) was achieved in the room temperature test of the reinforced titanium angle concept incorporating boron-epoxy composites. When compared with all-titanium SST designs, this represented a weight savings of 14%. The room-temperature test of the same concept incorporating boron-polyimide composites showed approximately the same results, and, when tested at 450° F (505° K), it fell well below its design ultimate but still showed a weight savings of 9% at the achieved load intensity of 13.3 kips/in. (2.33 MN/m). During this program, continuous processing problems were encountered with the polyimide systems. Also, testing of the above polyimide panels was modified to prevent peel failure modes as indicated by shorter crippling specimens.

In general, significant weight savings were demonstrated by comparing test results obtained with composite-reinforced metal aircraft structure with equivalent all-metal structure. Studies showed that these weight savings could be obtained in a cost-effective manner because of the relatively small amounts of composite required to accomplish significant weight savings with the reinforcement concept.

APPENDIX A

CONVERSION OF U.S. CUSTOMARY UNITS TO SI UNITS

The international system of units (SI) was adopted by the Eleventh General Conference on Weights and Measures, Paris, October 1960 (ref. 1). Conversion factors for the units used herein are given in the following table:

Physical quantity	U.S. customary unit	Conversion factor (*)	SI unit
Length	in.	0.0254	meters (m)
Temperature	($^\circ$ F + 460)	5/9	degrees Kelvin ($^\circ$ K)
Density	(lbm/in^3)	27.68 x 10^3	kilograms per cubic meter (kg/m^3)
Load	lbf	4.448	newtons (N)
Mass	lbm	0.4536	kilograms (kg)
Modulus, stress	psi = lbf/in^2	6895	newtons per square meter (N/m^2)

*Multiply value given in U.S. customary units by conversion factor to obtain equivalent value in SI units.

Prefixes to indicate multiple of units are as follows:

Prefix	Multiple
centi (c)	10^2
kilo (k)	10^3
mega (M)	10^6
giga (G)	10^9

APPENDIX B

TEST SPECIMEN FABRICATION

Tape Fabrication

All boron-adhesive tape material was fabricated by a drum-winding process. Tapes 10 in. (25.4 cm) wide by 72 in. (183 cm) long were wound, four at a time, on a cylindrical mandrel. All boron-epoxy tapes were wound on BP-907 adhesive film. All boron-polyimide tapes were wound on 35-520 Pyralin adhesive film. Tapes were wound at 208 filaments per inch of width with a filament tension of 0.15 to 0.22 lb pull. After winding, tapes were cut across the width, removed from the mandrel, individually packaged in plastic film, and marked with identification numbers. Figure B1 shows the winding machine with four completed tapes of boron-polyimide material.

The polyimide adhesive required softening during winding operation to ensure proper embedding of filament in the adhesive. In the first lots of polyimide material, steam was directed against the adhesive. In later lots, BR 34 solvent was gun sprayed onto the adhesive.

Sheet Lamination

Multiple sheets of boron adhesive material were laminated as follows: A flat tool plate was provided. Tapes were cut to length and placed side by side, with adhesive down, to form a ply of required width. Successive plies were laid, adhesive side down, on the first ply to stack up the required number of plies. A picture frame was placed around the periphery of the laminate to maintain edge thickness. The plate with laminated plies was then vacuum bagged and cured to form sheets of boron adhesive material. Figure B2 shows laminate plies being placed in picture frames.

Boron/BP-907 sheets were cured without bleeder materials under the vacuum bag.

Boron/35-520 Pyralin sheets were cured with additional peel plies and bleeders on both faces of the laminate to remove solvent and reaction products.

Cleaning

Cleaning of all components was essential to attaining a good adhesive bond. The cleaning operations were controlled by Boeing process specifications. The cleaning process for each material is summarized briefly as follows:

- Aluminum—Vapor degrease, alkaline clean, deoxidize, protective wrap, prime within 16 hr.

- Titanium-epoxy bonding—Emulsion or solvent clean, alkaline clean, deoxidize, phosphate fluoride conversion coat, protective wrap, prime within 16 hr.

- Titanium-polyimide bonding—Emulsion, vapor, or solvent clean; etch in nitric fluoride solution; Pasa Jel conversion coat, protective wrap, prime within 16 hr.

- Steel spacer blocks—Vapor degrease, alkaline clean, abrasive clean, alkaline clean, protective wrap, prime within 16 hr.

- Aluminum honeycomb—Vapor degrease, oven dry, protective wrap, assembly bond within 16 hr.

- Glass fabric honeycomb—Vapor degrease, oven dry, protective wrap, assembly bond within 16 hr.

Chemical Machining

Steps were chemically machined into the titanium step transition details that were bonded into the ends of composite details. The chemical machining process was controlled by Boeing process specifications. The titanium was cleaned, rinsed, and dried. Masking material was applied and cured. The masking material was removed from the first step area. Exposed surface was removed in a nitric-fluoride solution and a rinse used to stop action. Repeated dips and rinses were used to remove specific thicknesses of material. The masking material was removed from each successive step, and material was removed until the required steps remained. Drawing tolerances of ±1 mil were held on a typical step depth of 5.5 mils during fabrication.

Metal-Composite Lamination

This was essentially the same as sheet lamination except conversion coated and primed strips of chemically milled step transition were placed to form the ends of the laminate. Filler plies were placed to fill up to the level of the first step. Plies were cut to fit each step and progressively laid up until assembly was complete. Vacuum bagging and curing were the same as for sheet lamination. Figure B3 shows the first ply of boron tape being laid onto the first step of the titanium transition details.

Cavity Tool Lamination

This was essentially the same process as sheet lamination and primary bonding, but a net-size cavity was used to produce net specimen size. An upper pressure plate was used under a vacuum bag to provide pressure to the composite. This process gave difficulty with resin wash and thinning of composite between the metal transitions on the ends. With polyimide, it was difficult to adequately bleed composite faces during cure. Use was limited to smaller specimens. Figure B2 shows a picture frame tool that becomes a cavity tool if the pressure plates, at the right side of the tool, are installed over the cavities and under the vacuum bag.

Composite-to-Metal Bonding

Cured rough-machined boron composite details were bonded to metal details. All details were cleaned, titanium details were conversion coated, all detail faying surfaces were primed, adhesive films were applied, and assembly was completed. A cavity tool or a bonding fixture was used when required. The assemblies were vacuum bagged and cured. The primer system listed with each adhesive in the material section was used. The cures used for each adhesive are listed in table B1.

Figure B4 shows typical details ready for assembly bonding of a boron-composite strap-reinforced honeycomb panel. Figure B5 shows the panel assembled (with edge blocks to prevent core collapse at edges under vacuum) and the vacuum bag covering the assembly. Figure B6 shows a bonding assembly jig used to correctly position and hold details during the vacuum bag and cure operations.

Machining Recommendations

The recommended machining procedures to be used for composites and composite-reinforced metals are summarized in table B2.

TABLE B1.—ADHESIVE CURES

Adhesive type	Maximum temperature		Time,[a] min	Vacuum[b]	Maximum pressure	
	°F	°K			psi	N/m^2
BP-907	365	458	90	Yes	50	0.345
AF 126	250	394	90	No	100	0.690
FM 123	250	394	90	No	100	0.690
Epon 927[c]	165	347	120	Yes	None	None
Epon 927/933[c]	165	347	120	Yes	None	None
35-520 Pyralin	[d]610	[d]535	90	Yes	None	None
FM 34	[d]610	[d]535	120	Yes	None	None

[a]Time at maximum temperature

[b]Vacuum under bag was 25 in. of mercury

[c]Modified cure: 48 hr at room temperature under vacuum, 2 hr at 160° F (344° K)

[d]Postcure: initial cure at 350° F (450° K)

TABLE B2.—BORON FILAMENT COMPOSITE MACHINING RECOMMENDATIONS

|	Process	Unidirectional boron-epoxy composites	Aluminum- or titanium-faced unidirectional boron-epoxy composites
Band sawing	Cutter	High-carbon steel blades, 24 teeth per inch	High-carbon steel blade, 24 teeth per inch
	Cutting speed	290 sfpm	290 sfpm
	Cutting fluid	Dry air blast	Dry air blast
Shearing		Recommended for use only when the boron fibers are parallel to the shear blade. No data on blade wear. Blade clearance: 0.002 to 0.003 in. Photo paper cutter used for transverse shearing of uncured boron tape.	Same as for unidirectional boron-epoxy
Grinding	Cutter	Aluminum oxide grinding wheel grade 75C-46-J5 V52	Aluminum oxide grinding wheel grade 75C-46-J5 V52
	Cutting speed	5000 to 6000 sfpm	5000 to 6000 sfpm
	Cutting fluid	Hocut 3210 (30:1 aqueous solution)	(a) Hocut 3210 (30:1 aqueous solution) (b) Water plus rust inhibitor
Abrasive cutoff	Cutter	Abrasive wheel grade 37C-46-K88	Abrasive wheel grade 37C-46-K88
	Cutting speed	10 000 to 15 000 sfpm	10 000 to 15 000 sfpm
	Cutting fluid	Water and rust inhibitor	Water and rust inhibitor
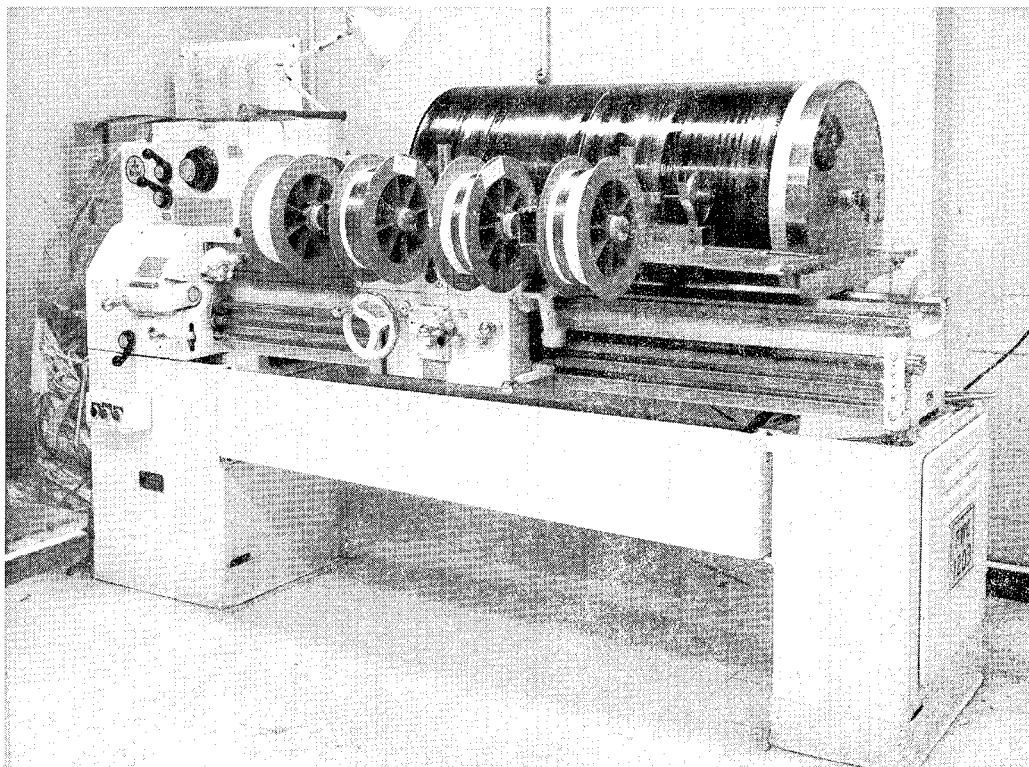
FIGURE B1.—TAPE WINDING MACHINE
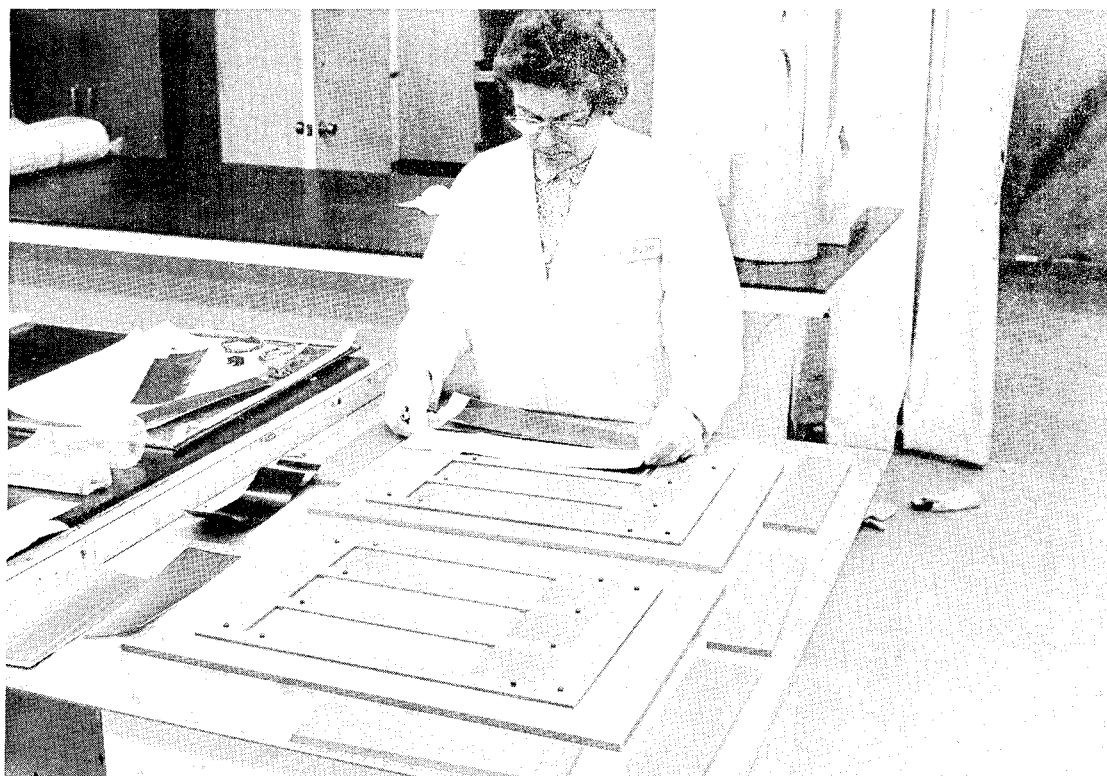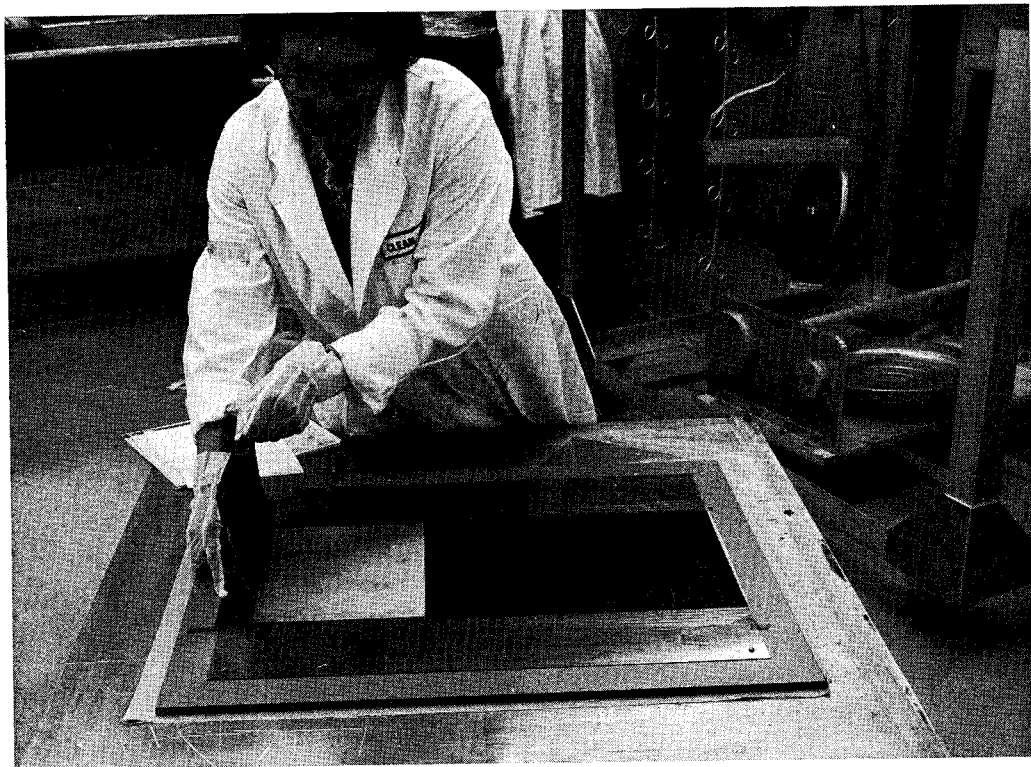

FIGURE B2.—SHEET LAMINATION
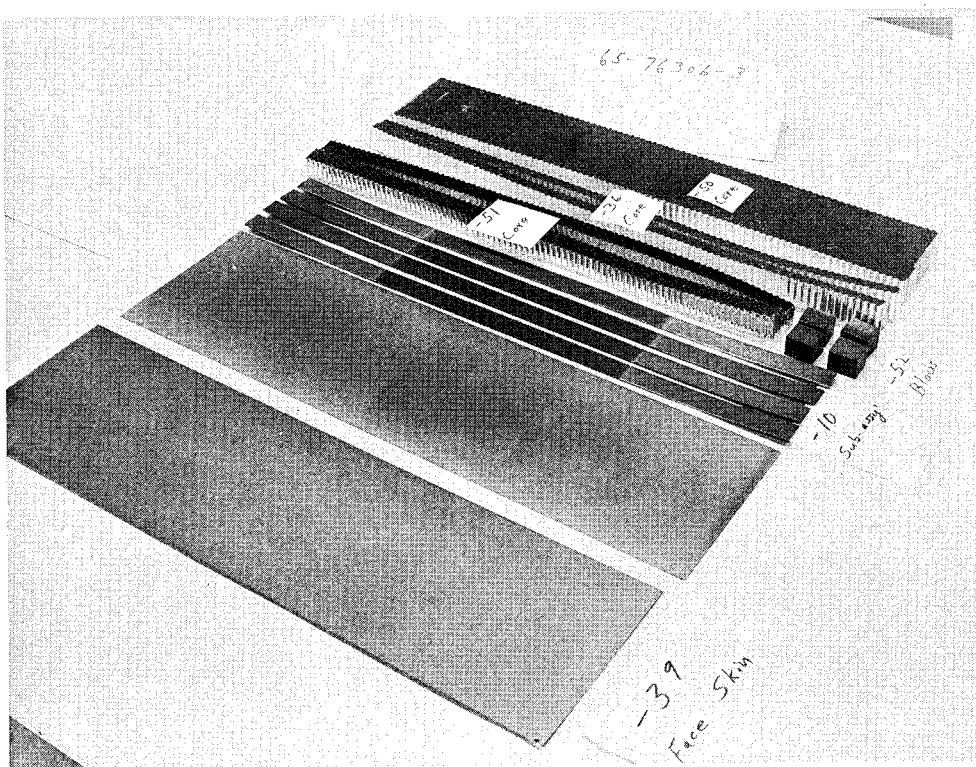
FIGURE B3.—COMPOSITE-TO-METAL BONDING

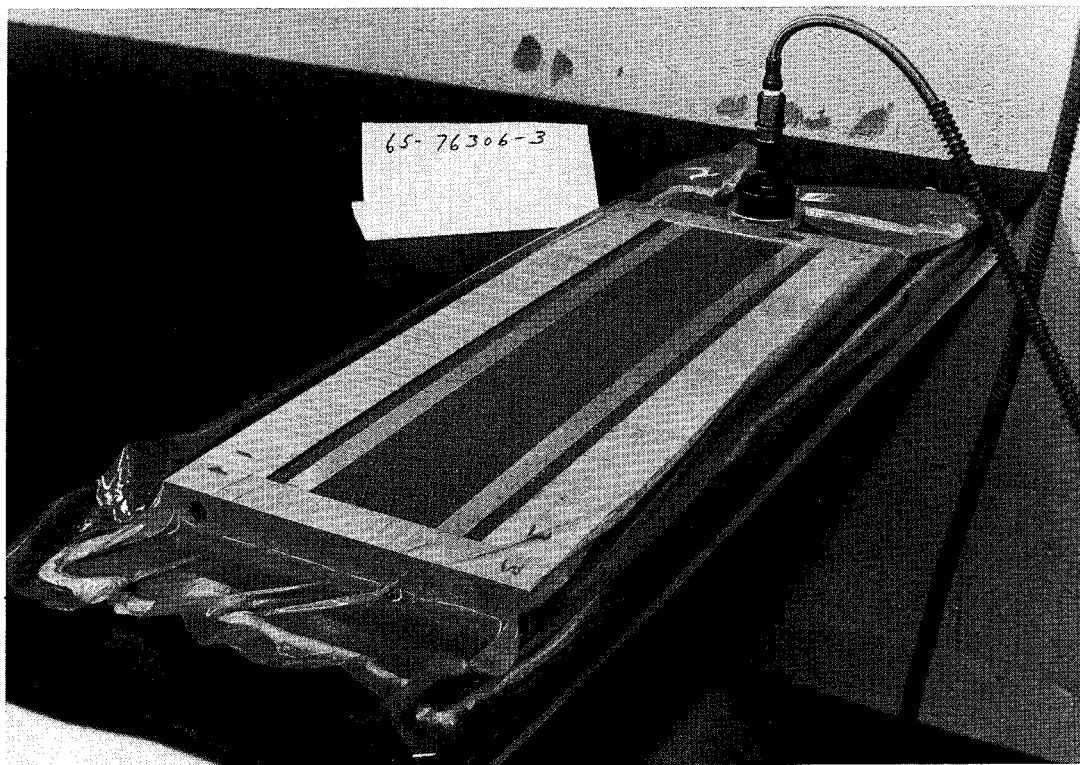FIGURE B4.—SANDWICH PANEL DETAILS

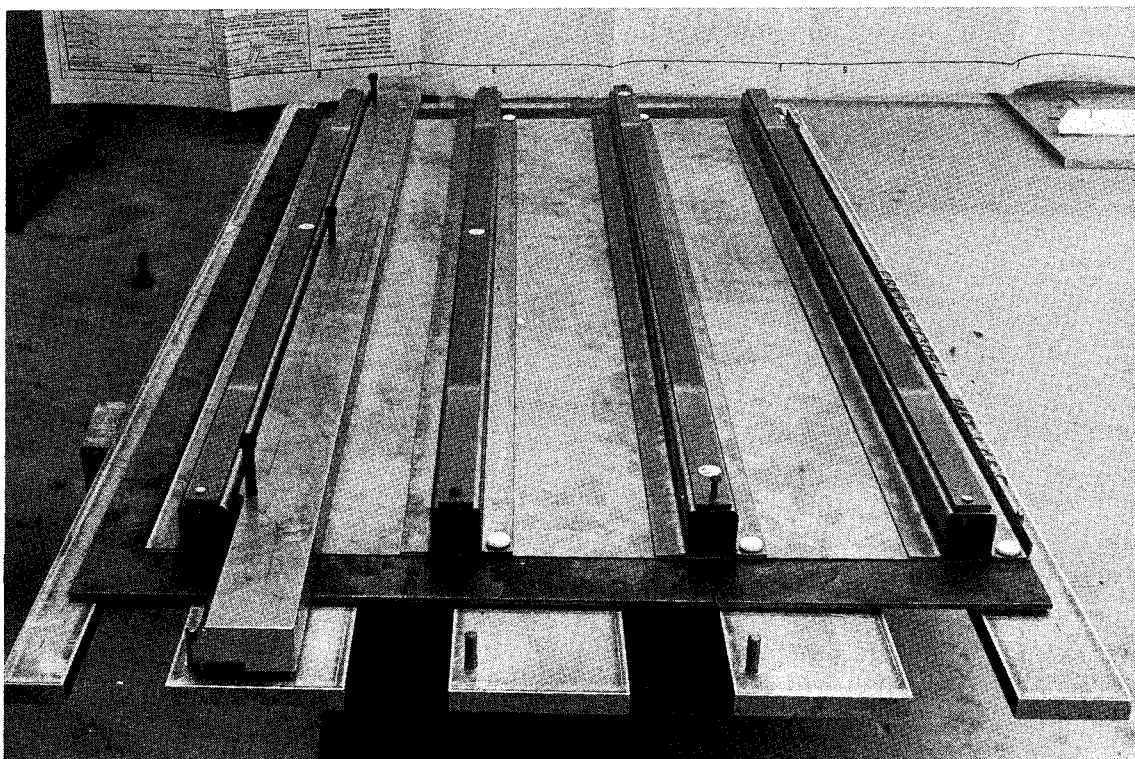FIGURE B5.—SANDWICH PANEL VACUUM BAGGED FOR CURE

FIGURE B6.—HAT SECTION PANEL IN BONDING FIXTURE

APPENDIX C

TEST SPECIMEN MATERIALS

Aluminum sheet and formed sections were alloy 7075-T6 per QQ-A-250/13.

Titanium sheet and formed sections were alloy 6Al-4V per MIL-T-9046F, type III, composition C, annealed or type III, composition C, solution treated and aged.

Steel spacer bars were annealed plain carbon steel per MIL-S-7952.

Aluminum honeycomb was per MIL-C-7438, type 8.1-1/8-20 (5052).

Polyimide-fiberglas honeycomb was HRH-324, 3/16-GF26-5.0 purchased from Hexcel Products, Incorporated.

Boron filaments were obtained from the Hamilton Standard Division of United Aircraft. These were 0.004-in. (0.010-cm) diameter filaments of boron vapor-deposited onto a tungsten wire substrate.

BP-907 adhesive was obtained from the Bloomingdale Department of American Cyanamid Company. This is a film adhesive of epoxy resin impregnated into a scrim of type 104 glass fabric. The material thickness is 0.003 in. (0.0076 cm). This is a latent cure material and has a shelf life of 6 months at room temperature. It is used primarily for drum winding with boron filament to form sheets of uncured boron-epoxy material. When used in adhesive bonding, liquid primer EC 2320 is used on all faying surfaces.

AF 126 adhesive was obtained from the Minnesota Mining and Manufacturing Company. This is a film adhesive of epoxy resin impregnated into a dacron fiber mat or veil. The material thickness is 0.005 in. (0.013 cm) for bonding plane surfaces or 0.015 in. (0.038 cm) for bonding honeycomb surfaces. Liquid primer EC 2320 is used on all faying surfaces.

FM 123-2 adhesive was obtained from the Bloomingdale Department, American Cyanamid Company. This is a film adhesive of epoxy resin impregnated into a dacron fiber mat or veil. The material thickness is 0.005 in. (0.013 cm) for bonding plane surfaces or 0.015 in. (0.038 cm) for bonding honeycomb surfaces. Liquid primer BR 123 is used on all faying surfaces.

FM 123-5 is a newer, higher room temperature strength adhesive than FM 123-2. It is used with corrosion-inhibitive primer BR 127.

Epon 927 adhesive was obtained from the Shell Chemical Company. This is a film adhesive of room temperature curing epoxy resin impregnated into a scrim of type 112 glass fabric. The material thickness is 0.005 in. (0.013 cm) and 0.010 in. (0.025 cm) for bonding only plane surfaces. Epon 927 surface conditioner is used to prime all faying surfaces.

Epon 933 adhesive was obtained from the Shell Chemical Company. This is the same epoxy resin used to manufacture Epon 927, but it is filled with a mixture of chopped fiberglass and asbestos to form a viscous material suitable for knife application to fill irregular bond surfaces.

The 35-520 Pyralin adhesive was obtained from E. I. du Pont de Nemours. This is a film adhesive of 2507 polyimide resin impregnated into a scrim of type 104 glass fabric. The material thickness is 0.003 in. (0.0076 cm). It is used primarily for drum winding with boron filament to form sheets of uncured boron-polyimide material.

FM 34 adhesive was obtained from Bloomingdale Department, American Cyanamid Company. This is a film adhesive of filled polyimide resin impregnated into glass fabric. The material thickness is 0.015 in. (0.038 cm) for plane surfaces and honeycomb core. BR 34 liquid primer is used on all faying surfaces.

The test specimen material properties used in analysis are listed in tables C1, C2, and C3. Unless otherwise noted, values were obtained from MIL-HDBK-5A (ref. 4).

TABLE C1.—ROOM TEMPERATURE PROPERTIES OF METAL AND BORON

Property	Ti-6Al-4V		7075-T6 Al	Boron filament
	Annealed	Heat treated and aged		
Tensile ultimate ksi (MN/m^2)	134(923)	157(1081)	76(523)	450(3100)
Tensile yield ksi (MN/m^2)	126(868)	143(985)	65(447)	–
Compressive yield ksi (MN/m^2)	132(909)	152(1047)	67(461)	–
Shear ultimate ksi (MN/m^2)	79(544)	98(675)	46(317)	–
Elongation %	8	3	7	–
Modulus of elasticity psi x 10^6 (N/m^2 x 10^9)	16.0(110.2)	16.0(110.2)	10.3(70.9)	60(413)
Compressive modulus psi x 10^6 (N/m^2 x 10^9)	16.4(113.0)	16.4(113.0)	10.5(72.3)	60(413)
Shear modulus psi x 10^6 (N/m^2 x 10^9)	6.2(42.7)	6.2(42.7)	3.9(26.8)	25(172)
Poisson's ratio	0.30	0.30	0.33	0.20
Coefficient of thermal expansion in./in. x 10^{-6} per °F (cm/cm x 10^{-6} per °K)	5.3(9.9)	5.3(9.9)	12.9(23.2)	2.7(4.9)

TABLE C2.—ROOM TEMPERATURE PROPERTIES OF BORON-RESIN COMPOSITES AND RESIN

Property	Material			
	Boron/BP-907	Boron/35-520	BP-907[a]	35-520[a]
Boron volume/adhesive volume	0.485	0.485	—	—
Tensile modulus longitudinal psi x 10^6 (N/m^2 x 10^9)	29.1(201)	[b]29.1 (201)	1.17(8.1)	1.94(13.4)
Tensile modulus transverse psi x 10^6 (N/m^2 x 10^9)	2.34(16.1)	[b]2.34 (16.1)	1.17(8.1)	1.94(13.4)
Compressive modulus longitudinal psi x 10^6 (N/m^2 x 10^9)	29.1(201)	[b]29.1 (201)	1.17(8.1)	1.94(13.4)
Compressive modulus transverse psi x 10^6 (N/m^2 x 10^9)	2.34(16.1)	[b]2.34 (16.1)	1.17(8.1)	1.94(13.4)
Shear modulus psi x 10^6 (N/m^2 x 10^9)	1.22(8.38)	[b]1.22 (8.38)	0.452(3.11)	—
Poisson's ratio	0.246	[b]0.246	0.30	—
Coefficient of thermal expansion in./in. x 10^{-6} per °F (cm/cm x 10^{-6} per °K)	3.1(5.8)	[b]3.1 (5.8)	15.0(28.0)	4.6 (8.6)

[a]Includes scrim

[b]Assumed values

TABLE C3.—COMPRESSIVE MODULUS OF MATERIALS AT TEST TEMPERATURES—psi x 10^{-6} (N/m^2 x 10^{-9})

Temperature		BP-907	35-520	7075-T6 Al	Ti-6Al-4V	Boron filament
°F	°K					
–65	220	[a]1.17 (8.10)	2.24(15.43)	10.0(68.9)	18.3(126.09)	[a]60 (413)
70	294	1.17(8.10)	1.94(13.4)	9.7(66.8)	16.4(113.0)	60(413)
165	346	[a]0.80 (5.51)	—	9.4(64.7)	—	[a]60 (413)
450	504	—	1.94(13.4)	—	14.1(97.1)	[a]60 (413)

[a]Assumed values

APPENDIX D

CALCULATIONS

Transformed Area Method

Boron-composite/metal element sections were converted to equivalent all-metal sections to facilitate use of design equations that involve section properties. Figure D1 shows a typical boron-composite/metal section. Figure D2 shows the metal equivalent of this same section.

The thickness of the section is known. The thickness of the metal portion is known. The thickness of the boron composite is

$$t_c = t - t_m$$

The composite area is

$$A_c = t_c B$$

The number of layers (n) of boron in the composite is known. There are 208 boron filaments per inch of width in each layer. The average diameter of a boron filament is 0.004 in. The boron section area in the composite is

$$A_B = \frac{208\pi d_B{}^2 Bn}{4}$$

The matrix area in the composite is

$$A_r = A_c - A_B$$

The metal equivalent area of the composite is

$$A_{me_c} = A_r \frac{E_r}{E_m} + A_B \frac{E_B}{E_m}$$

The values of E_r, E_B, and E_m are given in appendix C.

Residual Thermal Stress Calculations of Stress-Free Temperature

The stress-free temperature T_o was calculated using the following equation developed by S. Timoshenko (ref. 2) for bimetal thermostats:

$$\rho = \frac{h[3(1 + \alpha)^2 + (1 + \alpha\beta)(\alpha^2 + 1/\alpha\beta)]}{6(1 + \alpha)^2(\kappa_m - \kappa_c)\Delta T} \tag{1}$$

where:

h = total specimen thickness

ρ = radius of curvature

κ_m = thermal expansion coefficient of metal (see table C1)

κ_c = thermal expansion coefficient of composite (see table C2)

α = ratio of composite thickness to metal thickness

β = modulus ratio $= \dfrac{E_c}{E_m} = \dfrac{A_f}{(A_f + A_r)}\dfrac{E_f}{E_m}$

This approximation leads to a 1.7% error at 50% volume fraction. This error increases as fiber volume fraction decreases.

The thermal expansion coefficient of the composite is obtained from:

$$\epsilon_c = \kappa_c \Delta T \tag{2}$$

$$\epsilon_c = \epsilon_B = \frac{\sigma_B}{E_B} = \kappa_B \Delta T = \frac{E_r \Delta T E_B}{A_B E_B + A_r E_r}(\kappa_r - \kappa_B)A_r + \kappa_B \Delta T \tag{3}$$

$$\kappa_c = \frac{\epsilon_c}{\Delta T} = \frac{A_r E_r (\kappa_r - \kappa_B)}{A_B E_B + A_r E_r} + \kappa_B \tag{4}$$

Figure D3 shows how individual materials would expand due to a change in temperature and what happens to the titanium and the boron when held together by the matrix.

$$\text{Strain in boron} = \epsilon_B = \frac{\sigma_B}{E_B} + \kappa_B \Delta T = \frac{P_B/A_B}{E_B} + \kappa_B \Delta T \tag{5}$$

$$\text{Strain in titanium} = \epsilon_{Ti} = \frac{\sigma_{Ti}}{E_{Ti}} + \kappa_{Ti}\Delta T = \frac{P_{Ti}/A_{Ti}}{E_{Ti}} + \kappa_{Ti}\Delta T \tag{6}$$

$$\text{Strain in matrix} = \epsilon_r = \frac{\sigma_r}{E_r} + \kappa_r \Delta T = \frac{P_r/A_r}{E_r} + \kappa_r \Delta T \tag{7}$$

Where T is the change in temperature from the stress-free temperature T_o.

By equating the strains, the following equation is found:

$$\frac{P_B}{E_B A_B} - \frac{P_{Ti}}{E_{Ti}A_{Ti}} = \Delta T(\kappa_{Ti} - \kappa_B) \tag{8}$$

$$\frac{P_B}{E_B A_B} - \frac{P_r}{E_r A_r} = \Delta T(\kappa_r - \kappa_B) \qquad (9)$$

$$\frac{P_r}{E_r A_r} - \frac{P_{Ti}}{E_{Ti} A_{Ti}} = \Delta T(\kappa_{Ti} - \kappa_r) \qquad (10)$$

The equilibrium equation is:

$$P_B + P_{Ti} + P_r = 0 \qquad (11)$$

where P is the total load in any one of the three components.

Solving equations (5), (6), and (7) simultaneously gives

$$\sigma_r = \frac{\Delta T[(\kappa_{Ti} - \kappa_r)E_{Ti}A_{Ti} + (\kappa_B - \kappa_r)E_B A_B] E_r}{E_r A_r + E_B A_B + E_{Ti} A_{Ti}} \qquad (12)$$

$$\sigma_B = \frac{\Delta T[(\kappa_{Ti} - \kappa_B)E_{Ti}A_{Ti} + (\kappa_r - \kappa_B)E_r A_r] E_B}{E_B A_B + E_r A_r + E_{Ti} A_{Ti}} \qquad (13)$$

$$\sigma_{Ti} = \frac{\Delta T[(\kappa_B - \kappa_{Ti})E_B A_B + (\kappa_r - \kappa_{Ti})E_r A_r] E_{Ti}}{E_{Ti} A_{Ti} + E_r A_r + E_B A_B} \qquad (14)$$

The above equations are of the form $\sigma_i = \kappa \Delta T$ and may be plotted for different area ratios.

When the composite structure consists of fibers and resin only, equations (1) and (3) give

$$\sigma_B = \frac{E_r E_B \Delta T}{A_B E_B + A_r E_r} (\kappa_r - \kappa_B)A_r \qquad (15)$$

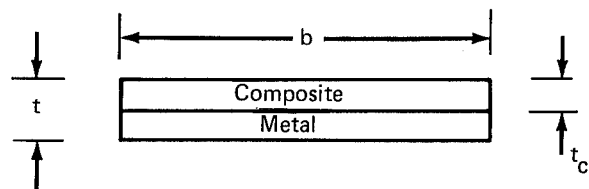$$\sigma_r = \frac{E_r E_B \Delta T}{A_B E_B + A_r E_r} (\kappa_B - \kappa_r)A_B \qquad (16)$$

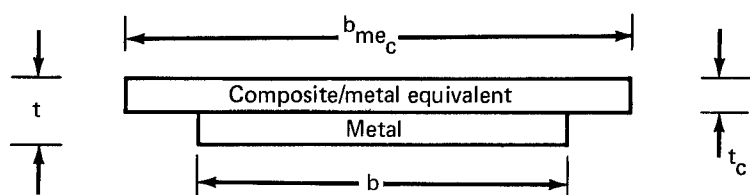FIGURE D1.—TYPICAL BORON COMPOSITE/METAL SECTION

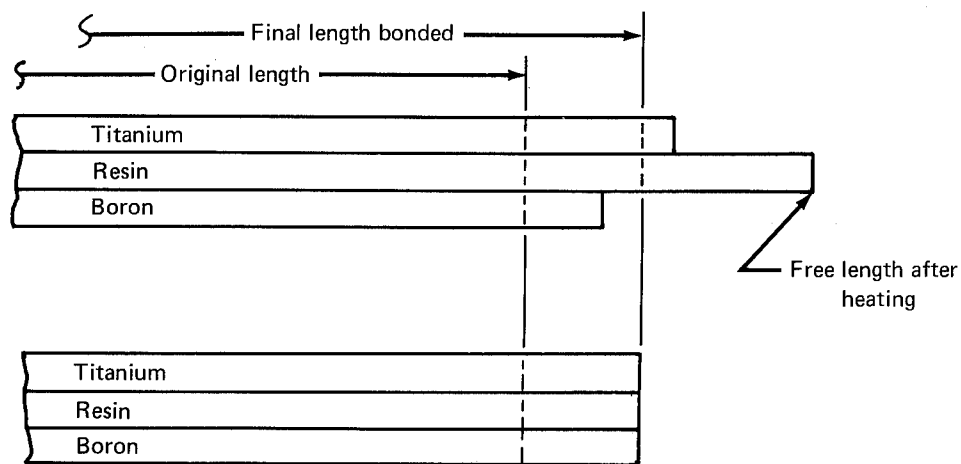FIGURE D2.—METAL EQUIVALENT OF BORON COMPOSITE/METAL SECTION

FIGURE D3.—TEMPERATURE EXPANSION OF INDIVIDUAL MATERIALS

REFERENCES

1. Comm. on Metric Pract.: ASTM Metric Practice Guide, NGS Handbook 102, U.S. Department of Commerce, March 10, 1967.

2. Timoshenko, S.: Analysis of Bimetal Thermostats. Journal of The American Optical Society of America, vol. II, 1925, pp. 233-255.

3. Zender, G. W. and Dexter, H. B.: Compressive Properties and Column Efficiency of Metals Reinforced on the Surface With Bonded Filaments. NASA TN D-4878, November 1968.

4. Anon.: Metallic Materials and Elements for Aerospace Vehicle Structure. Military Handbook MIL-HDBK-5, U.S. Department of Defense.

5. Viswanathan, A. V.; Soong, Tsai-Chen; and Miller, R. E., Jr.: Buckling Analysis for Axially Compressed Flat Plates — Structural Sections and Stiffened Plates Reinforced With Laminated Composites. NASA CR-1887, 1971.

001 001 C1 U 18 711203 S00942DS
DEPT OF THE ARMY
PICATINNY ARSENAL
PLASTICS TECHNICAL EVALUATION CENTER
ATTN: SMUPA-VP3
DOVER NJ 07801

POSTMASTER: If Undeliverable (Section 15 Postal Manual) Do Not Retu

"*The aeronautical and space activities of the United States shall be conducted so as to contribute . . . to the expansion of human knowledge of phenomena in the atmosphere and space. The Administration shall provide for the widest practicable and appropriate dissemination of information concerning its activities and the results thereof.*"

— NATIONAL AERONAUTICS AND SPACE ACT OF 1958

NASA SCIENTIFIC AND TECHNICAL PUBLICATIONS

TECHNICAL REPORTS: Scientific and technical information considered important, complete, and a lasting contribution to existing knowledge.

TECHNICAL NOTES: Information less broad in scope but nevertheless of importance as a contribution to existing knowledge.

TECHNICAL MEMORANDUMS: Information receiving limited distribution because of preliminary data, security classification, or other reasons.

CONTRACTOR REPORTS: Scientific and technical information generated under a NASA contract or grant and considered an important contribution to existing knowledge.

TECHNICAL TRANSLATIONS: Information published in a foreign language considered to merit NASA distribution in English.

SPECIAL PUBLICATIONS: Information derived from or of value to NASA activities. Publications include conference proceedings, monographs, data compilations, handbooks, sourcebooks, and special bibliographies.

TECHNOLOGY UTILIZATION PUBLICATIONS: Information on technology used by NASA that may be of particular interest in commercial and other non-aerospace applications. Publications include Tech Briefs, Technology Utilization Reports and Technology Surveys.

Details on the availability of these publications may be obtained from:

SCIENTIFIC AND TECHNICAL INFORMATION OFFICE

NATIONAL AERONAUTICS AND SPACE ADMINISTRATION
Washington, D.C. 20546